AD-A159 415 USE OF SPACE SHUTTLE PHOTOGRAPHY IN THE STUDY OF METEOROLOGICAL PHENOMENA(U) NAVAL POSTGRADUATE SCHOOL MONTEREY CA F J SVETZ JUN 85 1/2

UNCLASSIFIED F/G 4/2 NL

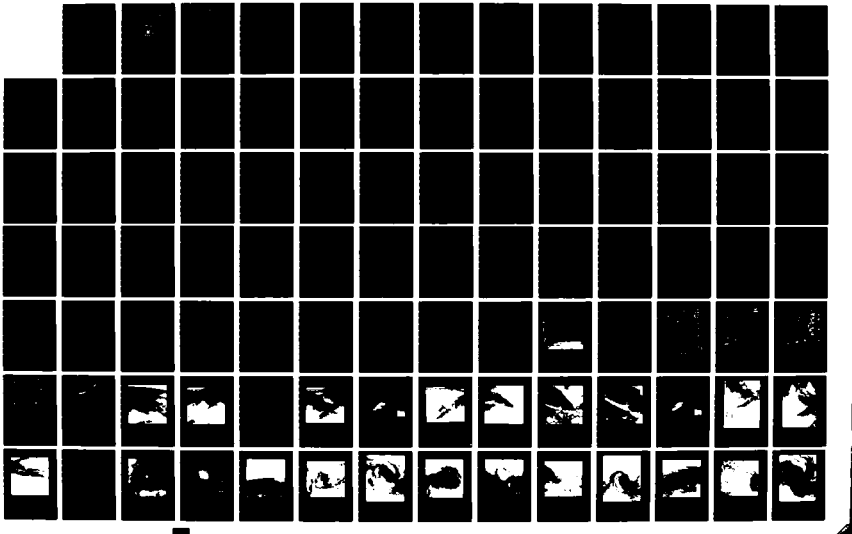

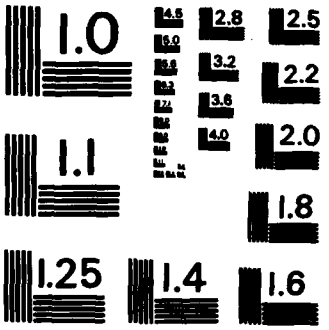

MICROCOPY RESOLUTION TEST CHART
NATIONAL BUREAU OF STANDARDS - 1963 - A

(2)

NAVAL POSTGRADUATE SCHOOL
Monterey, California

THESIS

USE OF SPACE SHUTTLE PHOTOGRAPHY IN
THE STUDY OF METEOROLOGICAL PHENOMENA

by

Frederick J. Svetz

June 1985

Thesis Advisor: C. H. Wash

Approved for public release; distribution is unlimited

UNCLASSIFIED

SECURITY CLASSIFICATION OF THIS PAGE (When Data Entered)

REPORT DOCUMENTATION PAGE		READ INSTRUCTIONS BEFORE COMPLETING FORM
1. REPORT NUMBER	2. GOVT ACCESSION NO. A159413	3. RECIPIENT'S CATALOG NUMBER
4. TITLE (and Subtitle) Use of Space Shuttle Photography in the Study of Meteorological Phenomena		5. TYPE OF REPORT & PERIOD COVERED Master's Thesis June 1985 6. PERFORMING ORG. REPORT NUMBER
7. AUTHOR(s) Frederick J. Svetz		8. CONTRACT OR GRANT NUMBER(s)
9. PERFORMING ORGANIZATION NAME AND ADDRESS Naval Postgraduate School Monterey, CA 93943		10. PROGRAM ELEMENT, PROJECT, TASK AREA & WORK UNIT NUMBERS
11. CONTROLLING OFFICE NAME AND ADDRESS Naval Postgraduate School Monterey, CA 93943		12. REPORT DATE June 1985 13. NUMBER OF PAGES 105
14. MONITORING AGENCY NAME & ADDRESS(if different from Controlling Office)		15. SECURITY CLASS. (of this report) Unclassified 15a. DECLASSIFICATION/ DOWNGRADING SCHEDULE

16. DISTRIBUTION STATEMENT (of this Report)

Approved for public release; distribution is unlimited.

17. DISTRIBUTION STATEMENT (of the abstract entered in Block 20, if different from Report)

18. SUPPLEMENTARY NOTES

19. KEY WORDS (Continue on reverse side if necessary and identify by block number)

space shuttle, photography, NASA, SSEOP, meteorology

20. ABSTRACT (Continue on reverse side if necessary and identify by block number)

Analysis of three atmospheric phenomena (squall line over the Gulf of Mexico on 9 April 1984, Hurricane Kamisy in the Indian Ocean 7-12 April 1984, and the Mauna Loa volcano smoke plume, Hawaii 7-12 April 1984) is performed using handheld-camera photographs from the Space Transportation System (STS) 41-C mission (6-13 April 1984). High resolution

DD FORM 1 JAN 73 1473 EDITION OF 1 NOV 65 IS OBSOLETE
S/N 0102-LF-014-6601

UNCLASSIFIED

SECURITY CLASSIFICATION OF THIS PAGE (When Data Entered)

#20 - ABSTRACT - (CONTINUED)

color photographs taken of the earth from the Space Shuttle Challenger were made available from the National Aeronautics and Space Administration (NASA) through the Space Shuttle Earth Observations Project (SSEOP).

Comparison is made to collocated meteorological satellite images (DMSP, AVHRR and GOES) and conventional meteorological data to illustrate the advantages and deficiencies of these new high resolution photographic data.

Approved for public release; distribution is unlimited.

Use of Space Shuttle Photography in the Study of Meteorological Phenomena

by

Frederick J. Svetz
Captain, United States Air Force
B.A., St. Mary's College of California, 1976

Submitted in partial fulfillment of the requirements for the degree of

MASTER OF SCIENCE IN METEOROLOGY

from the

NAVAL POSTGRADUATE SCHOOL
June 1985

Author: Frederick J. Svetz
Frederick J. Svetz

Approved by: _____
C.H. Wash, Thesis Advisor

_____
R.J. Renard, Second Reader

_____
R.J. Renard, Chairman,
Department of Meteorology

_____
J.N. Dyer,
Dean of Science and Engineering

ABSTRACT

Analysis of three atmospheric phenomena (squall line over the Gulf of Mexico on 9 April 1984, Hurricane Kamisy in the Indian Ocean 7-12 April 1984, and the Mauna Loa volcano smoke plume, Hawaii 7-12 April 1984) is performed using handheld-camera photographs from the Space Transportation System (STS) 41-C mission (6-13 April 1984). High resolution color photographs taken of the earth from the Space Shuttle Challenger were made available from the National Aeronautics and Space Administration (NASA) through the Space Shuttle Earth Observations Project (SSEOP).

Comparison is made to collocated meteorological satellite images (DMSP, AVHRR and GOES) and conventional meteorological data to illustrate the advantages and deficiencies of these new high resolution photographic data.

TABLE OF CONTENTS

I. INTRODUCTION 11

II. SHUTTLE ASTRONAUT PHOTOGRAPHY OPPORTUNITIES . . . 16

III. GULF OF MEXICO SQUALL LINE 19
- A. INTRODUCTION 19
- B. SYNOPTIC OVERVIEW 20
- C. ORBIT 46 22
- D. ORBIT 47 25
- E. ORBIT 48 29
- F. CONCLUSION 32

IV. HURRICANE KAMISY 34
- A. INTRODUCTION 34
- B. APRIL 7TH 35
- C. APRIL 8TH 40
- D. APRIL 9TH 42
- E. APRIL 12TH 44
- F. CONCLUSION 46

V. THE MAUNA LOA VOLCANO 48
- A. INTRODUCTION 48
- B. MEASUREMENTS 48
- C. CONCLUSION 51

VI. CONCLUSIONS / RECOMMENDATIONS 52
- A. CONCLUSIONS 52
- B. RECOMMENDATIONS 53

APPENDIX A: TABLES 56

APPENDIX B: FIGURES 58

LIST OF REFERENCES 103

INITIAL DISTRIBUTION LIST 105

LIST OF TABLES

I	Mission Data for STS 41-C	56
II	Hurricane Kamisy, 7-13 April 1984	57

LIST OF FIGURES

1. NASA-modified Hasselblad 500 EL/M Camera 58
2. Location of Windows in Shuttle Orbiter 59
3. Severe Weather Obs., Florida, 9 April 1984 60
4. STS 41-C Orbits 46, 47, and 48 Over the Gulf of Mexico 61
5. NMC Surface Analysis, 1200 GMT 9 April 1984 62
6. Boothville, Louisiana Sounding, 1200 GMT 9 April 1984 63
7. Tampa Bay, Florida Sounding, 1200 GMT 9 April 1984 64
8. NMC 500mb Analysis, Heights/Temperature 1200 GMT, 9 April 1984 65
9. NMC 300mb Analysis, Heights/Isotachs 1200 GMT, 9 April 1984 66
10. NMC 200mb Analysis, Heights/Isotachs 1200 GMT, 9 April 1984 67
11. NMC 100mb Analysis, Heights/Isotachs 1200 GMT, 9 April 1984 68
12. Vertically-coupled Upper- and Lower-tropospheric Jet-front Systems 69
13. Frame 2111: Gulf of Mexico Squall Line Orbit 46, 1208 GMT, 9 April 1984 (100-mm lens) 70
14. GOES IR: Gulf of Mexico Squall Line 1031 GMT, 9 April 1984 71
15. Severe Thunderstorm Vertical Flow in x-z Plane . . . 72
16. GOES IR: Gulf of Mexico Squall Line 1301 GMT, 9 April 1984 73
17. Tampa Bay, Florida Radar, 1340 GMT, 9 April 1984 . . 74

18. GOES VISIBLE: Gulf of Mexico Squall Line 1331 GMT, 9 April 1984 75
19. Frame 2130: Gulf of Mexico Squall Line Orbit 47, 1338 GMT, 9 April 1984 (100-mm lens) 76
20. Frame 2134: Gulf of Mexico Squall Line Orbit 47, 1338 GMT, 9 April 1984 (100-mm lens) 77
21. Frame 2008: Gulf of Mexico Squall Line Orbit 47, 1338 GMT, 9 April 1984 (250-mm lens) 78
22. Tampa Bay, Florida Radar, 1515 GMT 9 April 1984 79
23. DMSP VISIBLE: Gulf of Mexico Squall Line 1521 GMT, 9 April 1984 80
24. DMSP IR: Gulf of Mexico Squall Line 1521 GMT, 9 April 1984 81
25. Frame 2166: Gulf of Mexico Squall Line Orbit 48, 1516 GMT, 9 April 1984 (100-mm lens) 82
26. STS 41-C Orbits 14, 15, 16, 30 and 46 Over Hurricane Kamisy, 7-13 April 1984 83
27. Frame 1592: Hurricane Kamisy, Orbit 15, 1157 GMT, 7 April 1984 (100-mm lens) 84
28. Frame 1499: Hurricane Kamisy, Orbit 15 1157 GMT, 7 April 1984 (250-mm lens) 85
29. Frame 1608: Hurricane Kamisy, Orbit 16 1330 GMT, 7 April 1984 (100-mm lens) 86
30. AVHRR VISIBLE: Hurricane Kamisy 1205 GMT, 7 April 1984 87
31. DMSP IR: Hurricane Kamisy 1405 GMT, 7 April 1984 88
32. Frame 1661: Hurricane Kamisy, Orbit 30 1128 GMT, 8 April 1984 (50-mm lens) 89
33. Frame 1367: Hurricane Kamisy, Orbit 30 1128 GMT, 8 April 1984 (250-mm lens) 90
34. AVHRR VISIBLE: Hurricane Kamisy 1153 GMT, 8 April 1984 91

35. DMSP IR: Hurricane Kamisy 0714 GMT, 8 April 1984 92
36. Frame 2126: Hurricane Kamisy, Orbit 46 1239 GMT, 9 April 1984 (100-mm lens) 93
37. AVHRR VISIBLE: Hurricane Kamisy 1322 GMT, 9 April 1984 94
38. DMSP IR: Hurricane Kamisy 1322 GMT, 9 April 1984 95
39. Frame 1756: Unnamed Tropical Cyclone, Orbit 92 1330 GMT, 12 April 1984 (250-mm lens) 96
40. Frame 1780: Unnamed Tropical Cyclone, Orbit 93 1510 GMT, 12 April 1984 (250-mm lens) 97
41. Frame 1935: Unnamed Tropical Cyclone, Orbit 93 1510 GMT, 12 April 1984 (50-mm lens) 98
42. The Island of Hawaii, and Location of its Major Volcanoes 99
43. Frame 1538: Island of Hawaii, Orbit 21, 2051 GMT, 7 April 1984 (250-mm lens) 100
44. Frame 1688: Island of Hawaii, Orbit 37, 2205 GMT, 8 April 1984 (50-mm lens) 101
45. Frame 1807: Island of Hawaii, Orbit 96, 1951 GMT, 12 April 1984 (250-mm lens) 102

I. INTRODUCTION

The availability of continuous satellite images of the Earth has brought the science of meteorology to a new era. Since the introduction of orbital satellite imagery in 1960, a wealth of new data have been presented to the meteorological forecaster and researcher for consideration.

Although not without limitations, these weather satellites achieved what was previously impossible: the first visible-image time series of developing storms, precisely defining horizontal scales of motion. They illustrated the dynamic interactions of large-scale weather systems, located favored areas of genesis and dissipation and provided coverage for the data-sparse oceanic regions. Today they continue to be one of the most useful aids to the forecaster, and one of the most important data sources in meteorological research.

However, there are limitations on the usefulness of meteorological satellite imagery. Spatially and temporally, satellite coverage of the Earth is quite inflexible. Areal coverage is precisely determined and not readily changeable. As a result, interesting phenomena near or just beyond their boundaries will either be poorly defined due to distortion or lost completely. Necessarily rigid time schedules produce images that may completely miss weather features with short (less than 30 min) life cycles. Finally, circling the Earth at altitudes up to 40,000 km, the meteorological satellite simply cannot offer the image resolution necessary for accurate representation of small cloud elements and detailed cloud structures of mesoscale and synoptic systems.

Thus it is within this context that one must judge the usefulness of high-resolution photography from space. From its earliest beginnings in the Mercury, Gemini and Apollo missions, photographic images of the earth from a space platform have given scientists a perspective unavailable by any other means; a vitally important perspective that allows direct observation of features previously noted only in laboratory experiments. As one example, Chopra and Hubert (1965) found wake waves in stratus clouds formed in the lee of islands to be a quantitative analog to the vortex streets formed behind a solid cylinder comparable in size to the islands. For another, Black (1979) noted the similarity of classical wave reflection from a boundary to the atmospheric wave patterns found in fog on the coast of Nova Scotia.

Manned space flight has introduced an extra dimension to obtaining interesting Earth images. Human judgement does away with predetermined camera angles and rigid time schedules. Human observers can point cameras wherever they wish, and choose to photograph or not at their discretion. Utilizing the photographic equipment on board every space shuttle flight, large-scale events can be captured with a wide-angle lens, and a telephotographic lens can pinpoint smaller-scale phenomena that would otherwise never be noticed.

The product itself is superior to satellite imagery by several criteria. The addition of color enhances subtle textural variations to provide a three-dimensional effect in many of the photographs, making it easier to judge shape and spatial relationships between cloud masses. Stereophotography can provide important quantitative results in determining vertical scales of motion to a degree of accuracy unobtainable with radar or infrared (IR) satellite images. And lastly, sharply increased spatial resolution allows the cameras on board the current space shuttle

missions to resolve many detailed events on the order of tens to hundreds of meters.

The last of these advantages primarily results from the difference in orbital altitudes between the manned space platform and unmanned satellites. Meteorological satellites orbit at approximately 850 to 40,000 km above the Earth, compared to normal shuttle altitudes of 200 to 500 km. Consequently, while most satellite images from the Geostationary Operational Environmental Satellite (GOES) System, the United States Air Force Defense Meteorological Satellite Program (DMSP) and the Advanced Very High Resolution Radiometer (AVHRR) instrument on the TIROS-N satellite have a maximum resolution on the order of 1 km (and many of their products are restricted to features of several km size), the shuttle cameras on Space Transportation System (STS) 41-c mission, which produced the photographs in this thesis, had as their maximum ground resolution a fraction under 20 m (see Table I). Note that the figures in this table refer to a near-vertical orientation of the camera to the Earth's surface.

In the past, photography from space has yielded impressive results. In 1974, the 84 days of the Skylab mission alone produced a scientific goldmine. In the words of Gerald P. Carr, Commander of Skylab 4;

> I think that we have discovered a new national resource. With better equipment and more sophisticated training, space observers can capitalize on their initiative, discrimination and judgement to obtain information to better understand and manage our environment and to conduct Earth science experiments from space. Our 84 days in space...rewarded us with many spectacular scenes such as the luminescent red, blue and green plankton blooms in the intertwining ocean currents off the coasts of Argentina and New Zealand and the variety of shapes and colors that define agricultural patterns in many countries.... We photographically recorded the eruption of the volcano Sakura-zima in Japan and the vast extent of red dust clouds generated from the Sahara....
>
> When one realizes the vastness of the Earth, the complex interrelations of oceans, land and atmosphere, and the abundance of information required to understand and manage our environment, it is obvious that...man

will play an important role in the datagathering and interpretation phase of a total space system. (Carr, 1977)

From data gathered in those 84 days, the meteorological gains by themselves were outstanding: stereophotographs were used to determine heights and relationships of multilayered clouds in frontal systems (Skillman and Shenk, 1977); Karman vortex streets were examined and relationships established between them and orographic influences, stability and surface wind velocity (Fujita and Tecson, 1977); and clues for anticipating developing cyclonic systems were uncovered from examining cloud streets and their occurrence in conjunction with an unstable environment and strong low-level wind flow (Pitts, et al, 1977). In addition, persistent convective overshoot regions and convective waves were identified in developing tropical storms. Photographs of mature tropical storms supported a theory postulating the existence of outward-tilted eyewalls (Black, 1977). Overshooting convective turrets, internal gravity waves and transverse wave have all been identified as part of the small-scale dynamics of tropical storms--all due to the extremely high resolution and other unique features of hand-held photography from space.

Peter G. Black, a pioneer in the use of space photography for meteorological analysis, sums it up very well in a comment on his study of tropical storms: "Manned space flight offers a unique opportunity to observe tropical storms. The combination of human judgement and an Earth-orbiting platform enables off-track observations of tropical storms that could not be accomplished by other means. The ability to resolve small-scale features... and to obtain stereopair photographs is unparalleled by other observational techniques." (Black, 1977) Shuttle photographs are giving us unique views of commonplace meteorological

phenomena. And, in some cases, they are our only view of extraordinary events.

The goal of this thesis will be to use this high-resolution photography to more accurately interpret the routine satellite images available from the TIROS-N, GOES and DMSP meteorological orbiting satellites. In the three case studies to follow, I will point out the corrections and refinement of detail that can be made to previous analysis techniques applied to satellite images, and the value the use of these products will be to the teaching, forecasting, and research meteorologist.

II. SHUTTLE ASTRONAUT PHOTOGRAPHY OPPORTUNITIES

The aquisition of earth images by photography from space is organized by the Space Shuttle Earth Observations Project (SSEOP). It does not have the status or the mandate of other scheduled data-gathering experiments on the space shuttle, in that there is no set time of performance or, for that matter, any rigid requirement for the astronauts to complete any part of it. The entire project relies on the cooperation and the enthusiasm of the crew of the shuttle, to take time out from an exhausting schedule whenever possible to make photographs of terrestrial features of interest to scientists on the ground. Still, training and preparation for this undertaking are quite extensive. Basic photographic techniques must be learned, as well as the difficult art of identifying noteworthy physical features on the earth. The latter is not as easy as it may sound. Shuttle astronauts must be able to locate and identify features on the ground when passing over them in inverted flight, at high speed and peering through a relatively small window, sometimes with no reliable indication of which direction is north or south. Briefings in geology, oceanography and meteorology, in addition to reviews of previous manned-orbital photography play an important part in learning the reconnaissance cues vital to good performance of this role.

Real-time input to the shuttle crew is made by project scientists to direct the astronaut's attention to current areas of interest. Features especially sought for photographic study include hurricanes and other major storms, volcanoes, extreme pollution espisodes, floods, ice and fires. After the conclusion of the flight, the film is

processed and cataloged by the National Aeronautics and Space Administration (NASA).

All of the photographs used in this thesis were a product of the STS 41-C mission, in which the Space Shuttle Challenger (OV-099) completed 107 orbits in the time from liftoff at 6 April 1984, to landing seven days later on 13 April (see Table I). Nominal altitude for the first 16 orbits was 125 n mi, after which altitude was increased to 269 n mi in support of the Solar Max Repair Experiment.

The photography equipment used on this mission included two NASA-modified Hasselblad 500 EL/M 70-mm cameras (Fig. 1), equipped with Zeiss 50-mm Distagon C4.0, 100-mm Planar C3.5 and 250-mm Sonnar C5.6 lenses, and one NASA-modified Linhof Aero Technica 45 camera. The observations in this thesis are limited to the products of the 70-mm Hasselblad cameras exclusively. Kodak Ektachrome 64 Professional 6017 film was used. Ground resolution and ground coverage of these photographs (for angles near vertical) are presented in Table I The extreme resolution afforded the astronauts by these cameras made them uniquely qualified to capture small-scale (100 to 1000 m) events that had not been seen in such detail before this time.

Most of the photographs were taken through the overhead windows (Fig. 2). There are some obvious limitations to this method of obtaining photographs. First, taking any photograph through a glass surface (like the orbiter's window) introduces a chance of reflections degrading the quality of the photograph. The construction of the shuttle's windows make this almost an inevitability: the three panes of glass in each of the exterior windows have a total thickness of approximately ten inches. Indeed, in several of the frames, a clear reflection of the interior of the cockpit is discernable. Second, although there are several windows available for observations, not all viewing angles are

easily accessible at all times. Third, the space inside the cockpit is severely limited. Having several pieces of photography equipment to store and manipulate in such a confining space can only add to the workload of the astronaut. Since this program can only be conducted on a "target of opportunity", "time of opportunity" basis, anything that makes it easier and less time-consuming for the shuttle's occupants to bring us these fascinating products should become an item of high priority.

The case studies to follow include a squall line, a hurricane and two active volcanoes. Each takes advantage of the shuttle's unique observational ability to record information that could not have been obtained from any other source, and does it in a way to prove the value of the program to the entire meteorological community.

III. GULF OF MEXICO SQUALL LINE

A. INTRODUCTION

On 9 April 1984 a line of intense thunderstorms formed along a cold front traversing the state of Florida and the northern Gulf of Mexico. This line was part of a massive cyclone that stretched from the Great Lakes to the center of the Gulf of Mexico. The passage of the squall line through Florida was accompanied by several tornado sightings and one instance of severe hail (see Fig. 3) on 9 April alone. On that day, the Space Shuttle Challenger (STS 41-C) made three passes over the Gulf (see Fig. 4), capturing on film a detailed study of the structure of this squall line.

There are several limitations on our ability to properly analyze these photographs. On this mission, unlike following shuttle flights, a system had not been installed as yet to record the precise time a particular photograph had been taken. Even with a knowledge of the shuttle's route across the face of the Earth, unless identifying land marks are found in in the photograph, a precise location cannot be established for any feature of interest (El-Baz, et al, 1979; Maul and McCaslin, 1977). The time assigned tc each photograph was estimated by comparison to the shuttle's ground track and geographical area. Determining viewing angle is also somewhat of a challenge in many instances. Unless distinct shadowing is present and solar zenith angle is known (another function of time of day but here a gross approximation will suffice), even properly identifying the four cardinal directions becomes difficult (Terry, 1979). And without necessarily accurate timing data, it also becomes nearly impossible to construct useful stereopairs,

necessary for quantitative results (Black, 1977). Since this mission (STS 41-C), equipment has been procured tc ensure that every negative is imprinted with its exact time of exposure. Lacking still is any method of determining viewing angle relative to a vertical axis from the Earth. This precludes accurate determination of ground coverage in the photograph and properly establishing a sense of perspective when viewing individual features. Also, many of the figures included in this thesis are black-and-white copies of the shuttle photography, reduced in size to fit NPS thesis format. Some of the fine detail and small-scale phenomena are unfortunately not clearly shown in the black-and-white format.

B. SYNOPTIC OVERVIEW

The synoptic data corresponding to the time of the first photograph illustrate a classic setting for severe thunderstorm development along the Florida Gulf Coast. Fig. 5, a 1200 GMT surface chart for 9 April 1984, shows that the surface winds ahead of the front are from the south, forcing a warm, moist maritime tropical air mass to converge with the cooler, drier northwesterly flow behind the front.

Soundings from opposite sides of the front further illustrate the synoptic situation. In Fig. 6, the sounding from Boothville, Louisiana at 1200 GMT shows a typical example of the dry, stable continental air mass to the west of the cold front. It also provides a source for the mid-level (around 11,000 ft) intrusion of dry air seen on the Tampa Bay, Florida sounding in Fig. 7. This feature adds to the severe storm potential indicated in the Tampa sounding. As seen in Fig. 7, Tampa had a nearly saturated layer up to 11,000 ft, and above that a dry layer characterized by dewpoint depressions in excess of 25 deg C. Calculating

stability indices for this sounding gives a value for the Showalter's Index of -4.5, a Best Lifted Index of -6.5, and a SWEAT Index of 448. The tropopause level is 37,000 feet (215 mb).

An inversion, marked by wind shear (216 deg at 25 kt near 10,000 feet tc 252 deg at 51 kt just above 13,000 ft), and a pronounced temperature and humidity change, very likely contributed to the potential instability of the area. It serves to prevent deep convective overturning so that the air below became progressively warmer and more moist, while above the inversion conditions became drier and cooler. Under these conditions, potential instability would grow until some mechanism removed the inhibiting inversion.

Several possible "mechanisms" were present. The approaching cold front, a fast-moving (20-30 kt), organized field of vertical motion, would certainly have been sufficient. Secondly, the approaching line of thunderstorms ahead of the cold front could have produced enough turbulence to overcome this relatively weak feature. The next consideration would be surface heating provided by local sunrise, but perhaps this mechanism should be discounted. Convective activity in the Gulf, as evidenced by GOES images for the 9th, had been occurring throughout the night of 8 April 84, and began to develop into an organized band of severe storms between 0600 and 0800 GMT (not shown).

Of primary importance for the triggering of convective and potential instability in this synoptic situation is the pattern of intersecting upper and lower-level jet streams (Shapiro, 1983). From the surface chart (Fig. 5), 500 mb (Fig. 8), 300 mb (Fig. 9), 200 mb (Fig. 10), and 100 mb (Fig. 11) charts, we see the existence of an upper-level jet with a southern edge at 23N, and maximum winds centered at 26N. It crosses a weak surface jet parallel to the front as in Fig. 12a (Shapiro, 1983). Vertically, the maximum

winds in the upper jet appear at 200 mb, falling off sharply above that level. A gradual decrease in jet intensity is seen at 250 mb and 300 mb, corresponding very well with the illustration in Fig. 12b (Shapiro, 1983).]

By this jet configuration, a deep narrow plume of ascending motion is produced by the vertical alignment of the upper and lower circulations. The thermal lapse rate is substantially destabilized by the differential motion between the upper and lower fronts, producing a layer of convective instability. Satellite analysis (see Orbit 47) shows the squall line to follow this synoptic model closely.

C. ORBIT 46

The first photograph in this series, Fig. 13, was taken at approximately 1208 GMT (0708 local) with a 100-mm lens. The land mass of Florida is barely discernable behind the squall line in the top left corner of the picture. A 1031 GMT GOES image (Fig. 14) is provided for the reader to sense the orientation and extent of the line of thunderstorms. The shuttle is about to cross the line of storms, approaching from the west on orbit 46 (see Fig. 4).

In the photograph, individual cells of fair-weather cumulus are visible in the cold air behind the front, in sharp contrast to the relatively disorganized stratus on both sides of the squall line, at the base of the thunderstorms. The low-level thunderstorm outflow is made apparent by the organization found in this cold-air cumulus. Lines of small cumulus extend perpendicularly from approximately 40 km from the base of the squall to approximately 64 km. They end in a clear zone that has as its border similar lines of cumulus parallel to the squall. Here, apparently, the cold air moving in behind the front is encountering the thunderstorm outflow, suggesting a secondary line of convergence

parallel to the front. It is unclear whether the squall line has formed along the frontal zone or in the warm air ahead of the cold front, creating its own 'pseudo-cold front' by virtue of intense low-level outflow. Analysts have positioned the front more than 50 n mi behind the line of storms (see Fig. 5), but close examination of surface data, ship reports and buoy data failed to provide enough clues for precise positioning.

An unusual feature of this photograph is the apparent direction of movement of the cirrus deck spreading from the thunderstorm anvils. It appears to be spreading in two directions: one, along with the mean upper-level flow; and another, at nearly right angles to it. This is observed on the left side of the photograph, near the largest convective turrets. The mean flow in this case is directly from west to east.

This and other features tend to support a particular concept about severe storms that postulates a slope in their vertical development. Moist, unstable air is depicted as feeding the storms along their forward edges, rising and sloping toward the backs of the storms, away from the direction of movement (see Fig. 15). The sloping updraft in this model would tend to cause the highest towers to emerge near the rear edge of the storms. This structure is seen in the photograph in Fig. 13 (Zipser, 1977; Kropfli and Miller, 1975).

Rising through the cloud in this manner, the updraft is sheltered from direct mixing with dry environmental air, which would diminish its buoyancy. The intruding dry, mid-level jet is the drawn into the precipitation shaft produced by the sloping updraft, cooling the downdraft by evaporation and contributing to its downward velocity. This structure would also tend to form a small extension to the anvil not corresponding to the direction of the mean flow at that

altitude, but resulting from the horizontal directional component of the sloping updraft as it meets the tropopause.

Ground resolution of approximately 110 m in a near vertical view (see Table I), allows us to pick out individual convective turrets in the squall line. An oblique sun angle provides distinct shadows that outline the circular, stepwise intrusion these thunderstorms make into the tropopause. Knowing the tropopause height (1200 GMT sounding and radar returns from TBW indicate approximately 37,000 ft), and the scale of the ground coverage with a 100-mm lens (293.4 km x 293.4 km for a near vertical view) makes it possible to roughly estimate the height of various cloud layers using cloud shadows to determine vertical depth. In this photograph, the western edge of the stratus has a measured height of approximately 8,000 ft. The stratus turns into stratocumulus near the base of the thunderstorms and deepens to an estimated 14,000 ft. The thunderstorm anvils stretch another 24,000 ft above this layer, to a total cloud height of 38,000 ft. This corresponds to the levels indicated in a later GOES enhanced IR image, Fig. 16 (to be discussed in the next section, Orbit 47). But the photograph has the potential for far greater accuracy on small scales. IR images give approximate layer height, based on temperature. In the shuttle photograph, small perturbations of a cloud deck can be noted, and assigned a value distinct from the main cloud layer. The overshooting tops seen at the northern end of the line correspond to a 1223 GMT TBW radar report of max tops of 44,000 ft. From shadowing they appear to be approximately 4,000 ft above the top of the cirrus, for a total height of 42,000 ft: a close correlation to data from other sources (GOES IR, radar).

At low levels a several-miles-wide band of stratocumulus is visible at the base of the thunderstorms on their western side. It appears that a meso-high is being formed at the

base of the storms by the hydrostatic effect of the cold air downdraft, capping this intensely convective area with a stable layer extending for perhaps 50 kilometers from the squall line. This stable layer would explain some unusual phenomena seen in later photographs. Interestingly, if Fig. 5 showed a true location for the surface front, it would correspond very closely with the sharp line of the back edge (westerly side) of that stratus.

D. ORBIT 47

About one and one half hour later (94 min orbital period), the shuttle passed over the Gulf in its 47th orbit. The synoptic situation had changed little: the Tampa Bay radar image at 1340 GMT (Fig. 17) and the log entry for 1330 GMT show that the squall line's movement was still east to northeast at 20 to 30 kt, the maximum top to the cumulonimbus within radar range was still 44,000 ft and the orientation of the line was unchanged. The only difference appears to be that the entire line had moved closer to Tampa.

However, Fig. 18, a 1331 GMT visible light GOES image of 2 km resolution (at satellite subpoint), shows that the line had gained considerable organization and depth. It shows a distinctive wedge shape over the Gulf, and the back edge of the line is straighter and more filled-in. At its southernmost tip a thin line of convection stretched several tens of miles to the southwest, pointing out the weakening instabilty of the area to the south. This could be seen as a indication of a weakening front, but the location of the transition from deep convection to shallow cumulus corresponds very closely with the upper-level jet core noted previously (located at approximately 26N). In this image most of this line of shallow cumulus appeared as a solid

streak of white, with a few of the layer cloud elements appearing separately as brighter white "blobs".

Shadows produced by the early morning sun (0831 local time) help to give some detail to the west side of the squall line, but this solar angle also serves to "wash out" some of the features in the center and on the east side. Apart from the generally textured appearance of the cloud tops, a single large thunderstorm top can be picked out along the back edge of the squall line approximately 80 n mi from the southern tip of the line. From the image itself, little other information can be gained, but comparison with Tampa's radar report of 1340 GMT (Fig. 17) shows this area corresponding to a 44,000 ft top, 114 n mi from Tampa at 260 deg. This top overshoots the surrounding area by approximately 7,000 ft.

An enhanced infrared GOES image (Fig. 16) yields roughly the same information as the TBW radar. We can correlate the thunderstorm top in Fig. 18 to a pure black shaded area in this enhanced IR image. This shading in the "MB" enhancement scale indicates a temperature range of -58 to -62 deg C. Referring to the 1200 GMT 9 April 1984 Tampa Bay sounding in Fig. 7, -62 deg C occurs at a height of approximately 42,000 ft, only slightly less than the radar report. The surrounding area, in a dark gray shade, indicates a temperature range of -52 to -58 deg C, or roughly 36,000 to 39,000 ft, which matches closely an estimate of tropopause height of 37,000 ft made from the Tampa Bay sounding. As a result, the combining of these two images yields a good idea of large-scale structure and the rough locations and heights of its largest features.

A good example of the value of photography from space is the interpretation of the indentation in the cloud mass we see on the eastern side of the squall in this figure. It appears just to the south of the black area signifying the

highest cloud tops. We would normally interpret this as an area of lower cloud heights, induced by subsidence surrounding the massive updrafts in the thunderstorms. But infrared imagery has a shortcoming in this regard: it is impossible to tell from this image alone whether the cloud layer is at a lower altitude, or whether it is a thin cirrus deck that the IR sensor simply looks through (to a warmer environment below). Even the visible image in Fig. 18 does not conclusively answer the question.

Figs. 19 and 20 are shuttle photographs taken at 1338 GMT with a 100-mm lens. Taken only seconds apart, they offer both an oblique and a nearly vertical view of the same developmental stage of the squall line. A massive convective turret is visible (two hours later this thunderstorm will reach almost 50,000 ft), as are finely-detailed wave patterns in the low-level clouds. An interesting feature of Fig. 19 is the pattern in the low-level clouds found far ahead of the squall. Cuba is just visible in the top right-hand corner, and stretching from this island almost to the squall line itself are several sharply-defined cloud streets. These imply strong (20 to 30 kt) low-level flow into the line from the south, starting more than 100 n mi from the thunderstorms: an important contributing factor to the maintenance of strong convective activity.

This conclusion is supported by the surface reports and buoy data shown in Fig. 5, a 1200 GMT surface chart of the southeastern U.S. and Gulf of Mexico. In particular, buoy 42003, located at 26.0N, 85.9W, showed winds of 26 kt at 190 deg close to the forward edge of the squall line. Cloud streets are discernable in the GOES image (Fig. 18), but the degree of quantitative information we can derive from it is limited. A number of these cloud formations simply disappear in the GOES image, and those that can be seen have less visible length than their counterparts in the photograph.

The smallest cumulus at both ends fade away because their relatively small size (less than two km across) can't be resolved. Analyzing these cloud streets should yield information on the direction and intensity of the low-level flow ahead of the squall line. The precise information this photograph gives us may become an important tool in the hands of meteorologists attempting to forecast the intensity of Florida squall lines.

Fig. 21 was taken on the same orbit as Figs. 19 and 20, but with a 250-mm lens that provides a ground resolution of approximately 43 m. Shuttle orientation is to the west of the squall line, and it continued on to pass directly overhead. In this we can distinctly see thin cirrus on the east side of the overshooting top, and even have some impressions of the lower cloud deck the IR sensor is seeing through the cirrus. This is not the only demonstrable advantage of the shuttle photography. Fine wave patterns, invisible in the GOES products, are observable in the stratus and stratocumulus that extends outward from the base of the thunderstorms. The waves propagate along the stable layer apparently provided by the meso-high, in an apparently incoherent pattern influenced by interference and convective turbulence.

Gravity waves have been observed in cyclonic systems for some time, but their origin, maintenance and dissipation, as well as their interaction with larger scales of motion, are not well understood. That their occurrences are linked to intense precipitation events, however, is generally accepted, as is the necessity for a lower tropospheric stable layer to serve as a propagation channel. Both of these factors are present in this case.

At upper levels we can pick out the wind direction by the cirrus outflow pattern: west-southwest. The same immense convective turret (as seen in Figs. 19 and 20) can be seen

breaking through the tropopause in the center of the photograph. It appears as a series of rising plateaus on its southern side, sloping down dome-shaped on the north. The extreme detail of this photograph gives it a three-dimensional appearance, enhancing our sense of proportion when comparing one cloud feature to another. None of the separation of cloud layers, or of the small-scale (less than 1 km wavelength) wave patterns in the stratocumulus are visible in the GOES products. Of interest is the deep cleft in the squall line just to the south of the huge overshooting top. Possibly caused by induced subsidence around the deep convection, it is an identifying feature in both the GOES images and these photographs. An important difference is that in the photograph cloud detail is visible even within the shadows of the cleft. Just visible in the upper left-hand corner is another cleft, and a series of ridges leading upward to another overshooting top. This is the top identified in radar reports and in the IR GOES image (Fig. 16) as reaching 44,000 ft. The top in the center of the photograph is a "mere" 39,000 ft.

There are wave patterns between these two convective turrets, propagating along the stable trpopause with a wavelength of approximately 1 to 2 km. Without a higher resolution product, even these relatively coarse features would not be readily apparent on the 2 km resolution GOES products.

E. ORBIT 48

On its 48th orbit, at approximately 1516 GMT, 9 April 1984, the shuttle again passed close enough to the squall line to capture an oblique view of the storm. Radar returns indicated that the line of storms was nearly over Tampa Bay, and that the maximum recorded cloud top was up to 49,000 ft.

The location of the largest cell had moved closer to Tampa, but had retained its position in the line (see Fig. 22).

DMSP images, both visible and infra-red, were available to cover this time period. Fig. 23 is a 1521 GMT visible image of 2.7 km resolution. Higher resolution DMSP images were not available for this area at this time. Due to a higher zenith angle of the sun than in earlier images, most of the cloud top structure has been lost. There is a faint shadow (visible on the original data, but not on this smaller-scale reproduction), however, delineating the position of an overshooting convective turret in roughly the same position as the massive thunderstorm dome shown so clearly in Figs. 19, 20 and 21. This is in itself remarkable because it means this feature has persisted for more than three hours, far beyond the average thunderstorm life of 90 min.

Faint cloud streets are visible across the island of Cuba, indicating that the strong low-level flow still remains at this time. As in Fig. 18, quantitative information is lost by the lack of resolution: many of the streets are not visible, and those that are visible do not show their full extent. A thin bright line extends southwest from the tip of the squall. It indicates shallow convection continuing far to the south of the thunderstorms, along the line established by the storms. Identifying individual features in this line or in the stratus deck surrounding it is impossible. The solitary cloud elements that make up the line are too small to be resolved individually by this imaging system.

Fig. 24, the 1521 GMT infrared image, confirms that the streak is composed of individual cumulus cells, diminishing in size to the southwest. Little more can be gained from the information it presents. Its coarse resolution causes the cloud tops of the squall line to appear as a solid white mass.

All of these features are set in perfect perspective in Fig. 25, taken on orbit 48 with a 100-mm lens. This shuttle photograph was taken at approximately 1516 GMT on 9 April, nearly simultaneously with the DMSP images in Figs. 23 and 24 . Yet compared to DMSP, which shows only a vague stratus layer in both sides of a diminishing line of cumulus, Fig. 25 places precisely every cumulus buildup and its relationship to other cloud formations around it. Only the brightest tops show in the DMSP products, while every small-scale buildup in the line as well as that occurring in the stratocumulus on the sides of the squall line, are clear in the shuttle photograph.

Of interest in this figure is the extent of the propagation of gravity waves visible in the stratus south of the squall line. Distinct wave patterns perpendicular to the line of thunderstorms, are plainly visible (in the original data) at a distance of more than 150 km from the nearest cumulonimbus. As a mechanism for triggering the development of other thunderstorms, thunderstorm outflow boundaries have been the subject of much interest in the scientific community in the past few years. Could this outflow have the power to both create a stable layer for propagation (the meso-high discussed earlier) and then impel gravity waves to travel along it for this distance?

In this last figure, all the signs of a classic cold-front squall line are illustrated. Cloud streets reaching all the way from Cuba attest to the strong low-level inflow from the south, constantly resupplying moisture to the convective system. Cumulus towers along the back edge of the line show that the low-level inflow slopes toward the back of the line as it moves upward, drawn into an explosively unstable environment. Cirrus blowoff streaming west-southwest points out the strong shear between upper and lower-level wind directions, while a small rim of cirrus

stretching westward completes the scenario of an updraft sloping from east tc west, reaching the stable tropopause and mushrooming out against the predominant wind flow at that altitude.

F. CONCLUSION

The important factors that undermined the usefulness of these photographs were lack of recorded time of exposure, lack of identifiable land features and an inability to determine camera angle relative to an Earth vertical axis. Since this mission (STS 41-C), provision has been made for times to be imprinted on each roll of film as the exposure is made, but there has been no attempt to record camera angle.

This case study concerned the development of a squall line, and succeeded in illustrating its mesoscale structure from the intense low-level inflow to the cirrus blowoff. It tended to confirm a concept concerning organized severe thunderstorms that specifies a tilting updraft, with the highest convective turrets occurring at the back of the squall line. It also provided a detailed look at very small-scale gravity waves propagating along the stable stratus layer at the base of the thunderstorms, and provided measured values for wavelength and horizontal extent.

Compared to visible and infrared satellite images, the photographs provided far more detailed height differences between cloud layers, and yielded a useful estimate of overall height from cloud shadow measurements. It also provided clear images of cloud height and structure in cases where infrared images were vague (e.g., in the case of thin cirrus). Because very high resolution DMSP images were not available, comparisons with relatively low resolution (2 and 2.7 km) images resulted in a predictable advantage for the

shuttle photographs. But even very high resolution meteorological satellite images do not have these significant advantages: oblique sensor angles, color imagery, and most importantly, human judgement.

Regardless of individual merits, none of the meteorological satellite images are able to give the details of mesoscale thundersorm dynamics as the shuttle photographs. As a teaching tool for mesoscale dynamics, the photographs would be invaluable.

IV. HURRICANE KAMISY

A. INTRODUCTION

In April 1984, Hurricane Kamisy brought 110 kt winds to the island of Madagascar in the Indian Ocean. Kamisy's winds reached a maximum of 135 kt in its mature stage, at which point its spiraling outflow bands spanned nearly 1000 n mi. For five days, covering a period from initial rapid development to loss of hurricane status and final dissipation, the Space Shuttle Challenger (STS 41-C) orbited overhead, providing an outstanding series of photographs of the life and death of a hurricane.

Fig. 26 charts the shuttle's orbital path (moving from left to right on the chart) and Kamisy's reported positions at 12-hour intervals, taken from warning positions issued by the Joint Typhoon Warning Center (JTWC) at Guam. A list of corresponding wind intensities is available in Table II.

The earliest available indication of Kamisy's inception was from Tiros-N polar hemispheric mosaics (National Oceanic and Atmospheric Administration, 1984). Cyclonic circulation, organizing widespread convective activity, was evident on the 0220 GMT, 4 April 1984 satellite image. By 0313 GMT on 6 April, a Tropical Cyclone Warning had been issued by JTWC. The 0600 GMT warning position put Kamisy at 12.8S, 65.0E (about 900 n mi east of the northern tip of Madagascar), with winds estimated at 65 kt, gusting to 80 kt. Movement over the previous six hours was reported as 270 deg at 9 kt, and the radius of 50 kt winds was estimated at 50 n mi.

B. APRIL 7TH

The first usable views of the developing hurricane (earlier photographs exist but they are either too oblique or at too great a distance to be useful) given by the shuttle's cameras were taken at approximately 1157 GMT 7 April 1984, on the shuttle's 15th orbit. A Hasselblad camera with a 100-mm lens was used for Fig. 27, from an orbital position slightly northeast of the storm. The shuttle's altitude on orbits 1 to 16 was approximately 125 n mi (this increased to 269 n mi after the 16th orbit in order to complete the Solar Max repair). By this time Kamisy had moved almost directly west from its last warning postion to 12.6S, 58E. Maximum winds had increased to 80 kt gusting to 100 kt, and the radius of 50 kt winds had increased to 70 n mi.

The eye in the phctograph is well developed and plainly visible, almost perfectly circular and approximately 9 km across (distance across the image is roughly 136 km--see Table I). There is a ring of convective turrets circling it on three quadrants, with an approximate diameter of 20 km. Beginning low in the southwest quadrant, the turrets are large (diameter of 1 to 2 km) and widely spaced, becoming progressively smaller and more numerous in a counterclockwise direction. A thin, smooth cirrus layer is apparent extending a short distance inward from just below the tops of these turrets, masking the true position of the eyewall.

A series of waves appears to emanate concentrically from the eyewall into the southeast quadrant, ending at a point where they intersect with Kamisy's main outflow channel. Scaling the distance from crest to crest against the known distance across the image gives a wavelength of approximately 3.4 km. This compares very closely with measurements done by Black (1977) on several tropical storms. He found wavelengths of 1.5 to 12.4 km, with a peak at 2.2 km. There

also appears to be a wave pattern extending radially for more than 30 km from the circle of convection surrounding the eye. It occurs in the northwest quadrant and has an approximate wavelength of 4.5 km.

Structure and location of a hurricane's outflow channels are controlling factors in their development or dissipation. When the air rising in the eyewall reaches the strongly stable region at the tropopause, it is forced outward from the center, usually in one or two cyclonically curving jets. Spinning in a cyclonic motion, conservation of angular momentum forces a rapid decrease in their cyclonic rotation as the air moves away from the center of the storm. At some point (usually around a radius of 300 km), they will acquire an anticyclonic component (Anthes, 1983). These curving jets (the outflow channels), control the rate of mass evacuation from the top of the hurricane. By this mechanism they can either enhance the updraft and contribute to hurricane intensification, or cap the updraft and cause the storm's eventual dissipation. Only traces of Kamisy's extensive outflow channels can be seen in Fig. 27. To the north and extending outward to the northwest is the main channel, while the second starts directly south of the eye, and rapidly sweeps off to the southeast. This structure will become more apparent in later photographs and satellite images.

The only other convective activity apparent in this photograph occurs approximately 55 km northeastward from the eye, in the main outflow channel. Fig. 28 is another view of the storm taken just seconds prior to Fig. 27, but with a 250-mm lens. Distance across the image is just 54.5 km (see Table I), and in this case the camera appears to be positioned almost directly above the eye. This is supported by the crew's opinion that the shot was near vertical. There are difficulties when attempting to pinpoint the position of

the camera vertically above a feature on the ground, as previously mentioned. Without precise timing of the photographs and an indication of the camera angle relative to vertical, this has to be relegated to the category of an educated guess. If it is accepted for the moment that the camera appears to be directly over the eye, it would also appear that the eye is somewhat tilted to the west or southwest. An interesting correlation is that the area of least convection surrounding the eye occurs to the west, and, as we shall see in the following photographs, retains that orientation for the rest of its recorded existence. It should be remembered that the direction of motion of the storm at this time is also toward the west.

In Fig. 28, we can see the interior structure of the eyewall itself. Huge scooping slices out of the cloud mass of the eyewall attest to turbulent entrainment caused by the downward rush of subsiding air through the center of the storm. And down to the smallest cumulus buildups, every part of the low-level inflow is cyclonically organized.

Black (1977) documented several instances of recorded eyewall tilt, most notably in Skylab photography of Hurricane Irah in the eastern Pacific Ocean on 24 September 1973. He concluded that tilts of 45 degrees are fairly common, especially at altitudes above four kilometers. Irah differed from Hurricane Kamisy in several important aspects. First, the observed tilt reached 45 deg on Irah's west side, and Kamisy's tilt is barely recognizable. Second, the wall cloud diameter for Irah was approximately 35 km at its top, tapering down to approximately 15 km at its base. The top of Kamisy's wall cloud had a diameter of less than 10 km. Still, there was one very important similarity: both eyes tilted away from the region of most intense convection, and it seems, towards the direction of motion.

The issue concerning tilt in the vertical structure of a tropical storm is an intriguing one. Anthes (1983) states that the main driving force in tropical storm development is the release of latent heat in intense convection. It could be argued that for a tropical storm to reach hurricane intensity, a tilt is necessary for the same reasons given for severe thunderstorms: updrafts in competition with downdrafts can only hamper intense convection, and result in storm dissipation. In the circular structure of a hurricane, however, a tilt would enhance convection on one side of the circle (opposite the direction of tilt), and necessarily discriminate against convection on the other (towards the direction of tilt). There is some evidence of this structure in Fig. 27.

Ninety-four min after orbit 15, at approximately 1330 1330 GMT, the shuttle made another pass over the Indian Ocean on orbit 16. Fig. 29 was taken with a 100-mm lens, from a position approximately 600 n mi southeast of the center of the hurricane (see Fig. 26). It offers an oblique perspective that covers a much greater area than the preceeding photographs, facilitating comparison with other sources of storm imagery.

The main structure of the storm is shrouded by a streaky cirrus layer that graphically displays the upper-level outflow pattern, but several observations can still be made. The ring pattern of overshooting convective turrets is wider and better organized along the outflow lines, indicating continued development of the storm (Anthes, 1982). The area of least convection is still predominantly to the west, in line with the direction of movement. Visible beneath the outer edges of the cirrus are mid-level cumulus clouds, implying a significantly deep moisture layer and a very unstable surrounding environment. Clusters of thunderstorms are visible on the periphery of the storm to the southeast

and northwest, and a broken pattern of shallow concentric waves about the eye is still apparent. In another case study by Black (1977), similar waves ranged from 3.0 to 4.2 km in wavelength, and occurred solely on the eastern semicircle. Assuming that their movements were also to the west, the similarities would lead us to speculate upon a connection between intense convection, gravity waves and the direction of movement of tropical storms. The overall appearance of the storm canopy is that of a flattened dome, declining in height at the outside edges in a series of wide, shallow steps.

Fig. 30 is a 1205 GMT 7 April 1984 blowup from an AVHRR (Advanced Very High Resolution Radiometer) visible-light image provided by the NOAA-7 satellite. Data from the AVHRR instrument are available in both 1.1 km and 4 km resolution, in two operational modes. Unfortunately, the 1.1 km resolu- image is not available for every location around the globe. the globe. Because of this restriction, in this chapter all of the AVHRR images are of 4 km resolution.

The most striking difference between the shuttle photographs and this figure is the homogeneous look of the cloud tops. The central area of the storm appears smooth, with little apparent difference of cloud top height from the center to the periphery. Any indication of a ring of convection surrounding the eye is lost. Only the massive buildups to the northwest and southeast within the outflow channels are apparent by faint shadowing and cloud-top brightness variations. A visual estimate of how far these buildups exceed the height of the surrounding cloud layer is impossible. Any gravity waves emanating from the eye of the storm are also lost to the coarser resolution of the satellite, and the structure of clouds within the eye itself is poorly observed. It is fortunate that the hurricane was centered in the field of view in this image. Examination of the image

only several deg latitude away from the center show the main drawback to AVHRR imagery: a loss of resolution along both edges of the scan line. If the feature of interest is more than a few deg from center, the obliquity of the sensor angle reduces resolution because of a fixed scan line.

Fig. 31 is a DMSP infrared image of 2.7 km resolution. Taken two hours later at 1405 GMT, it shows the same main features of Kamisy, but in a sharply degraded form. DMSP 0.3 km resolution imagery, which should compare very favorably with the shuttle photographs, was not available for this case study. One significant advantage DMSP has over AVHRR is that it modifies itself along each scan line to give good resolution edge to edge. But in this example, only infrared images were available for comparison, and any advantages DMSP enjoyed compared to AVHRR were lost for this reason.

The large eye is still quite obvious, but indicated only by a smooth black circle of no apparent depth. The outflow channels to the north and south still show large cumulus buildups, but the tops are represented as featureless white blobs. The heights of various cloud layers remain questionable: namely, are the gray shades lower than the white, or are they merely a result of thinner cloud layers that emit IR poorly?

C. APRIL 8TH

Fig. 32 was taken at approximately 1128 GMT, 8 April 1984. The shuttle's 30th orbit passed north of the storm, and this frame was taken as the spacecraft passed approximately 200 n mi to the northeast (see Fig. 26). The eye was located at 12.8S, 52.0E at that time, about 100 n mi east of the northern tip of Madagascar. Maximum winds were listed by JTWC as an estimated 100 kt gusting to 135 kt, and the

radius of 50 kt winds was essentially unchanged from the previous report.

The eye is still plainly visible, but appearing smaller and less circular. A dense cirrus shield covers most of the dome, signaling that Kamisy has reached its mature stage. The overall shape is almost completely symmetrical, with extensive outflow channels multiplying in number to the north and south. On the western side, and extending to the south, a line of deep convective activity oriented beside the main outflow channel produces the only break in the cirrus shield, with subsidence-induced clearing visible on both sides of the line of thunderstorms. Every overshooting top is precisely locatable, and if a stereophotograph had been made, the heights of each one relative to the storm's cirrus level would also have been known.

Only seconds earlier, a second camera with a 250-mm lens recorded Fig. 33: a close-up look at the eye. The eyewall appears to have "caved-in" towards the center, and the overshooting turrets have disappeared. The oblong shape of the eye measures approximately 23.4 km in the north-south direction, and 11.7 km in the east-west direction. Only a faint trace of the radiating wave pattern seen in earlier photographs is left. The enlargement of the eye and its loss of circular shape is confirmation that the storm has reached its mature stage and has begun to dissipate.

The AVHRR visible image (Fig. 34) from 1153 GMT 8 April 1984 captures Kamisy on the edge of the image. The reader should note: the reference 4 km resolution refers to an area within a few deg latitude from the satellite subpoint. When an interesting feature lies 7 or 8 deg latitude from this this point, as it does here, image quality is degraded. From this figure we are able to locate the eye and identify some large cumulus buildups near the outflow channel to the south, but very little else can be gleaned apart from the

overall size and shape of the storm. We are aided by the grid points for latitude and longitude, and the outline of nearby land masses to gain a sense of perspective, but comparison to the shuttle photograph is difficult.

The DMSP IR image from 0714 GMT (Fig. 35) is superior in some respects. It does manage to indicate the depth and structure of the eyewall, hinting at a tilted structure of very definite shape. Since this image was produced nearly five hours earlier than the others we have discussed, the eyewall deterioration is not yet visible. Coarse resolution in the IR, however, makes determination of the difference between thunderstorm tops and the surrounding cirrus very difficult.

D. APRIL 9TH

It was a full twenty-four hours later that the next photograph of Kamisy was taken. Fig. 36, taken on orbit 46 on 9 April at 1239 GMT, shows Kamisy's dissipation. Four large outflow bands can be identified, and their diffuse structure testify to Kamisy's weakening state. The eye cannot be located. We must assume a position somewhere in the center of the central dense overcast (CDO). This overcast is the result of old convective clouds and patches of layered clouds taking up the spaces between convective updrafts. Cirrus remnants (from the strong upward flux of water that occurred when the intense convection in the central portion of the storm was at its maximum intensity) also tend to smooth out the observable cloud features (Anthes, 1982). Most traces of surrounding convective activity are losing definition and organization. Mid-level clouds under the thin cirrus at the outside edges of the storm are again visible, and show markedly less organization and convective form than two days earlier in Fig. 29. The

astronaut's choice of an oblique angle and 100-mm lens provided a comprehensive look at the structure of Kamisy's demise.

Tropical Cyclone Warning NR06 from JTWC, Guam, confirms this conclusion. Maximum sustained winds had dropped to 85 kt from a peak of 110 kt the day before, and the radius of 50 kt winds had decrease from 70 n mi to 30 n mi. The storm made a brief land fall at the northern tip of Madagascar on the 9th, and in the next twenty-four hours continued west over the Mozambique Channel.

Comparison of the 9 April shuttle photographs with AVHRR and DMSP images follows a pattern similar to previous days: AVHRR losing detail on the edges, and DMSP fairing poorly because of the lack of availability of a visible-light image. Fig. 37 is an AVHRR visible-light image produced at 1322 GMT 9 April 1984. In it, Kamisy's entire eastern half loses resolution as a consequence of being too far from the satellite's subpoint. Yet because of the loss of image quality caused by reproducing the shuttle photographs, AVHRR in this instance appears to be comparible in detail to the shuttle photograph in Fig. 36 .

However, dissipation of the storm is apparent here too: the center of the storm has essentially the same appearance as in the shuttle photograph, but only by virtue of the lack of definable features occurring in the smooth CDO. Convective turrets, piercing the smooth cirrus canopy, are also visible to the north of the center, but individual tops are blurred, tending to merge several into a few bright dots. Low-cloud orientation below the cirrus in the periphery of the storm is impossible to define. Even the existence of clouds not part of the upper-level circulation is not apparent in this image.

A comparable DMSP IR image is available from less than two hours later than Fig. 37. Fig. 38 was taken at 1504 GMT,

and again offers far less detail than that from the NOAA-7 satellite. Location of the center of the CDO for accurate positioning of the storm becomes very difficult compared to the other images because of the complete lack of apparent depth depicted in the cirrus overcast. What may be a weak eye is seen on the western side of the cloud mass. But with only this data, postulating the existence of massive cumulus buildups north of the center of the storm only could be regarded as speculation.

For the next two days (10 and 11 April), there are no shuttle photographs of Hurricane Kamisy. From satellite images and storm bulletins we find that the storm started to redevelop once it left Madagascar for the waters of the Mozambique Channel, and by the 11th had started to turn southeast, back towards the northeastern coast of Madagascar.

E. APRIL 12TH

The next series of photographs came from orbits 92 and 93, on 12 April. All three photographs appear to have been taken of Kamisy from a shuttle position either directly overhead the storm or distinctly northward. Because the photographs bear little resemblance to the available DMSP and AVHRR images, a catalog of observations was consulted (Nowakowski and Palmer, 1984). Kamisy was identified as the subject of the photographs.

Investigation of the position of shuttle orbits and a Tiros-N strip produced at 1245 GMT 12 April 1984 indicate that the vortex is not Kamisy, but a very large cyclone positioned approximately at 30S, 40E. It was not listed as a developing tropical storm in warnings published for the period by JTWC. Apparently it never became severe enough to attract attention. The three photographs (Figs. 39, 40 and

41) are included because they may be of some interest to other researchers and because they are still an excellent illustration of the value of high-resolution photography from space.

Fig. 39 was taken with a 250-mm lens on orbit 92 at approximately 1330 GMT 12 April 1984, and offers an oblique view of the storm. The shuttle's position appears to be to the northeast. The other two photographs were taken on the next orbit (orbit 93) at approximately 1510 GMT, when the shuttle passed almost directly over the center of the storm. Fig. 40 was also a product of a 250-mm lens, but here it provides a close-up view of the center. There is no distinguishable eye in either of the photographs, but a very distinct center of low-level cyclonic motion. Directly east of the center at a distance of approximately 60 n mi, a massive convective turret is visible, with waves radiating concentrically from its center in a manner similar to those emanating from Kamisy's eyewall. To the south and southeast of the center of the storm, gravity waves of an extremely short wavelength (less than 1 km) radiate in a pattern seemingly unrelated to the center of the storm. In one case they appear to extend along the main flow lines (directly south of the center), and in another they form perpendicular to the flow (southeast of the center). The origin of these waves is not easily deduced.

As the shuttle moved away from the storm to the east, one last photograph was made, this time with a 50-mm lens that allows us to put the storm into perspective with the surrounding circulation. The wide-angle lens lacks the resolution of the 100-mm and 250-mm lenses, and as a result the fine detail in the center of the storm and the gravity wave patterns disappear, leaving only relatively large-scale features visible. But even here, the height difference between various layers of clouds is distinct, and identifying cloud types and their distribution is positive.

F. CONCLUSION

The advantages of higher-resolution photography from space are well-illustrated in this case history. The ease of locating particular small-scale features, and the accuracy of making height estimates relative to other cloud structures is of particular benefit. Small-scale features such as gravity waves, hurricane eyewall features, individual cumulus turrets, stratiform cloud configuration, and precise information of the location and condition of the eye itself, not only give information about tropical storm dynamics in the mesoscale, but in some cases define the large-scale circulation to a degree beyond our current ability.

Several similarities to Black's (1977) results were noted. The structure of the semi-circle of intense convection surrounding the eye, and its relationship to eyewall tilt were of primary interest. The recorded gravity waves, propagating across the top of Kamisy's stable cirrus dome, conform almost exactly to those seen in several of his case studies in both wavelength and orientation. What was not observed was any indication of a large circular convective cloud feature, but this may have been due to the large temporal spacing of the photographs.

For the teacher, it is a superb set of nearly three-dimensional illustrations of developing and dissipating tropical storms. For the researcher, it adds to the available data concerning eyewall tilt, and provides measurable length and height scales of mesoscale tropical cyclone structure. For the forecaster, it would be invaluable for post-storm analysis and forecaster training. Beyond illustrating eye formation and collapse over the lifetime of a tropical storm, and beyond providing exact eye location even when the storm is covered in dense cirrus overcast, these pictures provide a total picture of the storm in which the

entire structure is visible, allowing the forecasters to better interpret the subtleties of DMSP and AVHRR images. Also, were these photographs to be made available in stereo-pairs, individual cloud formations could be isolated to common levels. Combined with continuous satellite coverage of the movement of these cloud features, the large-scale wind pattern could be precisely defined. This has been acknowledged to be a vital piece of information for hurricane forecasters (Anthes, 1982).

V. THE MAUNA LOA VOLCANO

A. INTRODUCTION

On 25 March 1984, Mauna Loa, the world's largest active volcano, erupted with its biggest lava outpouring in nearly 35 years. According to the New York Times published on that date, eruptions consisted of a curtain of flame reaching approximately 150 ft high (observations were made by members of the United States Geological Survey's Volcano Observatory), and continued for twenty-two days. On March 30, the Times reported that a second volcano less than 20 mi away had joined Mauna Loa. With fountains of lava generally less than 100 ft high, Kilauea's eruption spouted from a 250-ft-high cinder cone that had been building for several days. Radical weather changes were soon noted. The immense heat, along with copious amounts of smoke and volcanic dust injected into the atmosphere, resulted in unseasonable thunder, lightning and even snow.

The 13,677-ft-high Mauna Loa is located on the island of Hawaii (see Fig. 42), the largest island in the state. Kilauea is at the 4000-ft-level on the southeast slope of Mauna Loa. Although both eruptions were minor in size compared to previous events, the large amount of dust and smoke introduced into the atmosphere during their twenty-two days of activity will serve well to illustrate a unique value of shuttle photography.

B. MEASUREMENTS

By April 12, Mauna Loa had been in continuous eruption for nineteen days; Kilauea for fourteen. By then, the Space Shuttle Challenger had photographed Hawaii three times: on

orbits 21, 37 and 96. The photographs in Figs. 43, 44 and 45 reveal evidence not only of the expected volcanic smoke plumes, but also of a dense pall of smoke (and to a lesser amount volcanic dust) steadily accumulating in the lee of the island.

Qualitative measurements of this dense aerosol cloud conceivably could be of interest to meteorologists in several fields. Air pollution meteorologists could compare the spatial and temporal scope of this natural manifestation to manmade pollution in many parts of the world. Satellite meteorologists could compare variances of satellite-detected upwelling radiance from clear areas and those contaminated by the volcanic aerosols. Boundary-layer meteorologists could determine how atmospheric turbidity measurements are affected by unusually high levels of aerosols.

But common to all of these scientists' goals is the need for accurate measurment of the amount (density) of the aerosols present in the area being studied. It is here that the increased resolution of photography from space shows its value.

Determination of aerosol amounts from space by two common means--contrast reduction calculations and brightness measurements--are facilitated by space shuttle photography. As explained by Kaufman (1979), reduction of contrast due to atmospheric extinction is a function of aerosol amounts, and can be represented in its simplest form by the following definitions:

$C = (I(1)-I(2))/I(2)$ = contrast between surface (1) and surface (2).

$C(a)$ = apparent contrast (as seen from space).

$C(i)$ = inherent contrast (as seen near the object).

$\rho(i) = C(a)/C(i)$ = change of contrast due to atmospheric influences.

C(a) measurements are highly sensitive to the placement of the boundary between I(1) and I(2). Since the shuttle photographs serve to more clearly establish the location of boundaries (such as the coastline boundary between land areas on open ocean), often even through dense haze or smoke, it can contribute significantly to the accuracy of the contrast reduction calculations.

Brightness measurements have been used to calculate atmospheric turbidity (aerosol optical depth) in several studies (Norton, et al, 1982; Hering, 1981; Koepke and Quenzel, 1979). A limiting factor to accuracy common to all of these works is the inability to properly identify small cumulus in the subject area (brightness values for an area contaminated with the inclusion of highly reflective clouds would necessarily be biased towards higher values). In a study of the optical thickness of Saharan dust by Norton, et al (1982), the problem is explained; "...a more serious problem is distinguishing between clouds and dust.... Here there may be small clouds (primarily trade cumulus) which do not fill the sensor's field of view or thin clouds of optical thickness comparable with that of dust."

In general, the measurement of turbidity is straightforward. However, the judgement of a meteorologist is needed when selecting a representative digital count. The presence of small clouds, and thin clouds like cirrus, must be detected. It is here that the higher resolution of the space shuttle's photography would prove a distinct advantage over commonly-used sensors of 1 or 2 km resolution. In many cases, small cumulus on the order of hundreds of meters would be individually definable, and thin cirrus quite visible. This is vital for the next step: digital counts are selected from apparently cloud-free areas of at least 15 lines and elements. A representative digital count is then selected from a frequency distribution of digital counts for

the selected area. Because of the possibility of cloud contamination and inherent noise characteristics of the data, schemes for picking the best digital count from the histogram must be evaluated for the most consistent results. A computer then converts the selected digital count to a value of turbidity. (Norton, et al, 1982)

C. CONCLUSION

The increased spatial resolution of shuttle photography not only helps the observer to eliminate areas contaminated by small clouds that may not be visible to other sensors, but provides a greater number of data points for determination of brightness variations across a given area.

High-resolution photography from the space shuttle can be of great value to any study of aerosol concentrations, whether influenced by man (brush fires, burning of fossil fuels, contrails, ship trails), or natural (dust generated by wind, naturally induced forest fires, marine aeosol, smoke generated by volcanic activity). As demonstrated by Randerson (1977), air pollution studies, estimates of thermal energy release in a volcano contrail generation, and horizontal and vertical eddy diffusivity are but a few of the specific uses of this resource.

VI. CONCLUSIONS / RECOMMENDATIONS

A. CONCIUSIONS

In the three case studies presented here, examination of mesoscale features made visible by high-resolution photography from space has provided information on new and unusual phenomena, and brought additional insight to the well-known. Meteorological satellite images, while certainly not replaced by this photography, can be supplemented by it to refine present analysis techniques and more fully understand the small-scale dynamics of the features under observation.

For the teacher, it has provided a combination of oblique views and extreme detail that can take the student far beyond line drawings and into an understanding of real-world weather systems. In Chapter 3, photographs of the squall line in the Gulf of Mexico beautifully illustrate the high-speed low-level inflow, the tilted vertical structure, the upper-level outflow pattern and the surface effects of thunderstorm outflow that take place in thousands of severe thunderstorm outbreaks every year.

For the forecaster, it has proved the worth of extremely high-resolution imaging not only for precisely locating storm features (vital to hurricane forecasts), but for recognizing the current state of those features (e.g. eyewall size and shape). It has also served to introduce the possibility of other controlling factors in hurricane movement (regions of intense convection and eyewall tilt), or at least the need to look into this area further. And in combination with continuous satellite coverage, the ability to map the large-scale wind field around storm systems becomes a practical analysis tool. Of course, no real-time data

would be available. These products would be valuable only for post-storm analysis and forecaster training. Yet this could prove the desirability of adding continuous high-resolution imagery to the forecaster's set of tools.

But it is for those in meteorological research that this program holds the most promise. Shuttle photography introduces precise height and length scales for such small-scale phenomena as gravity waves, overshooting convective turrets, shallow cumulus cloud streets and volcanic smoke plumes. More precise aerosol measurement is made possible by eliminating areas contaminated with small clouds other sensors can't accurately show, and by more precisely positioning contrasting area boundaries in adverse conditions. Refinements to cloud height estimates made from infrared images can be made by the use of stereophotography, as well as final determination of height and structure of anomalous gray shades. In short, it fulfills one of the prime requirements in a reasearcher's work: greater accuracy.

B. RECOMMENDATIONS

Improvement of the space shuttle photography program can be approached from two sides. The first is making it easier for the astronauts to get good pictures. The second is making it easier for scientists on the ground to precisely define orientation of the camera relative to the ground and to determine the ground area covered by each photograph.

The astronauts currently manipulate several pieces of photographic equipment in a space-limited cockpit, and try to take pictures through a small window that imposes a limited field of view. At low altitudes (e.g. 225 km) the observation time available of a feature on the ground is only roughly 5 to 20 sec (Terry, 1979). Further, the possibility of reflections of the lighted cabin appearing in the

photographs has been confirmed with several mission's worth of phctographic data. One recommendation is to move the cameras to a gimballed pod in the cargo bay that can be remotely controlled by the astronauts in the cockpit. Aiming and triggering the exposures could be accomplished by reference to a television screen inside the cabin, connected to a televisior camera attached to the pod. The television camera could be oriented and adjusted to give the same image in the cabin that the cameras would see for their exposures.

Remote control offers the possibility of ground control of the photographic process while the astronauts are otherwise occupied. This is important because if a potential photograph is missed because of the imposition of other duties, simply waiting for the next orbit can not recreate the photographic opportunity. The shuttle moves approximately 23 deg farther west (at the equator) on every orbit. Nearly twenty-four hours must elapse before the shuttle is nearly (not exactly) over the same position. In addition to the slight change of position, few atmospheric features would remain unchanged over the twenty-four hours it would take for the shuttle to return. The option of a clock-controlled time sequence should also be available, as well as a precisely-timed (+/- 0.1 sec) automatic exposure interval to facilitate stereophotography.

Of benefit to analysts on the ground would be the addition of a recording device that would not only record the time of each exposure (as is currently done), but also the angle of the camera relative to the shuttle's vertical axis. A computer program would then be devised to compare the shuttle's attitude to an earth vertical axis, and the angle of the camera to the Earth's surface could be resolved. This, in combination with a knowledge of orbital path and precise time of exposure, would make possible the creation of latitude-longitude grid overlays for any photograph

worthy of study, and would finally resolve any questions produced by observations of cloud structure.

Finally, quality of the photographs would be enhanced by removing the cause of photographic reflections and by making it easier for the astronauts to locate and recognize features of scientific interest. It might even be possible to add a video display of shuttle movement over prominent land features to aid the astronauts in gaining a physical orientation for the features they are observing through the windows and on the screen. As mentioned by Terry (1979) in comments upon the Apollo-Soyuz mission: under less-than-optimal conditions, sometimes it is a choice of an astronaut either seeing the feature or taking a picture, and losing the benefit of one or the other by that decision. Utilizing these recommendations, both should be possible at all times.

APPENDIX A

TABLES

TABLE I

Mission Data for STS 41-C

Launch:	6 April 1984, 8:58 a.m. EST from Kennedy Space Center, Florida		
Landing:	13 April 1984, 8:38 a.m. EST at Edwards Air Force Base, California		
Orbits:	107		
Vehicle:	Challenger (OV-099)		
Altitude:	269 n mi (Photographs taken on orbits 1 through 16 are from an altitude of approximately 125 n mi.)		
Inclination:	28.5 degrees		
Crew:	Commander, Capt. Robert L. Crippen, USN		
	Pilot, Mr. Francis R. Scobee		
	Mission Specialists		
	Mr. Terry J. Hart Dr. George D. Nelson Dr. James D. van Hoften		
Ground Coverage: (Orbits 1-16)	586.8 x 586.8 km (272.7 x 272.7 km)	(50-mm lens)	
	293.4 x 293.4 km (136.3 x 136.3 km)	(100-mm lens)	
	117.4 x 117.4 km (54.5 x 54.5 km)	(250-mm lens)	
Ground Resolution: (Orbits 1-16)	213.8 m (99.3 m)	(50-mm lens)	
	106.9 m (99.3 m)	(100-mm lens)	
	42.9 m (19.9 m)	(250-mm lens)	

TABLE II

Hurricane Kamisy, 7-13 April 1984

DATE/TIME (GMT)	POSITION	MAX WINDS (kt)
06/0600	12.8S, 65.0E	65 G80 (G = maximum gusts)
07/0600	12.2S, 59.6E	80 G100
07/1800	13.0S, 56.0E	95 G115
08/0600	13.0S, 52.9E	110 G135
08/1800	12.5S, 51.8E	100 G125
09/0600	12.5S, 48.9E	90 G110
09/1800	13.1S, 46.5E	85 G105
10/0600	13.0S, 46.3E	75 G90
10/1800	13.3S, 44.7E	80 G100
11/0600	14.8S, 45.3E	80 G100
11/1800	15.2S, 45.4E	80 G100
12/0600	16.2S, 47.2E	60 G80
12/1800	16.5S, 47.2E	50 G65
13/0600	18.0S, 51.2E	40 G50
13/1800	19.0S, 50.7E	35 G45

APPENDIX B

FIGURES

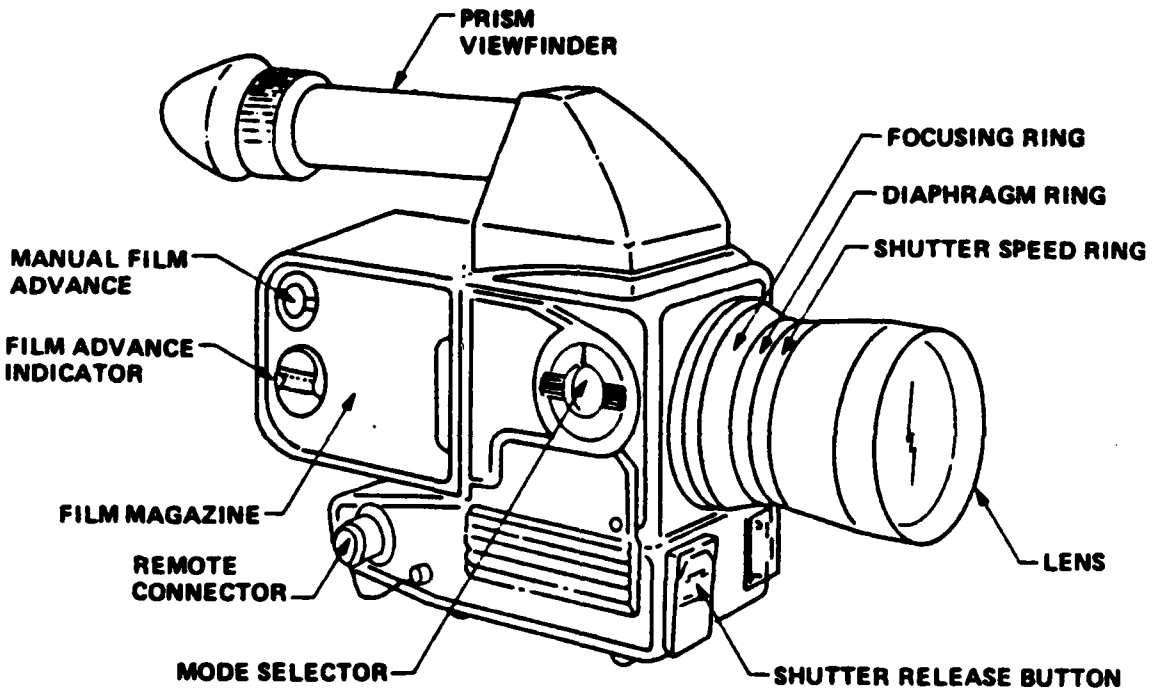

Fig. 1 NASA-modified Hasselblad 500 EL/M Camera (Nowakowski and Palmer, 1984).

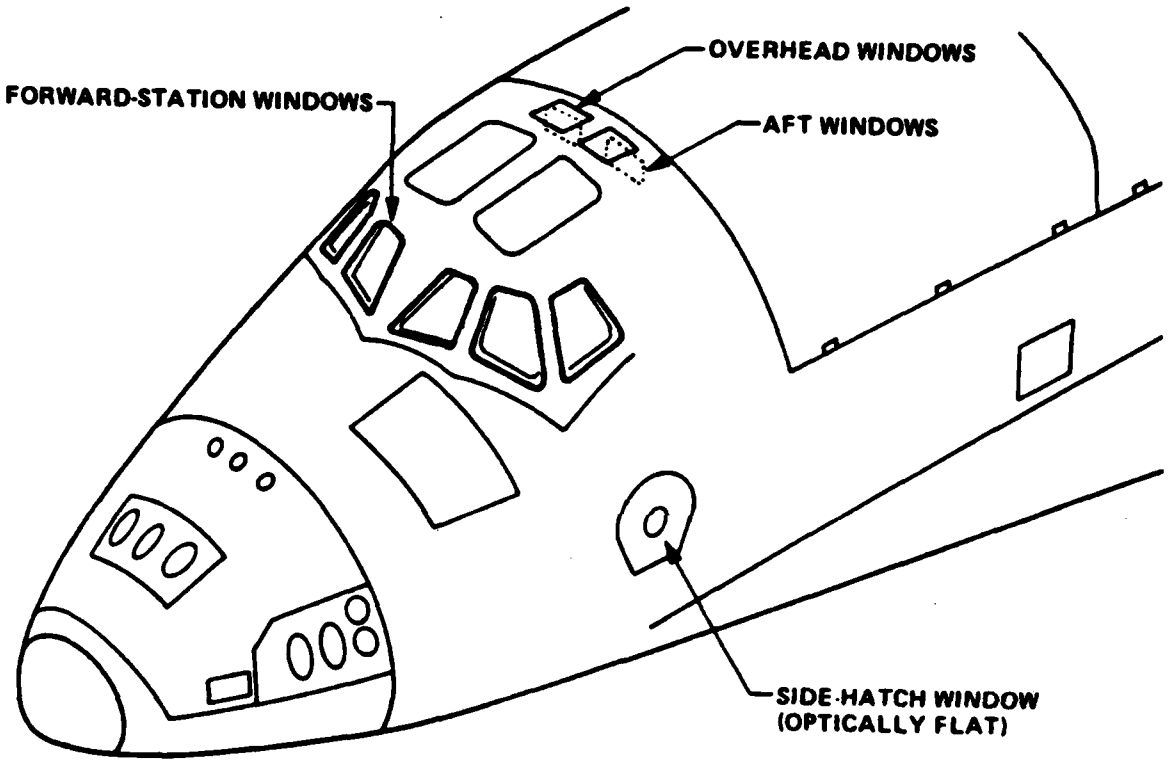

Fig. 2 Location of Windows in Shuttle Orbiter (Nowakowski and Palmer, 1984).

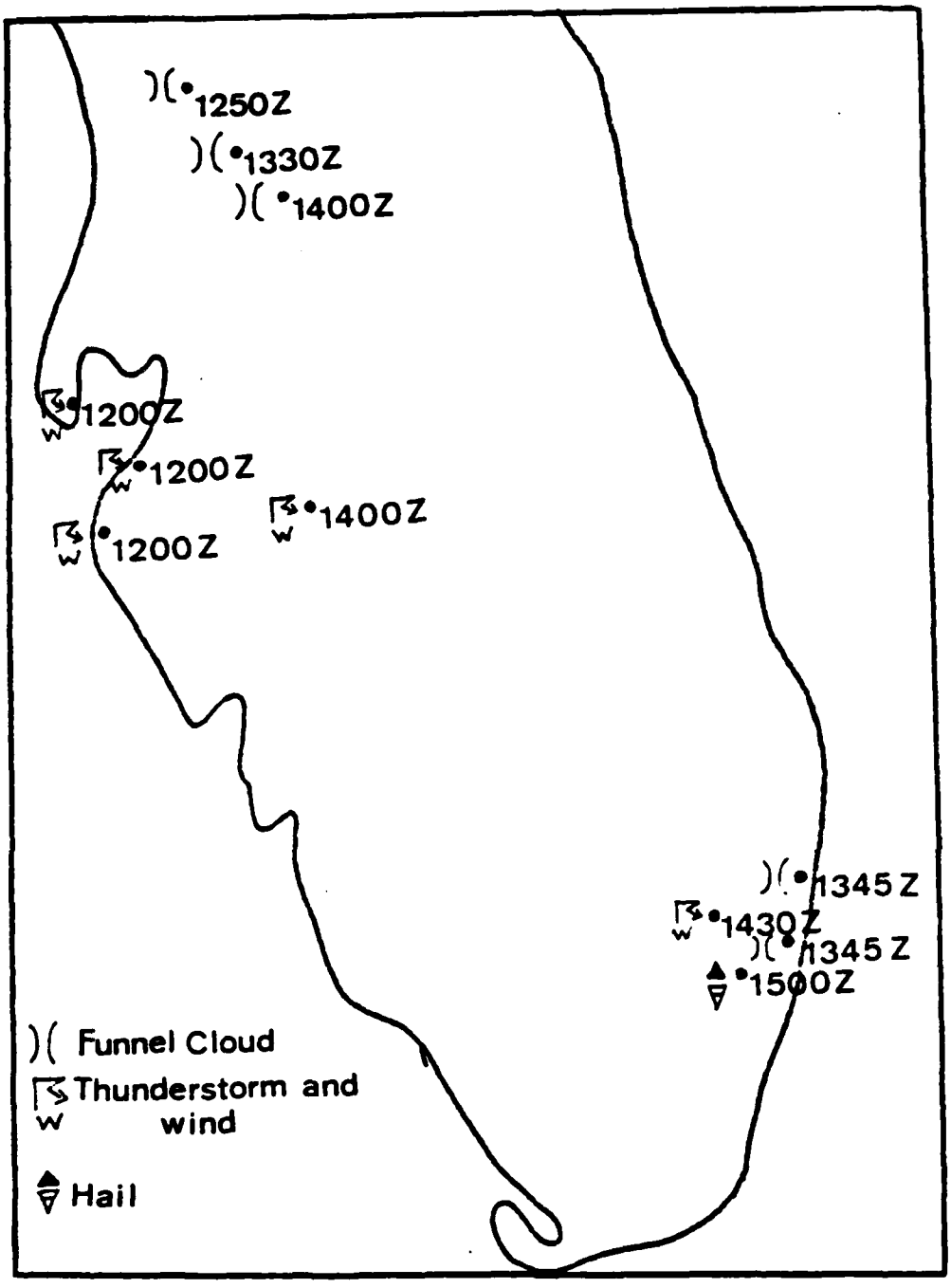

Fig. 3 Severe Weather Obs., Florida, 9 April 1984.

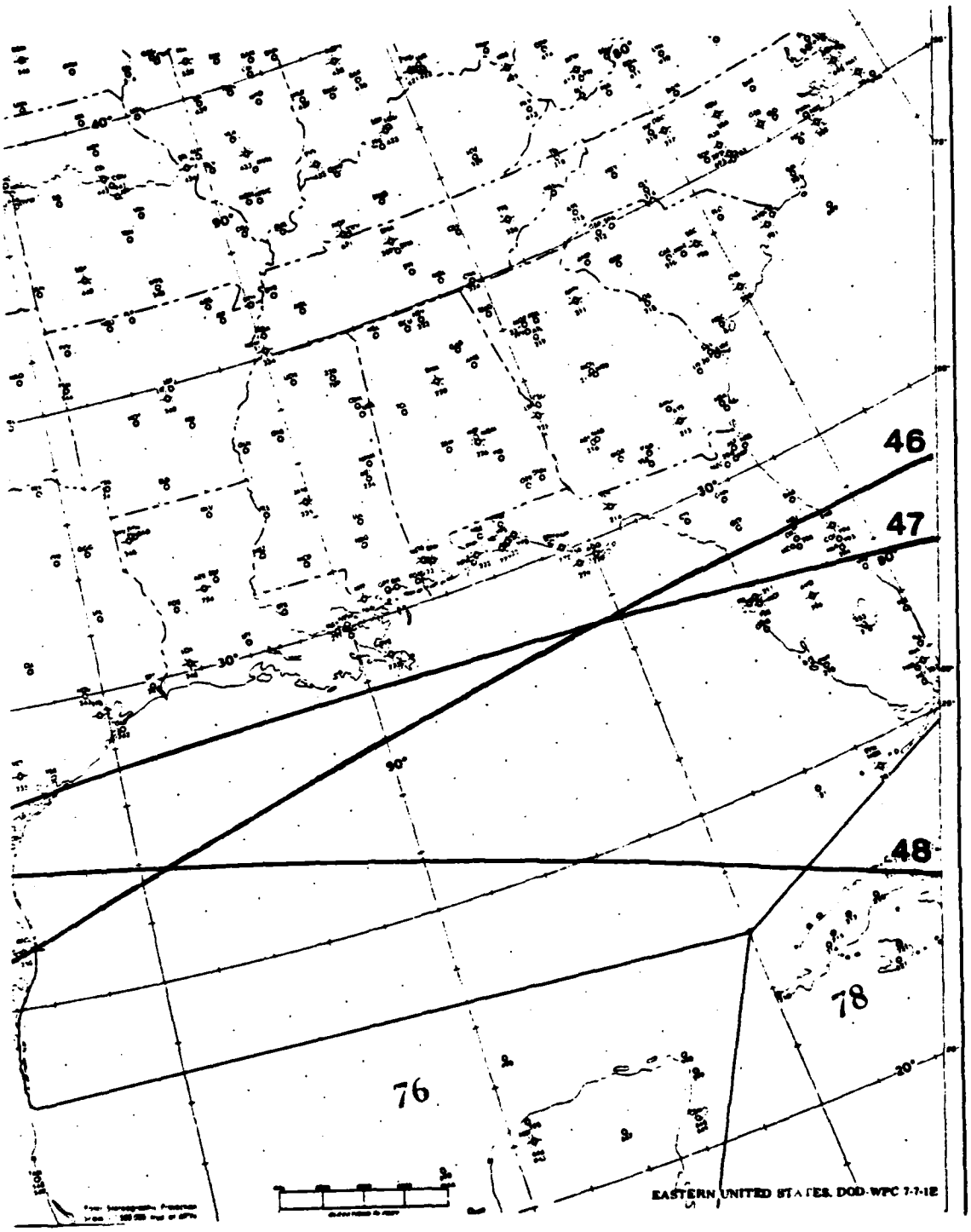

Fig. 4 STS 41-C Orbits 46, 47, and 48 Over the Gulf of Mexico.

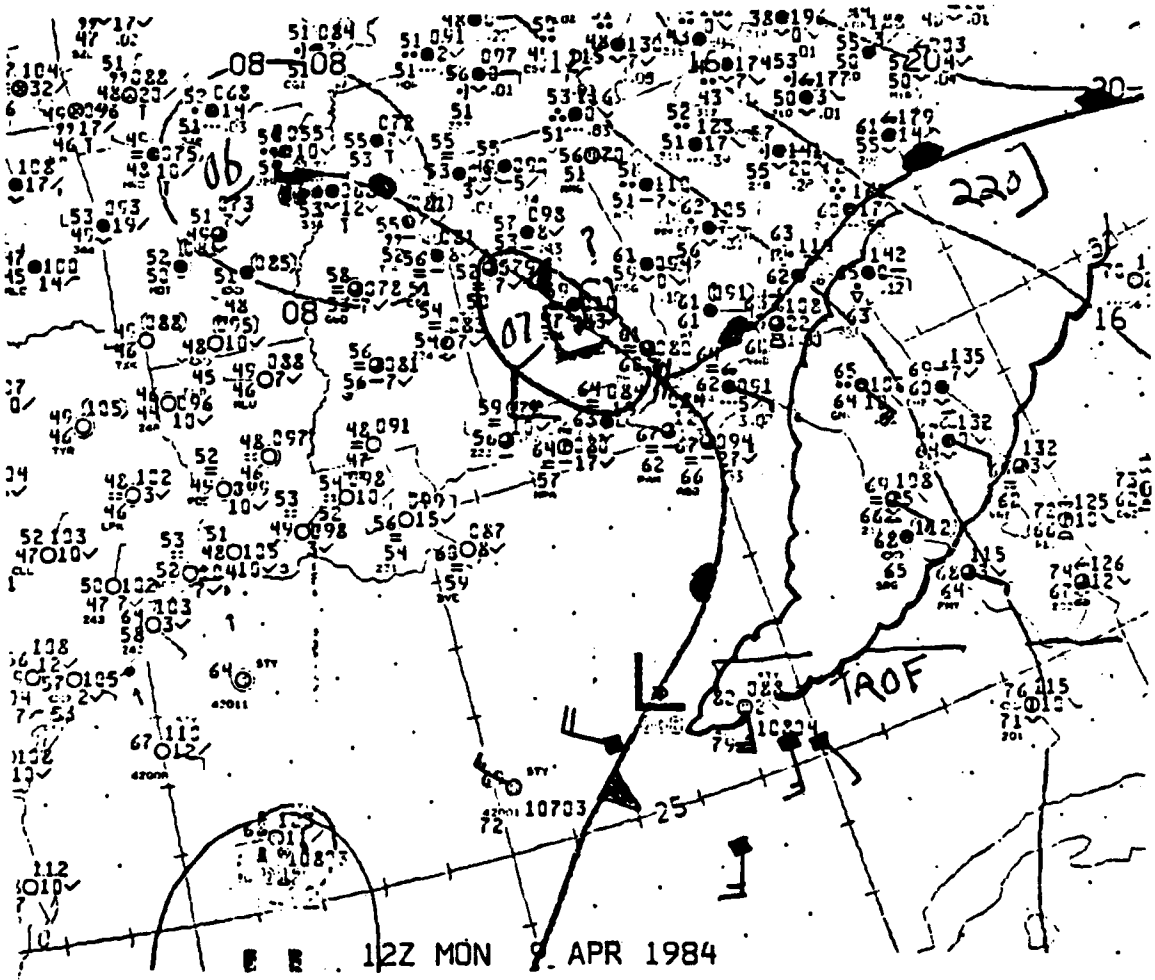

Fig. 5 NMC Surface Analysis, 1200 GMT 9 April 1984.

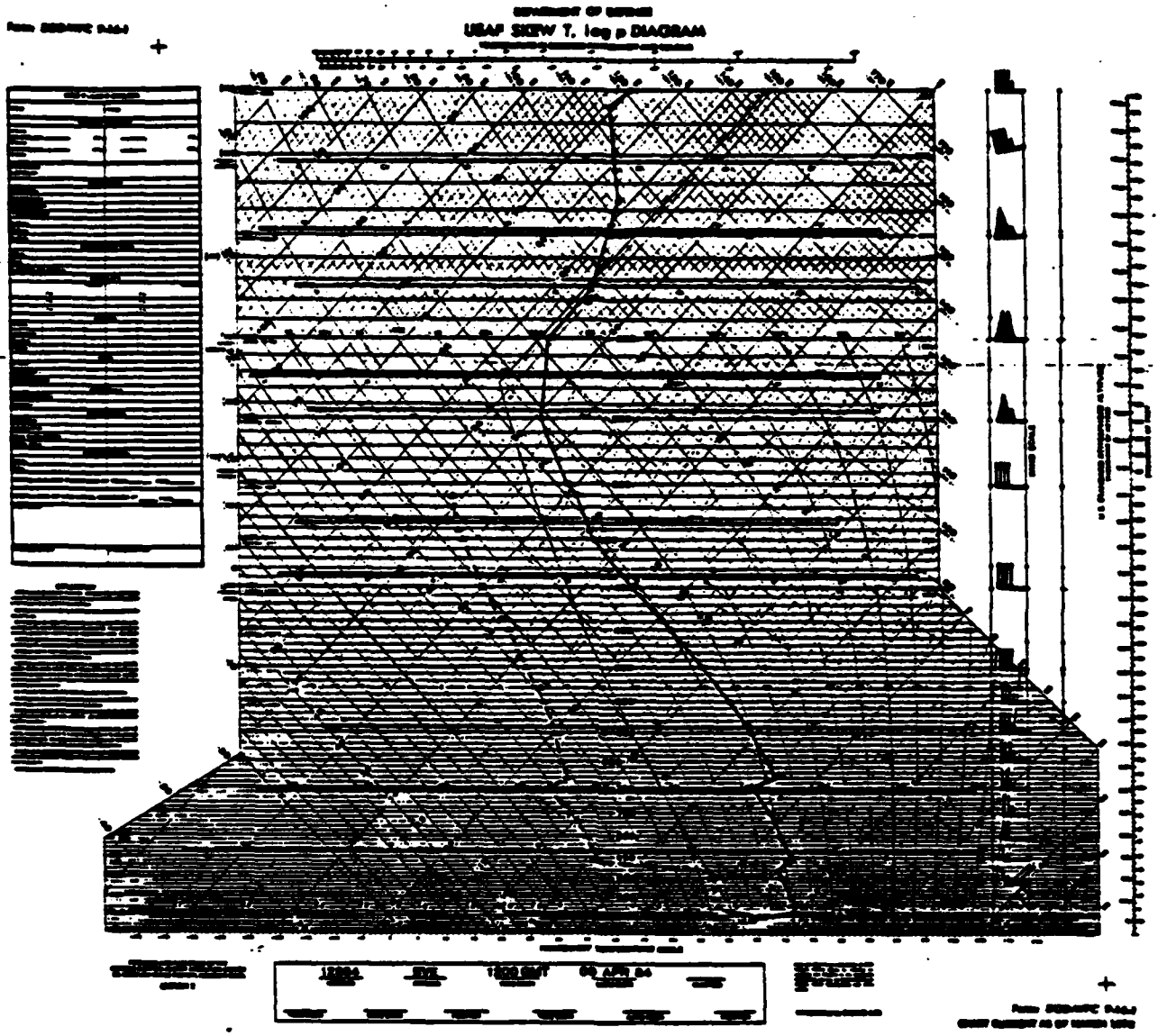

Fig. 6 Boothville, Louisiana Sounding, 1200 GMT 9 April 1984.

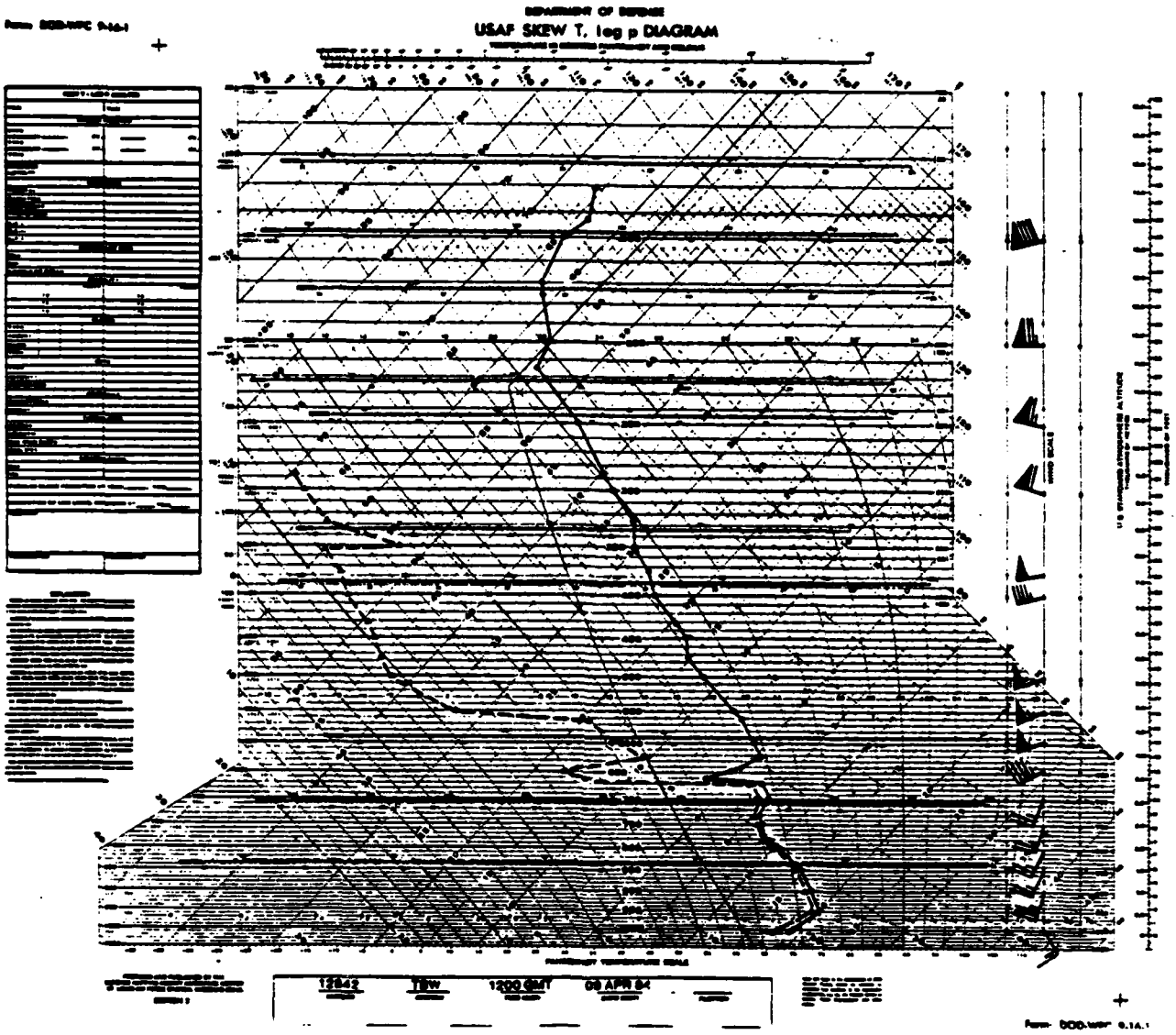

Fig. 7 Tampa Bay, Florida Sounding, 1200 GMT 9 April 1984.

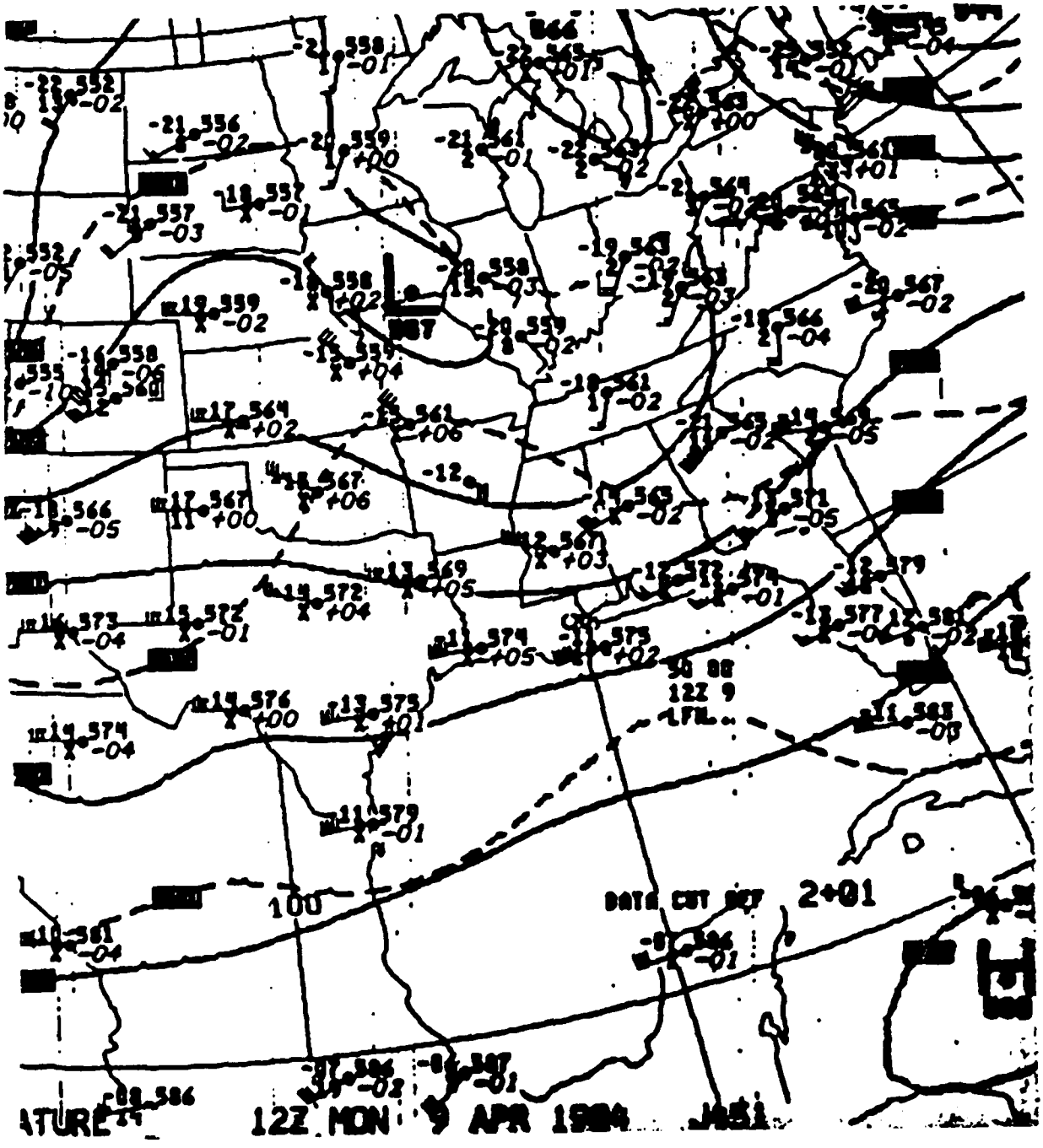

Fig. 8 NMC 500mb Analysis, Heights/Temperature 1200 GMT, 9 April 1984.

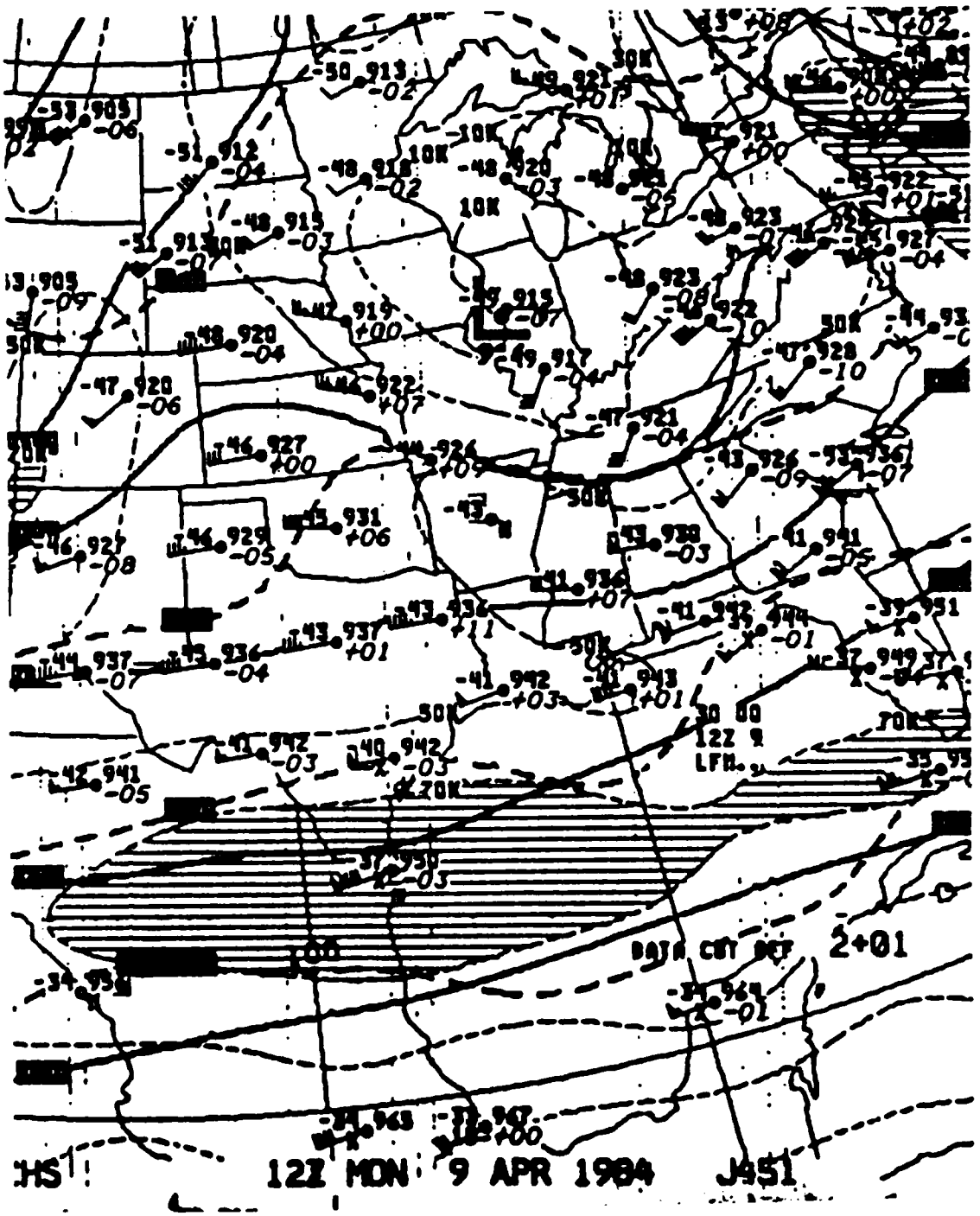

Fig. 9 NMC 300mb Analysis, Heights/Isotachs 1200 GMT, 9 April 1984.

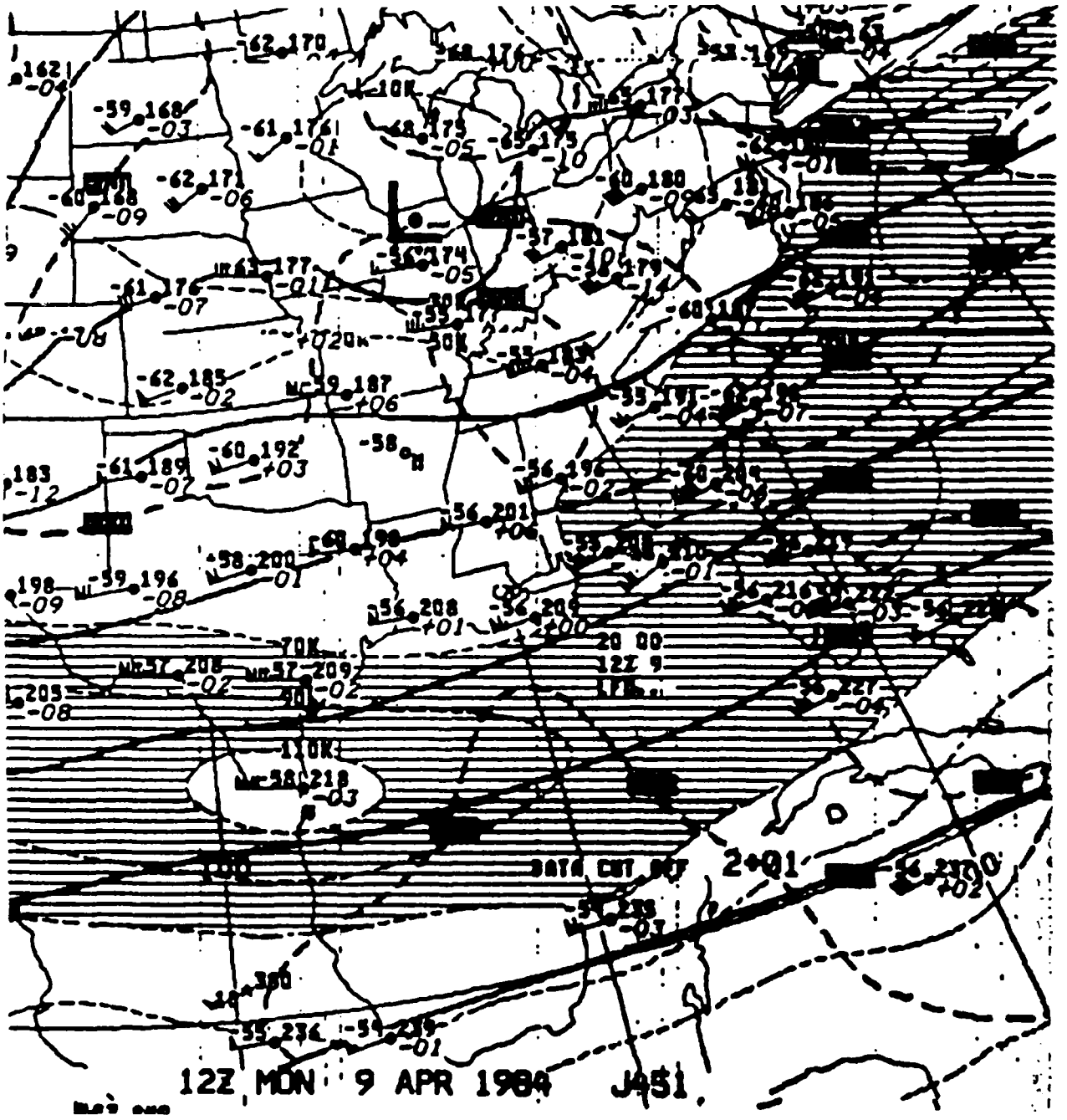

Fig. 10 NMC 200mb Analysis, Heights/Isotachs 1200 GMT, 9 April 1984.

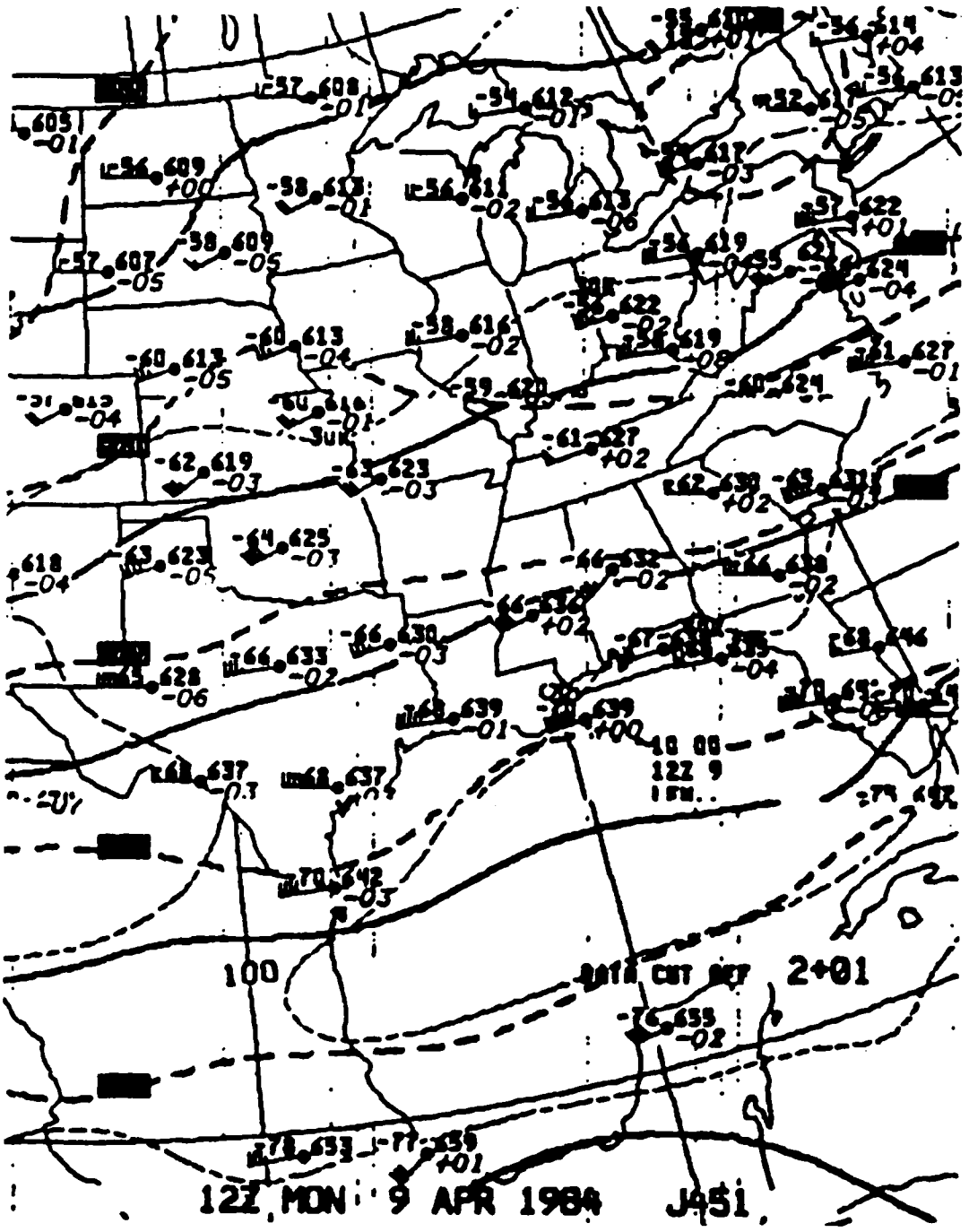

Fig. 11 NMC 100mb Analysis, Heights/Isotachs 1200 GMT, 9 April 1984.

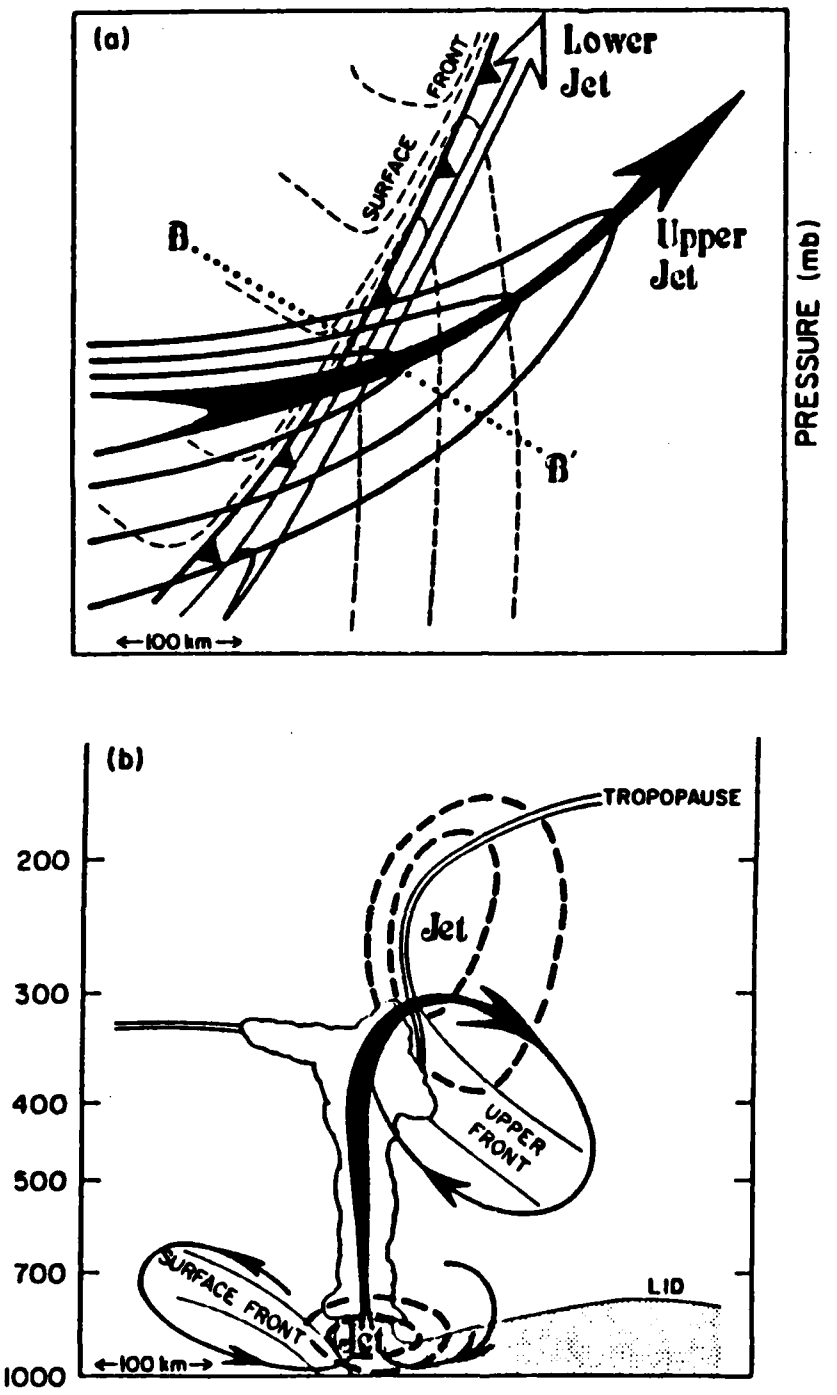

Fig. 12 Vertically-coupled Upper- and Lower-tropospheric Jet-front Systems (Shapiro, 1983).

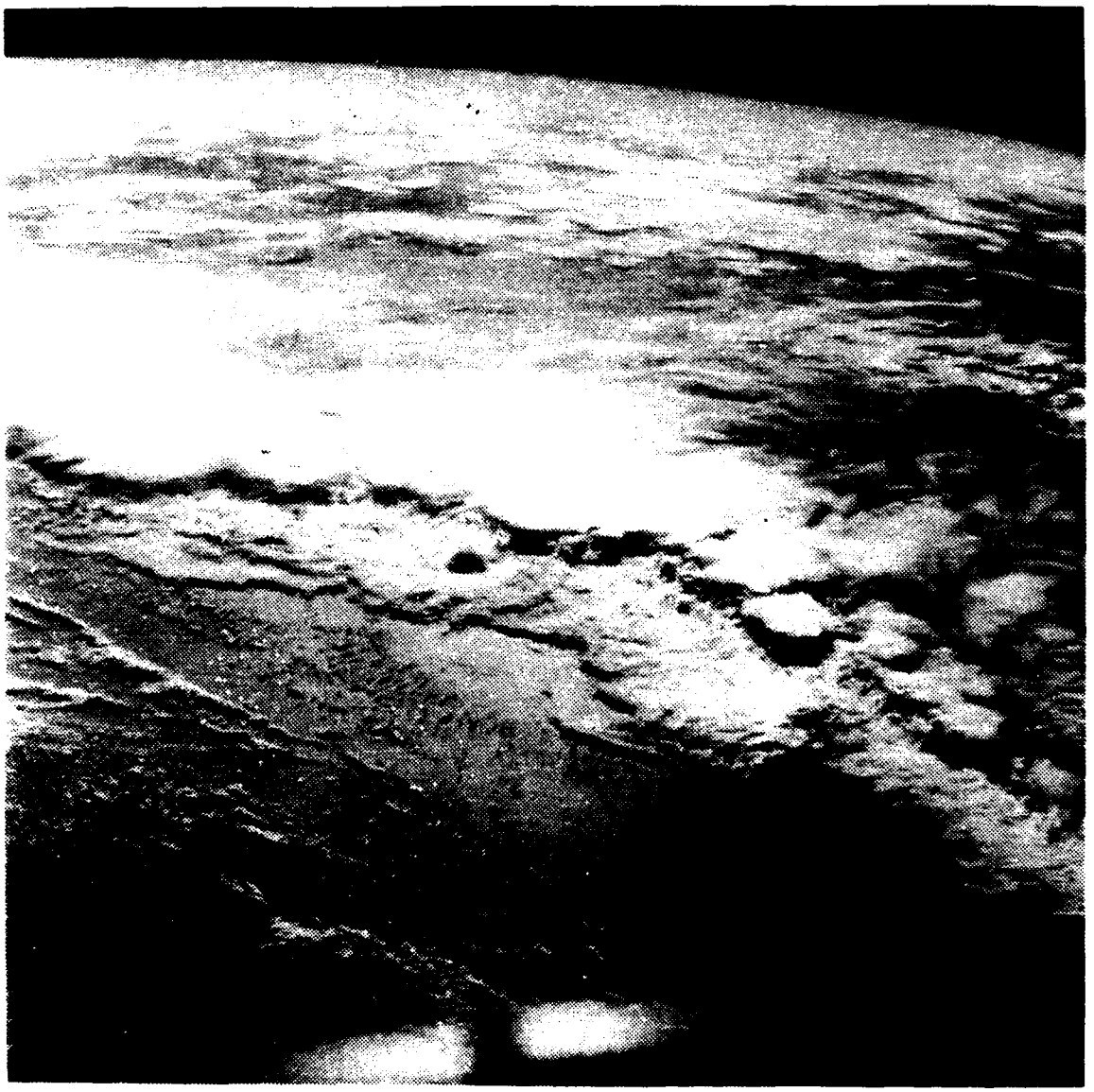

Fig. 13 Frame 2111: Gulf of Mexico Squall Line
Orbit 46, 1208 GMT, 9 April 1984 (100-mm lens).

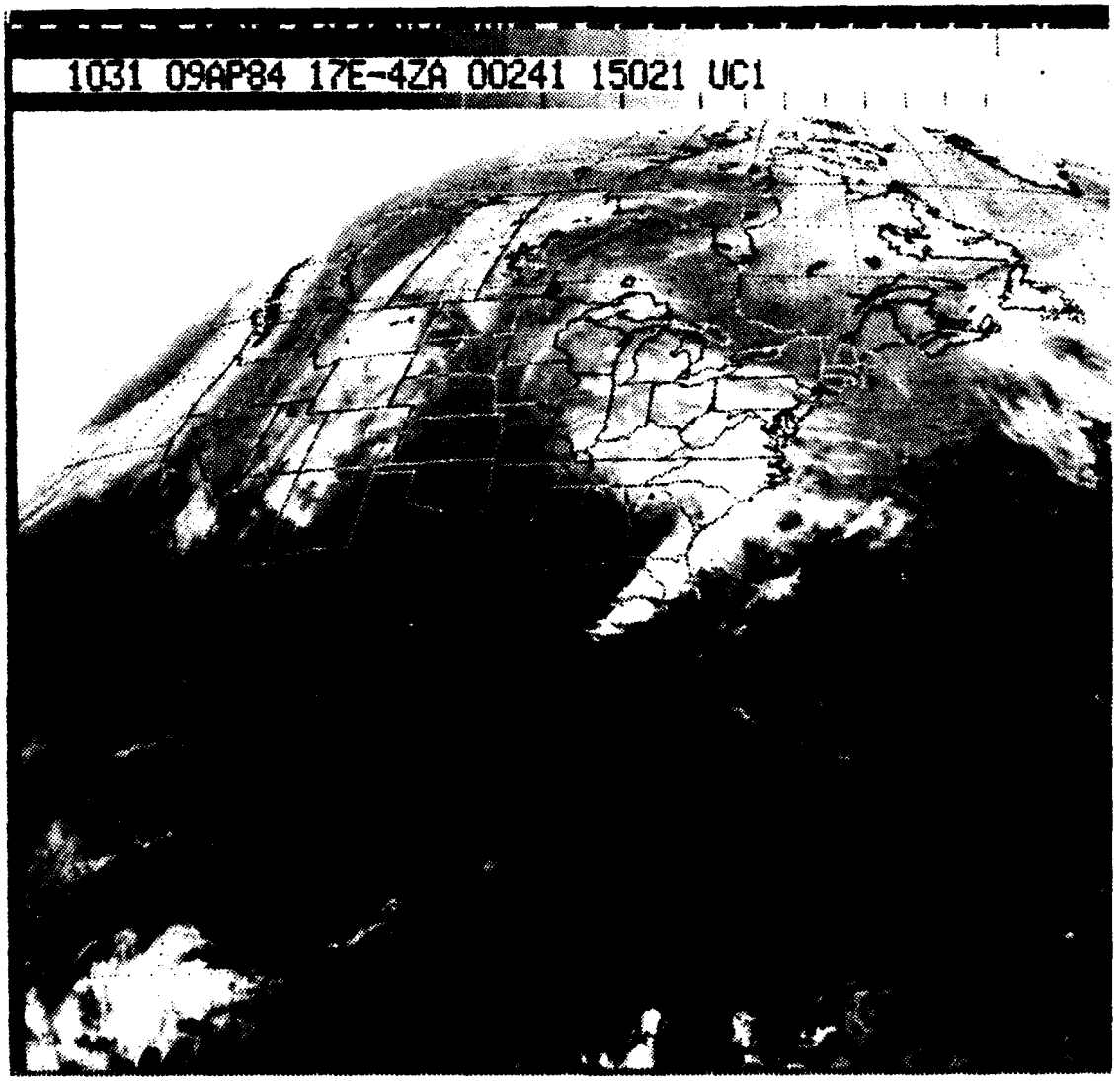

Fig. 14 GOES IR: Gulf of Mexico Squall Line
1031 GMT, 9 April 1984.

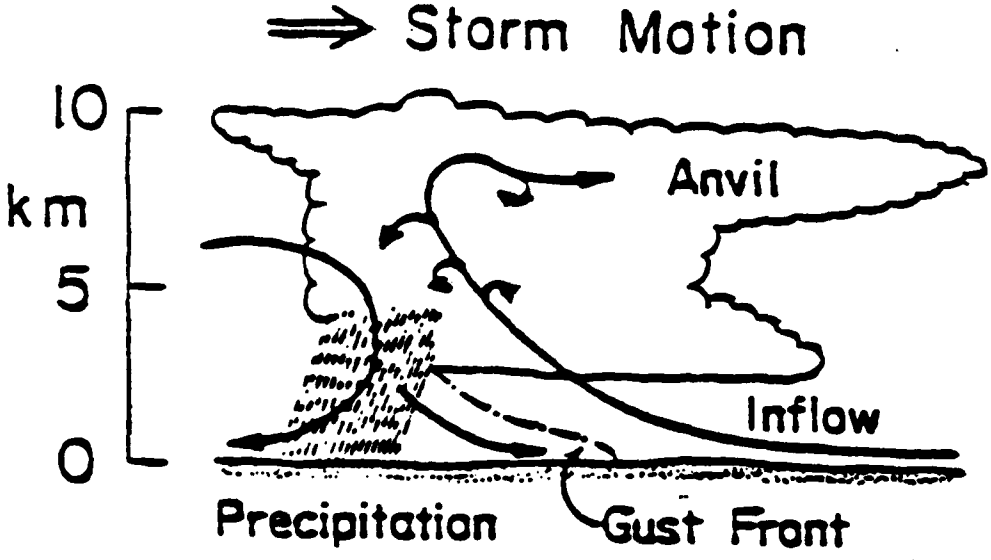

Fig. 15 Severe Thunderstorm Vertical Flow in x-z Plane (Kropfli and Miller, 1975).

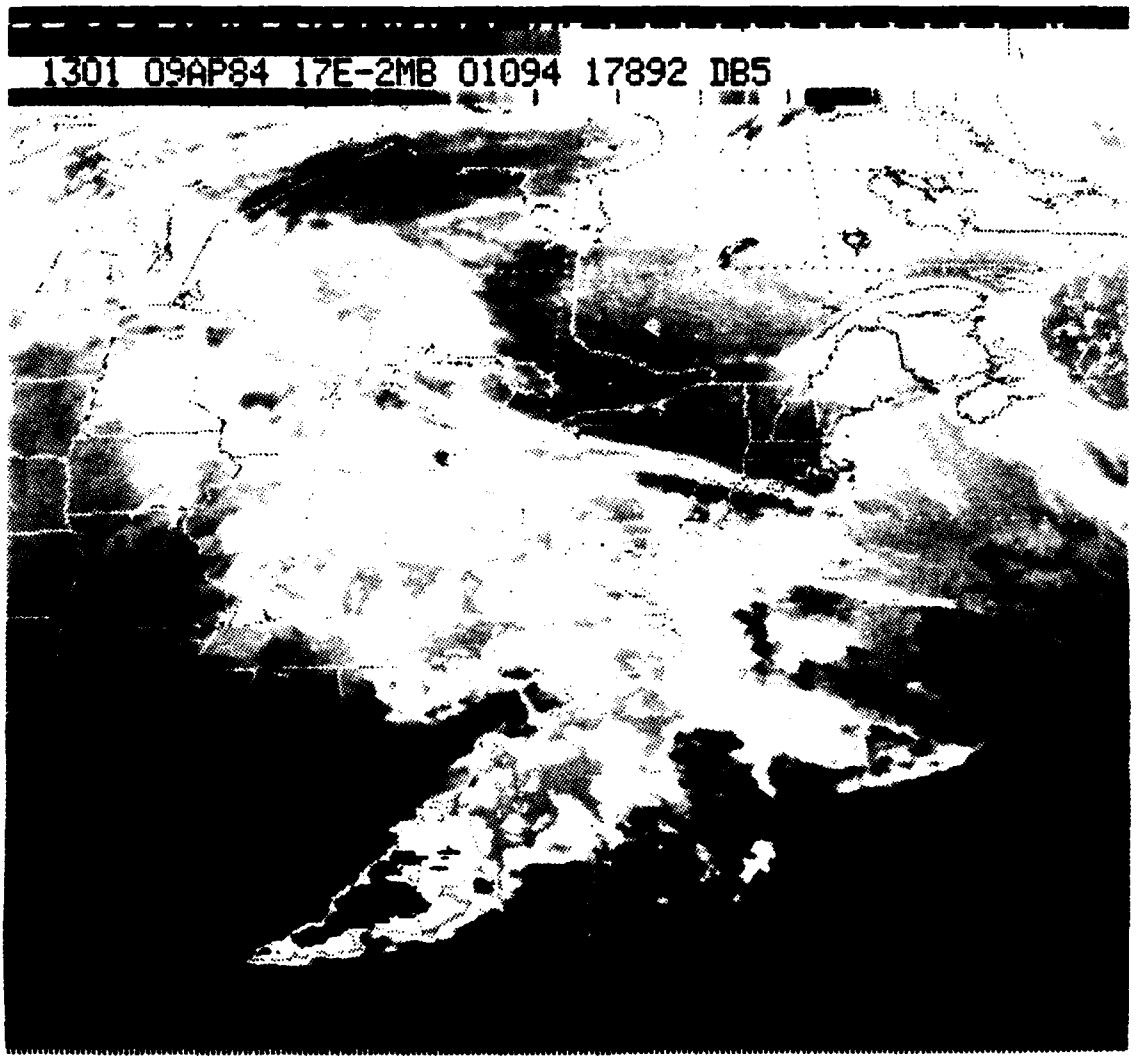

Fig. 16 GOES IR: Gulf of Mexico Squall Line 1301 GMT, 9 April 1984.

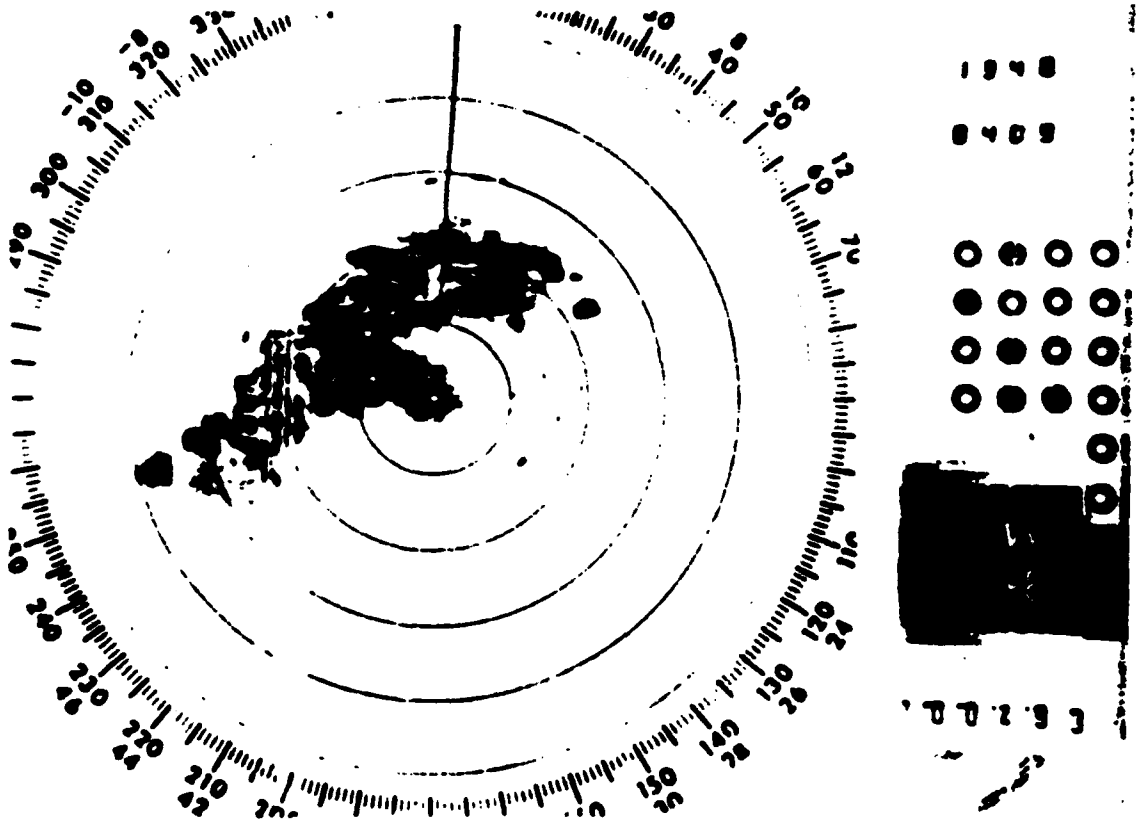

Fig. 17 Tampa Bay, Florida Radar, 1340 GMT 9 April 1984.

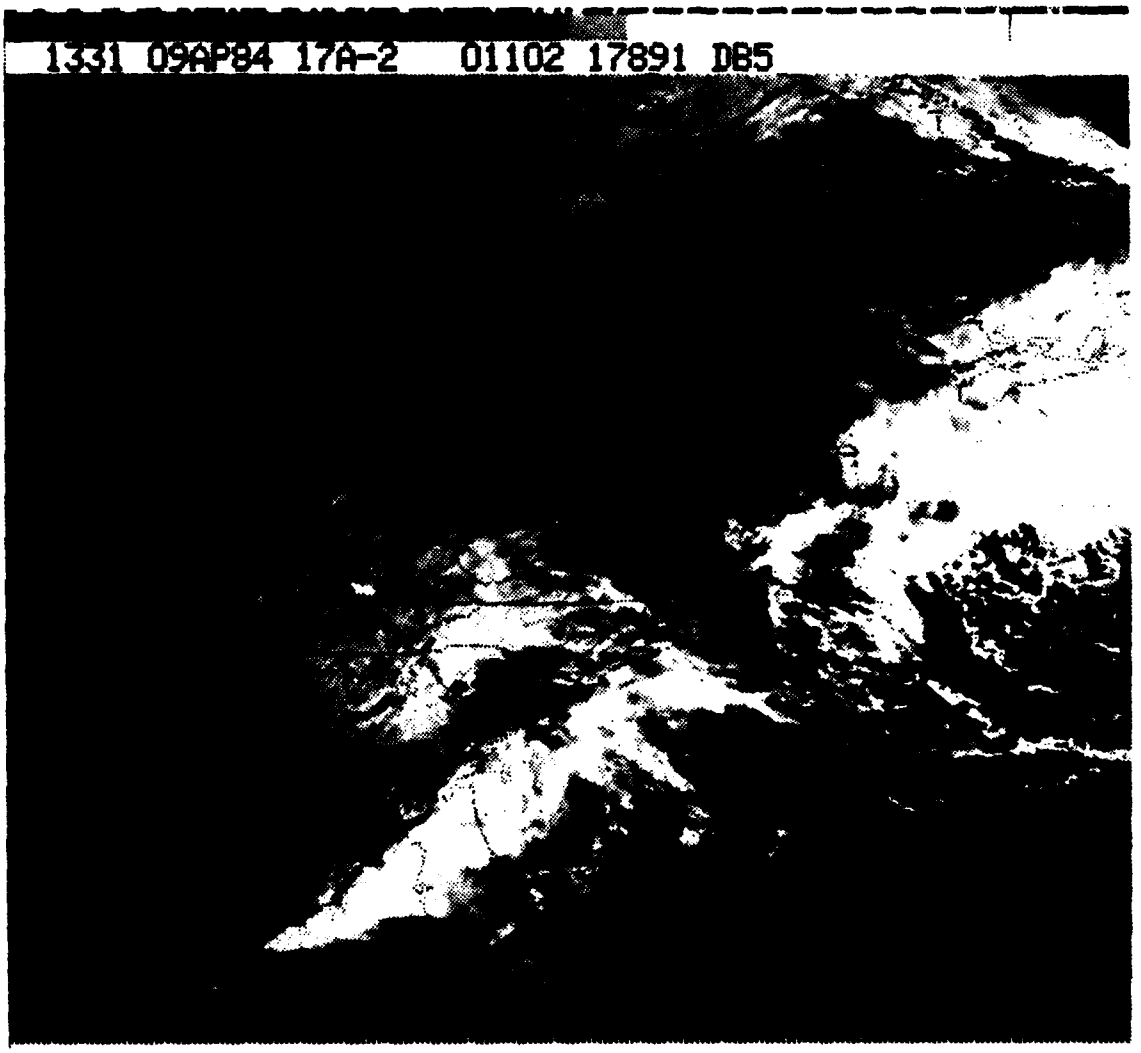

Fig. 18 GOES VISIBLE: Gulf of Mexico Squall Line 1331 GMT, 9 April 1984.

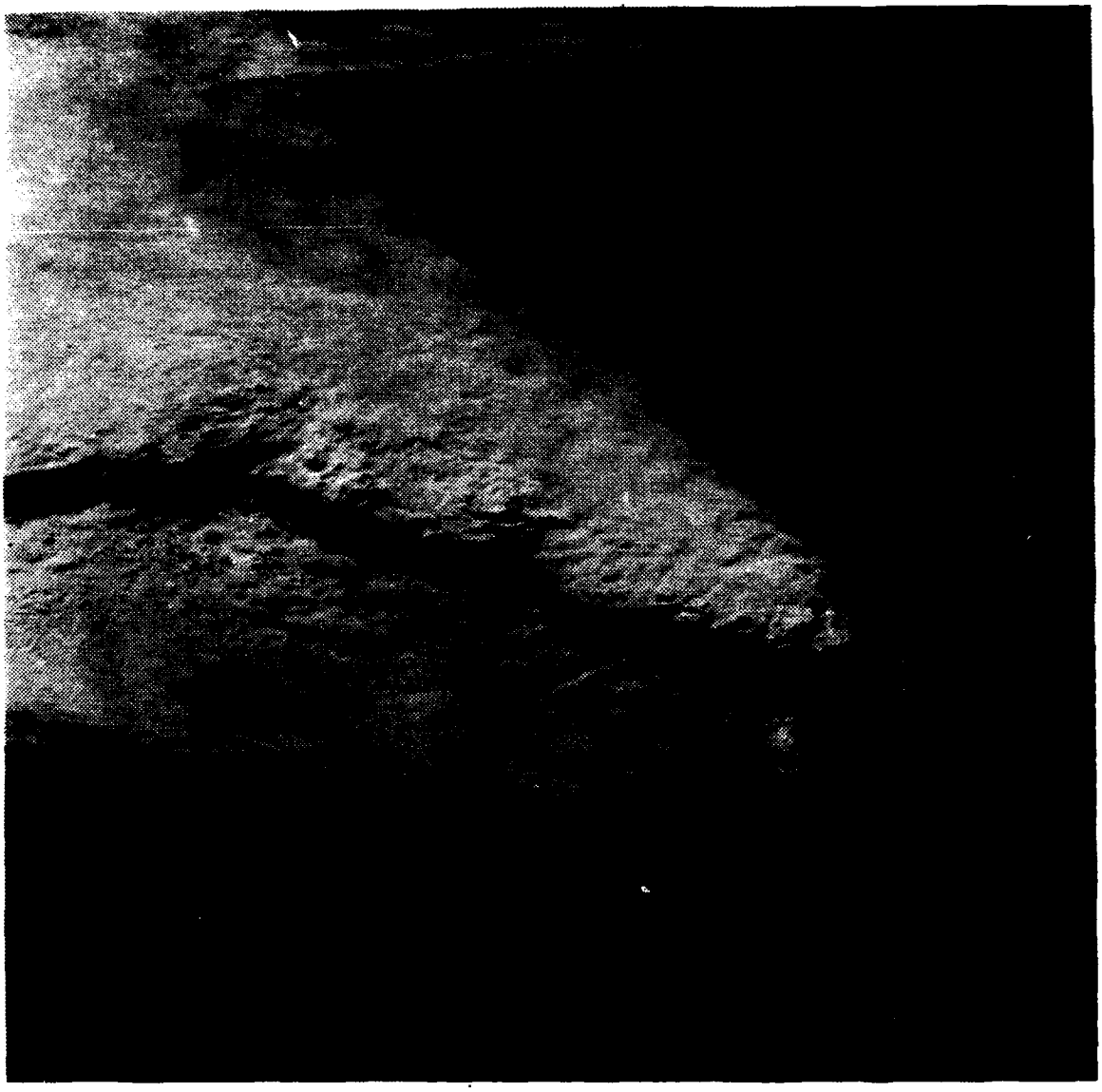

Fig. 19. Frame 2130: Gulf of Mexico Squall Line
Orbit 47, 1338 GMT, 9 April 1984 (100-mm lens).

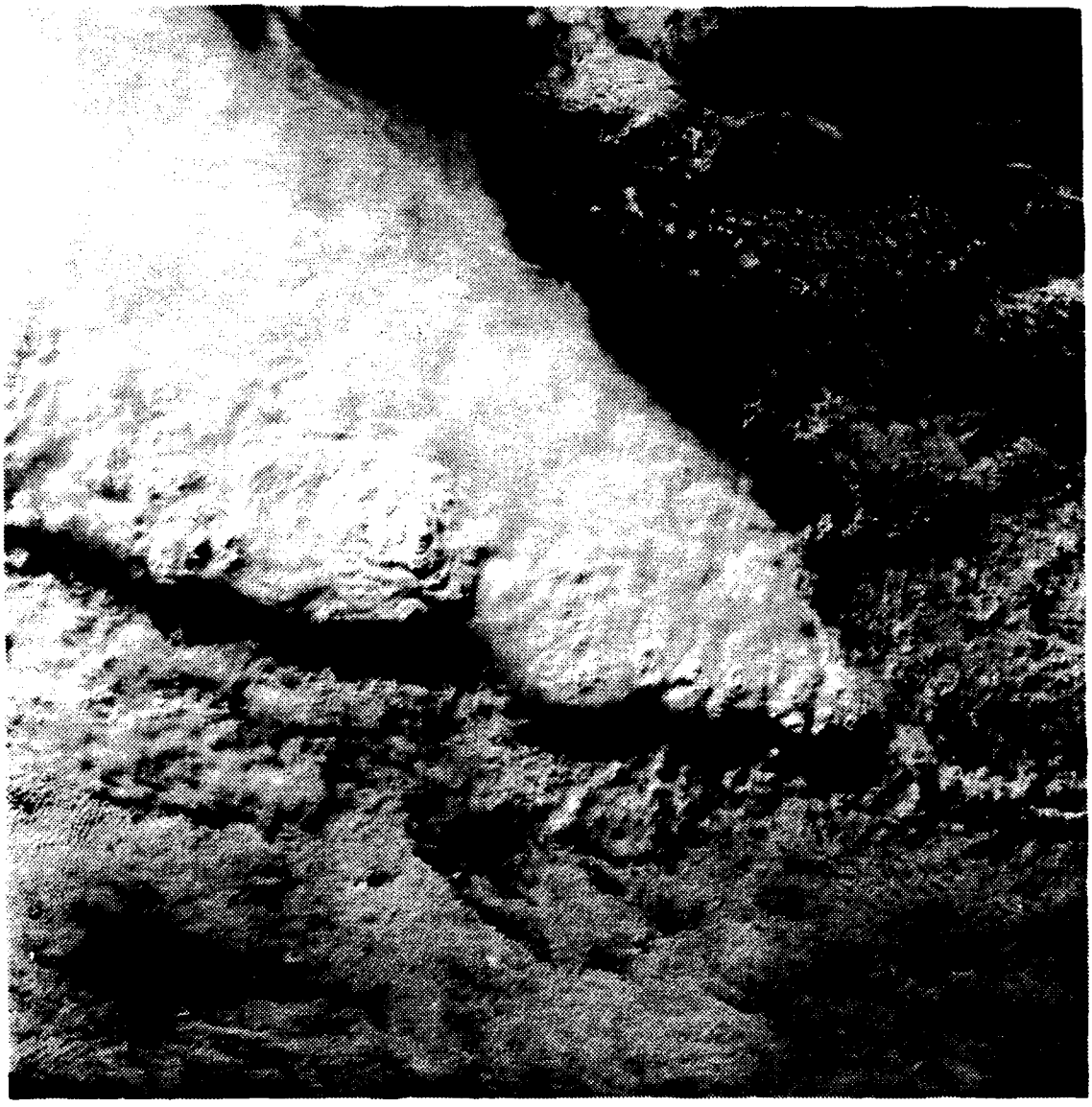

Fig. 20. Frame 2134: Gulf of Mexico Squall Line Orbit 47, 1338 GMT, 9 April 1984 (100-mm lens).

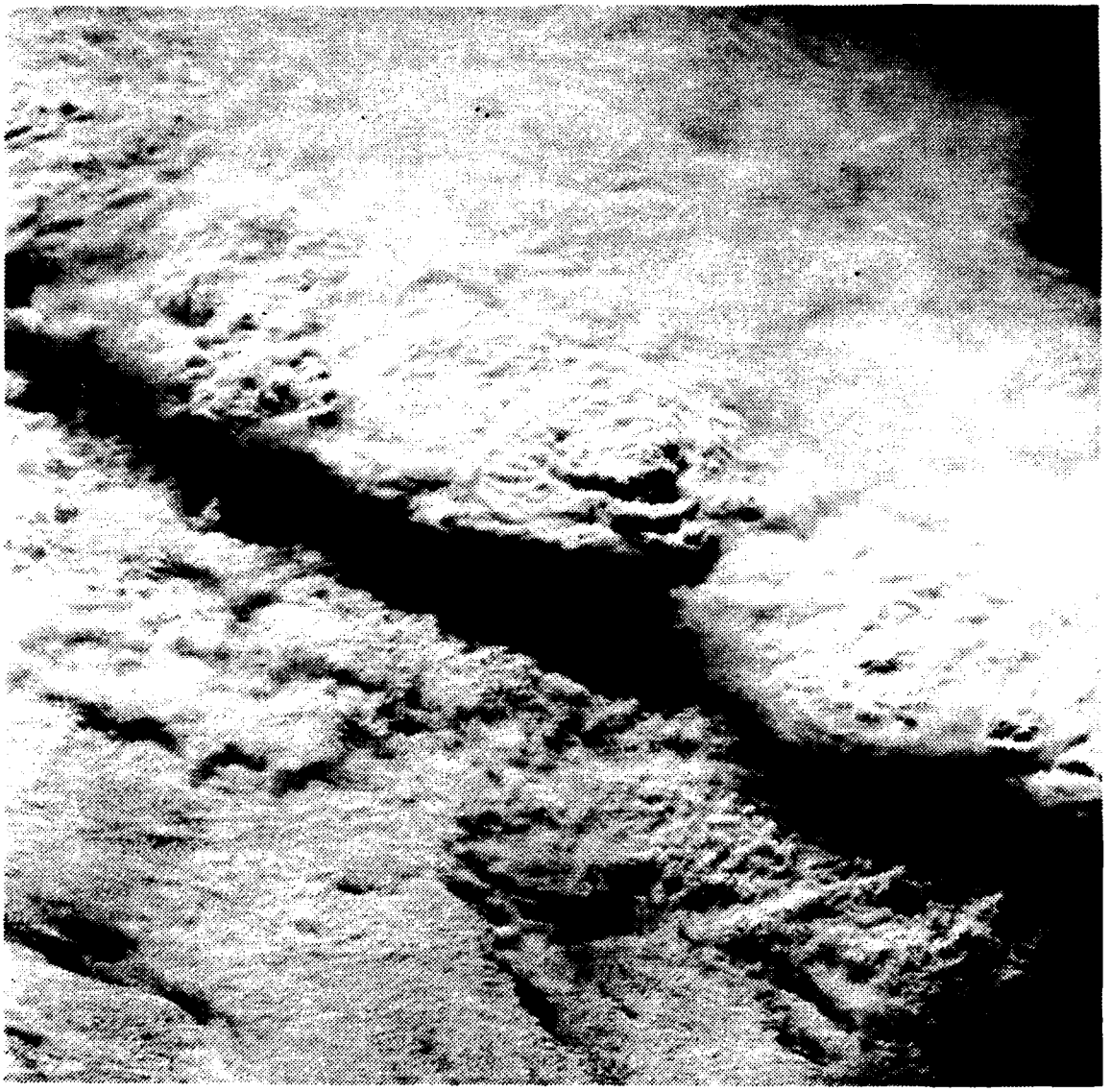

Fig. 21. Frame 2008: Gulf of Mexico Squall Line Orbit 47, 1338 GMT, 9 April 1984 (250-mm lens).

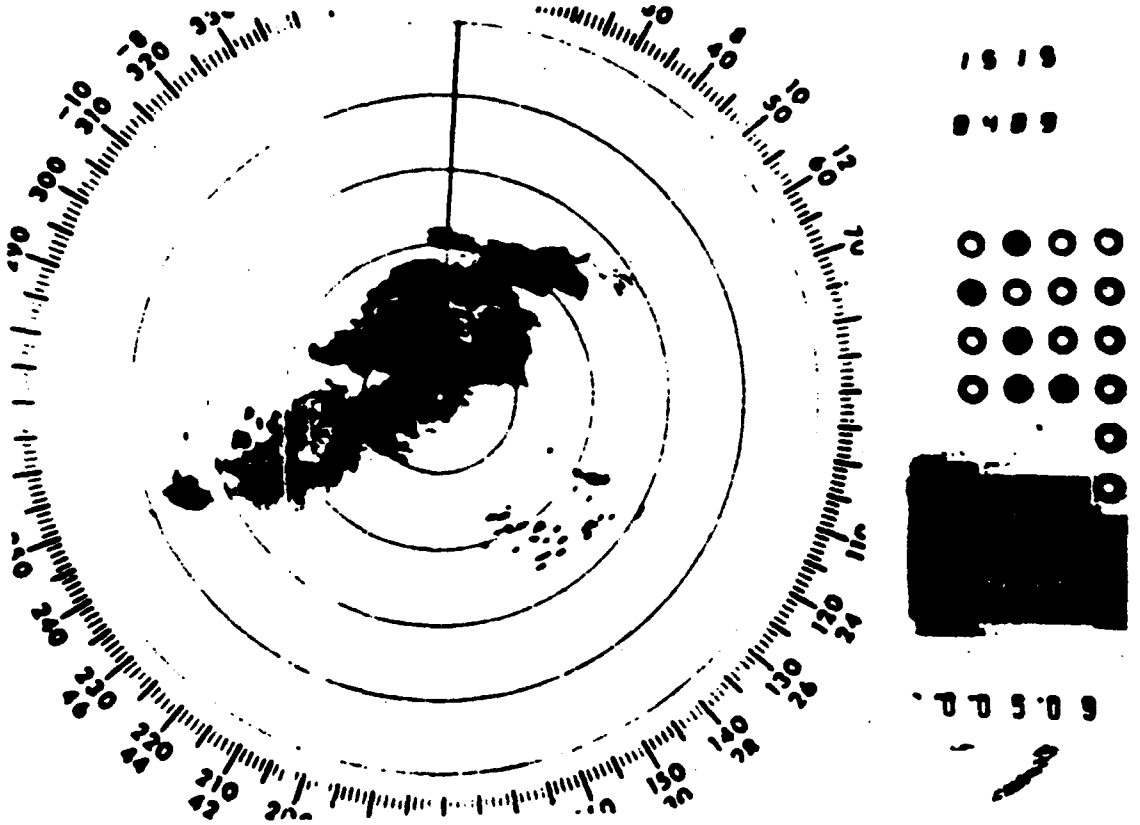

Fig. 22 Tampa Bay, Florida Radar, 1515 GMT 9 April 1984.

Fig. 23 DMSP VISIBLE: Gulf of Mexico Squall Line 1521 GMT, 9 April 1984.

Fig. 24 DMSP IR: Gulf of Mexico Squall Line 1521 GMT, 9 April 1984.

Fig. 25, Frame 2166: Gulf of Mexico Squall Line
Orbit 48, 1516 GMT, 9 April 1984 (100-mm lens).

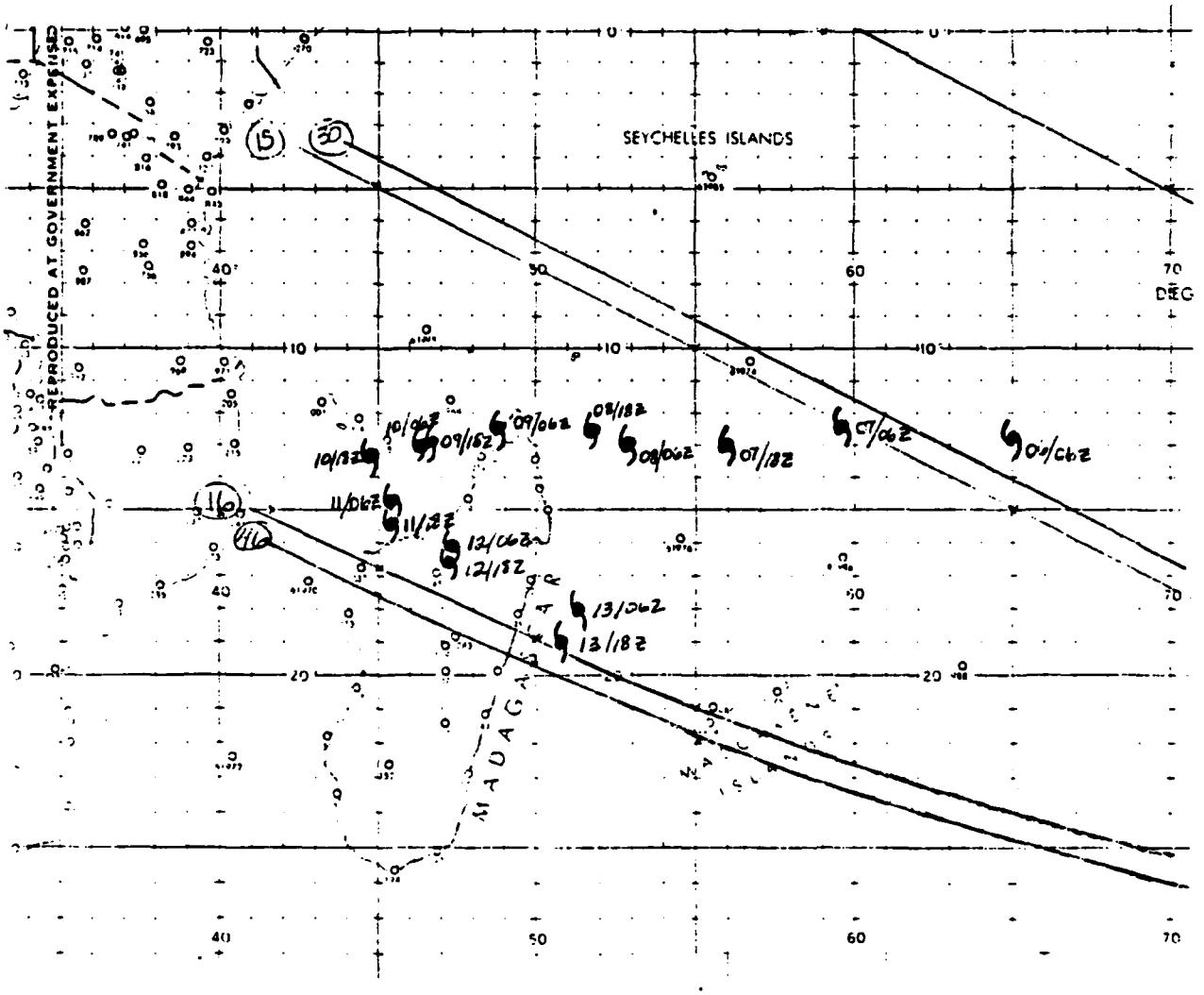

Fig. 26 STS 41-C Orbits 14, 15, 16, 30 and 46 Over Hurricane Kamisy, 7-13 April 1984.

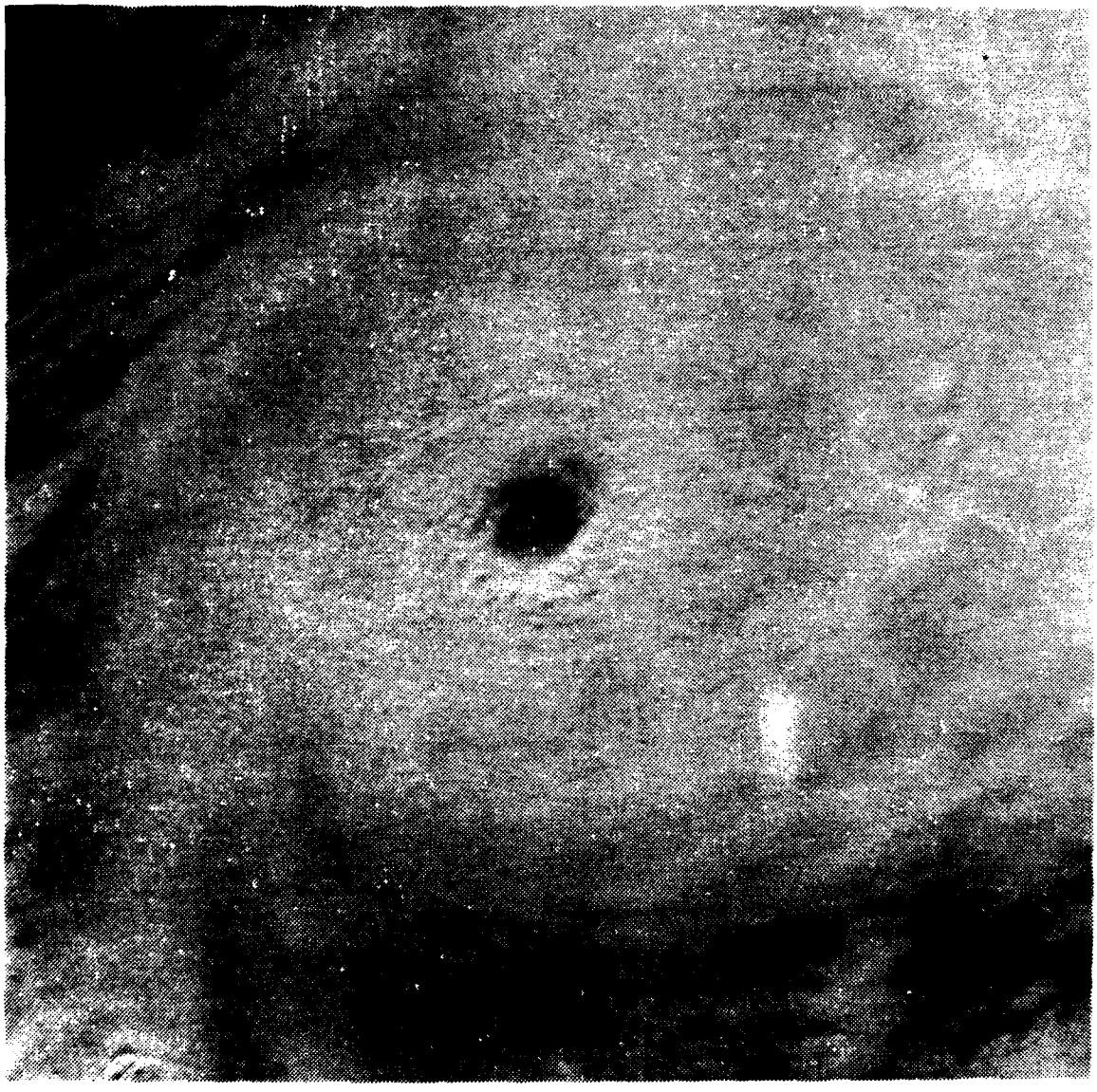

Fig. 27 Frame 1592: Hurricane Kamisy, Orbit 15 1157 GMT, 7 April 1984 (100-mm lens).

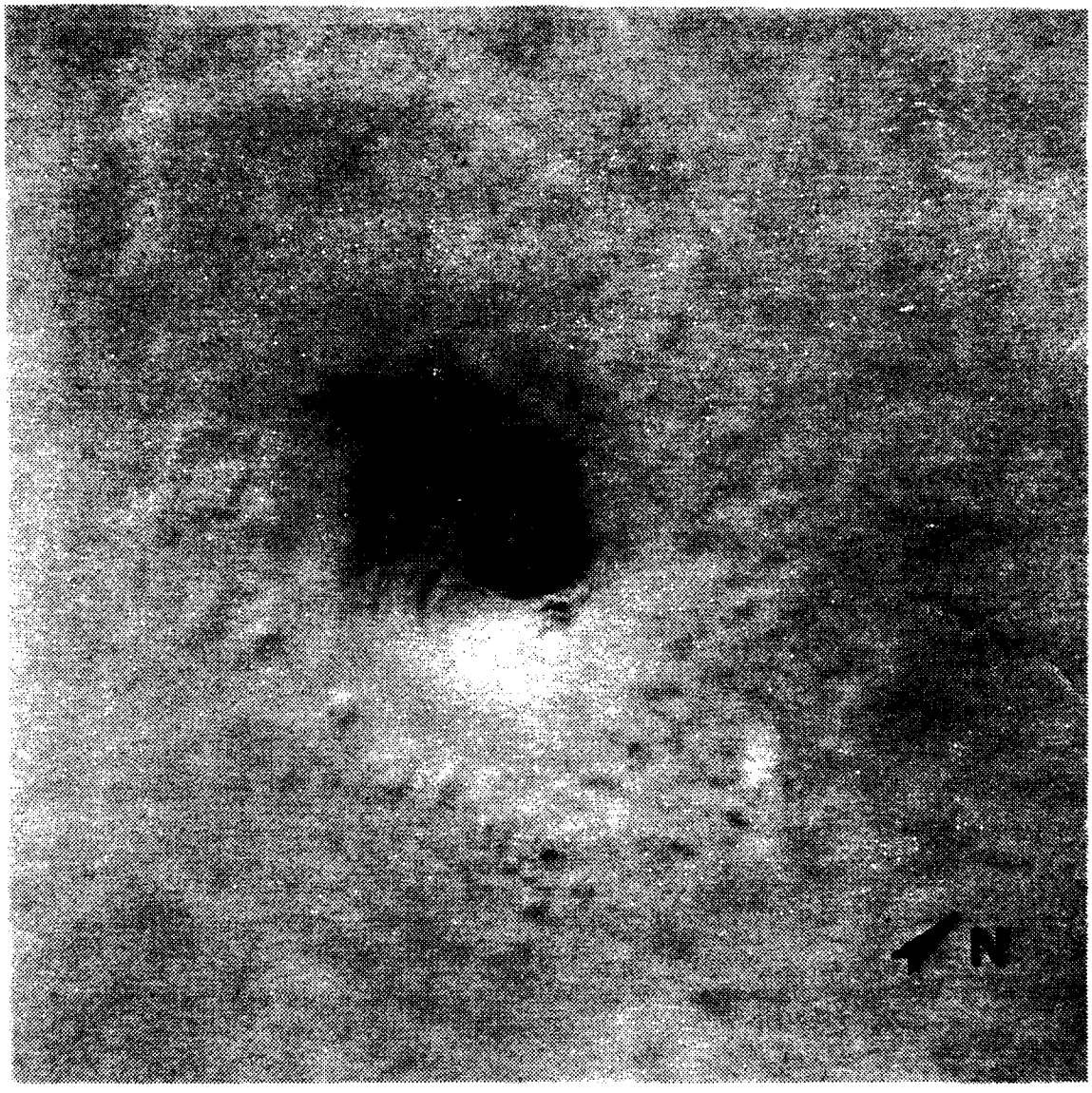

Fig. 28 Frame 1499; Hurricane Kamisy, Orbit 15 1157 GMT, 7 April 1984 (250-mm lens).

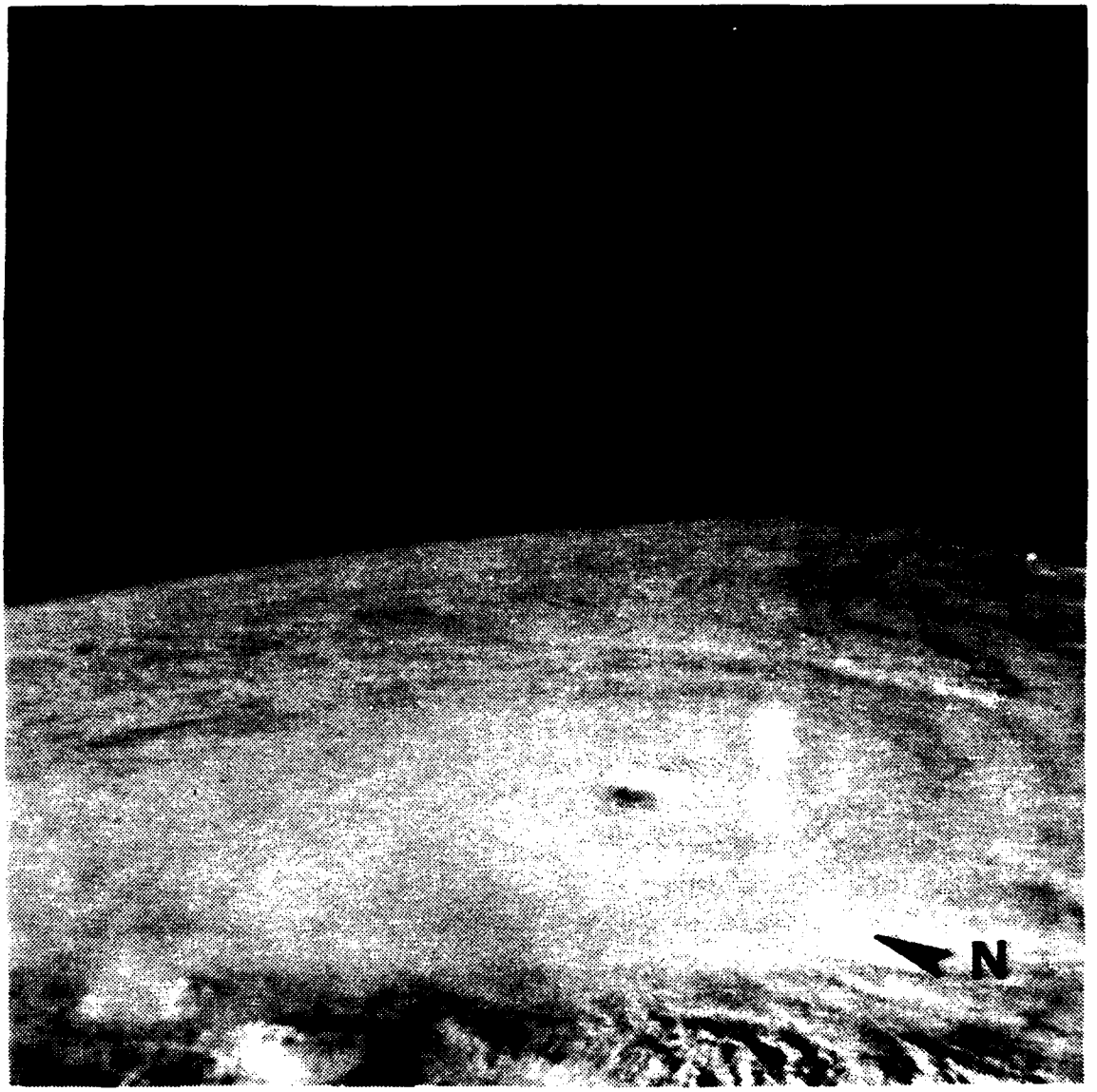

Fig. 29 Frame 1608: Hurricane Kamisy, Orbit 16
1330 GMT, 7 April 1984 (100-mm lens).

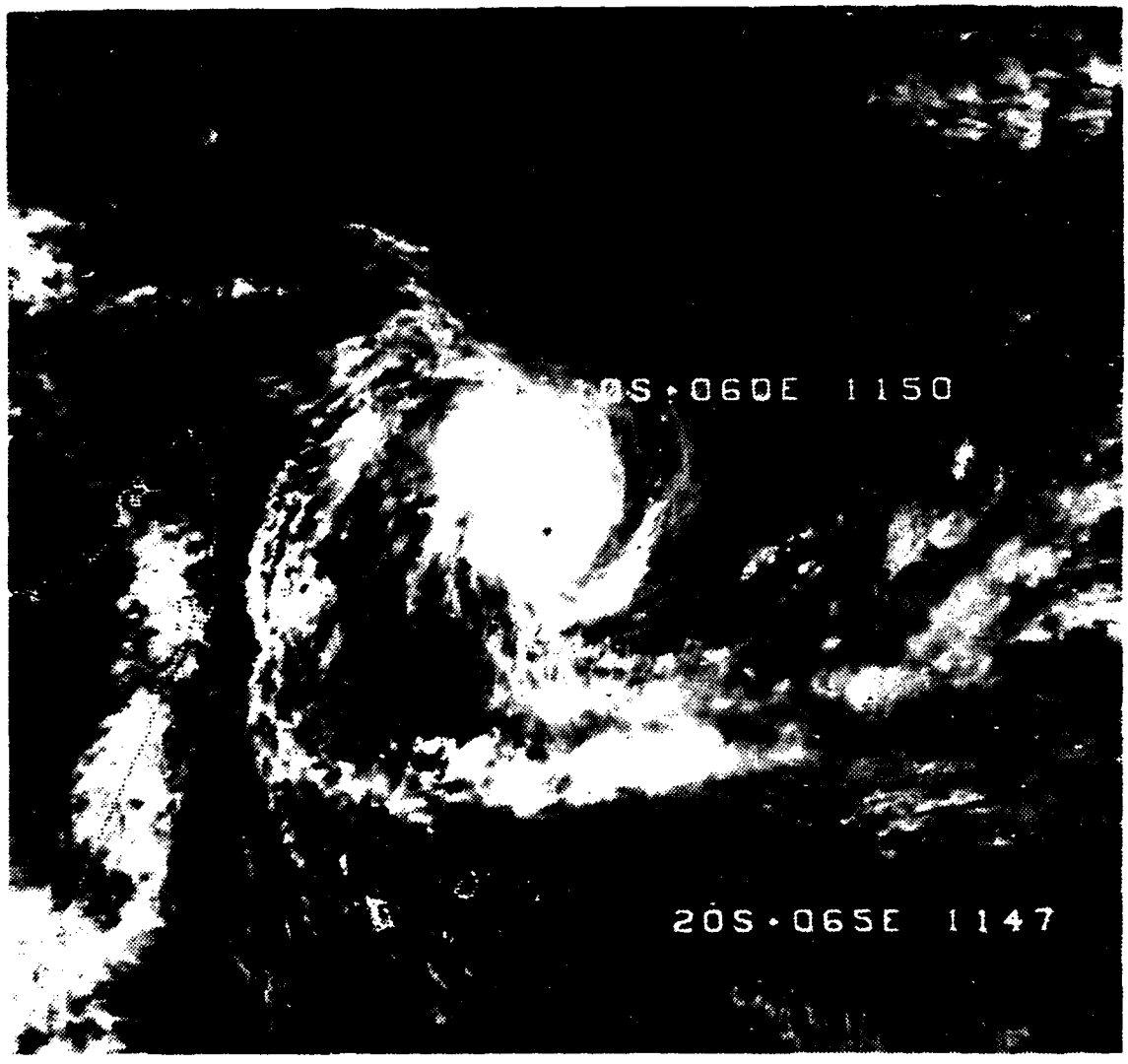

Fig. 30 AVHRR VISIBLE: Hurricane Kamisy
1205 GMT, 7 April 1984.

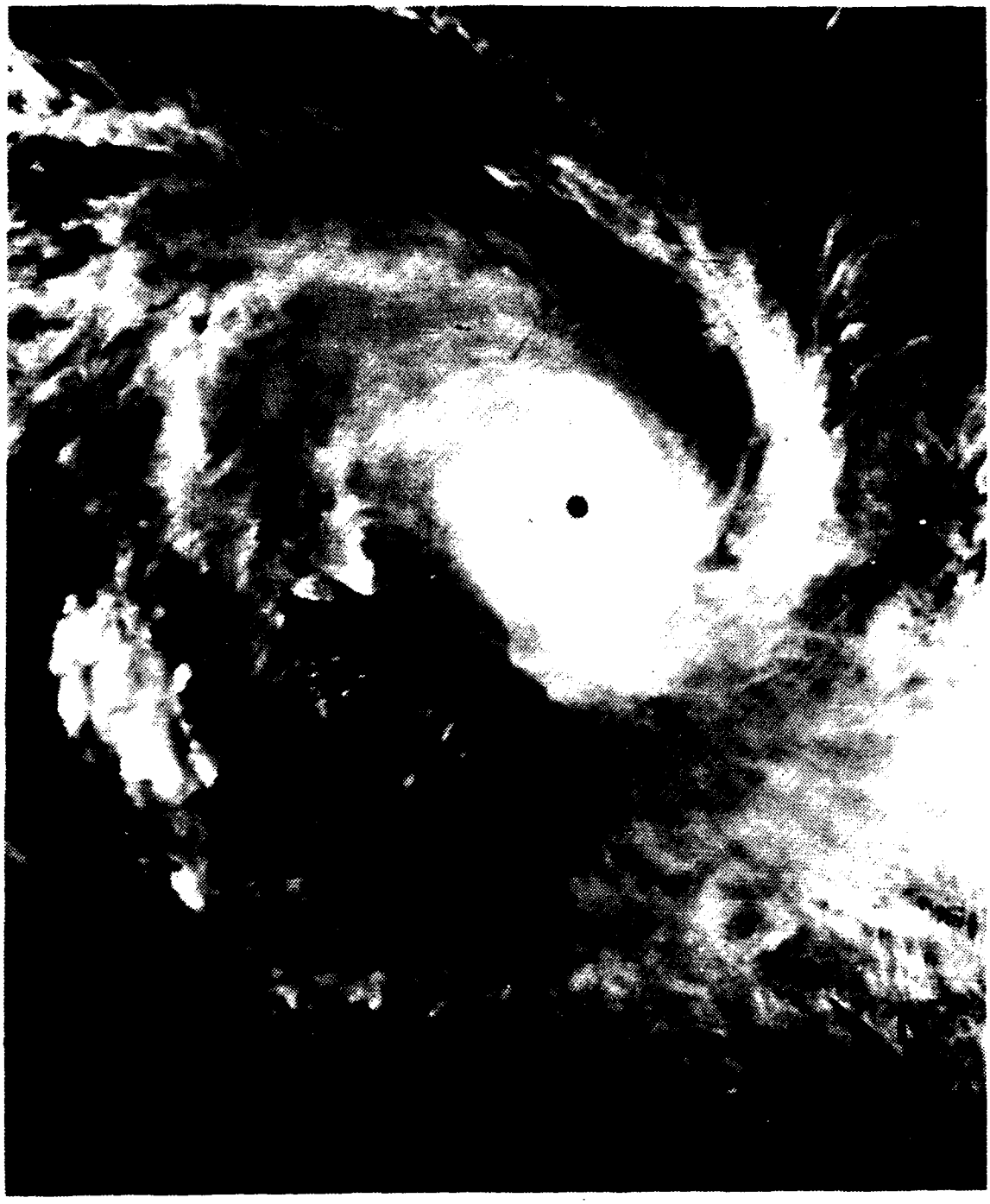

Fig. 31 DMSP IR: Hurricane Kamisy
1405 GMT, 7 April 1984.

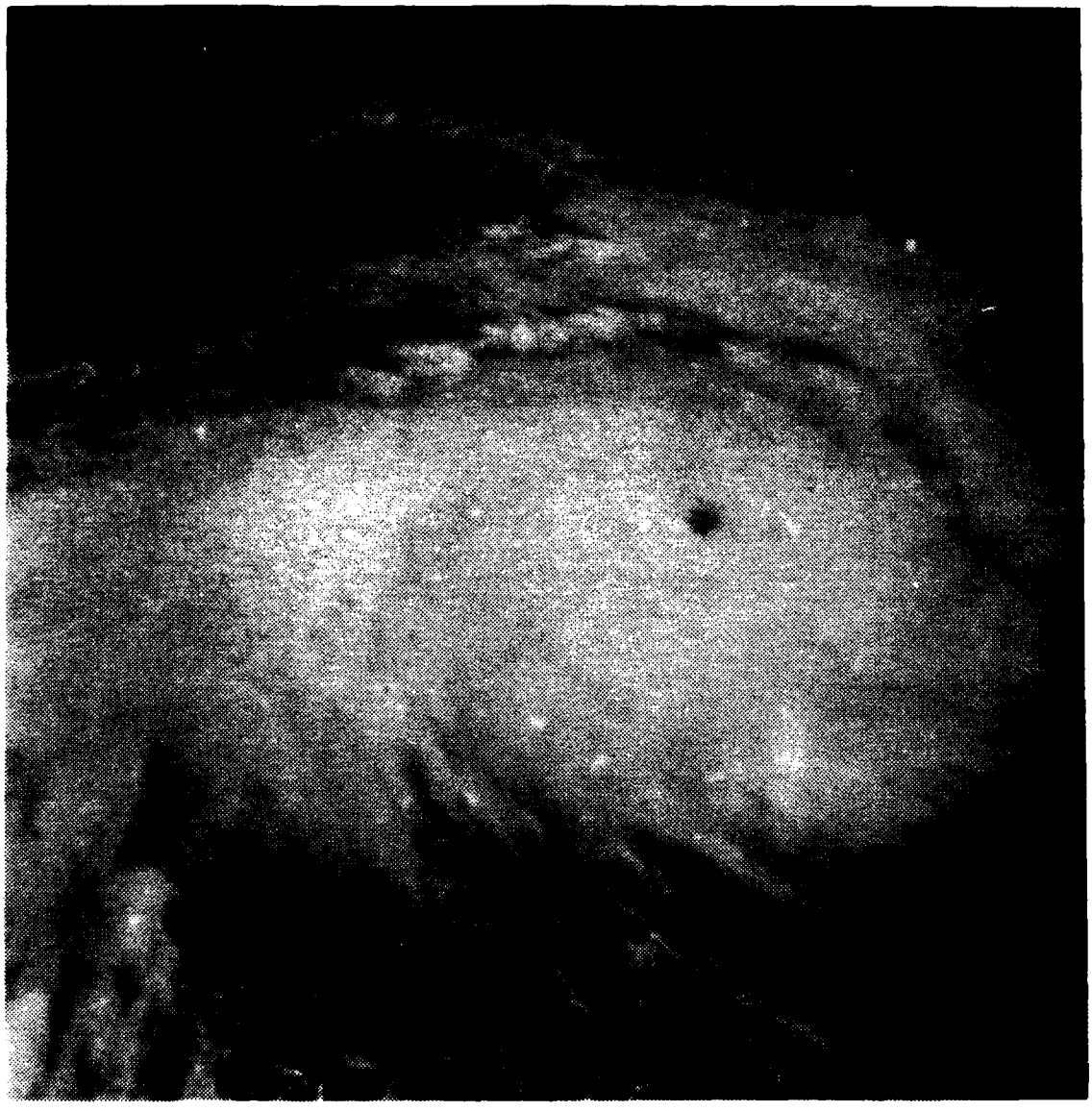

Fig. 32 Frame 1661: Hurricane Kamisy, Orbit 30 1128 GMT, 8 April 1984 (50-mm lens).

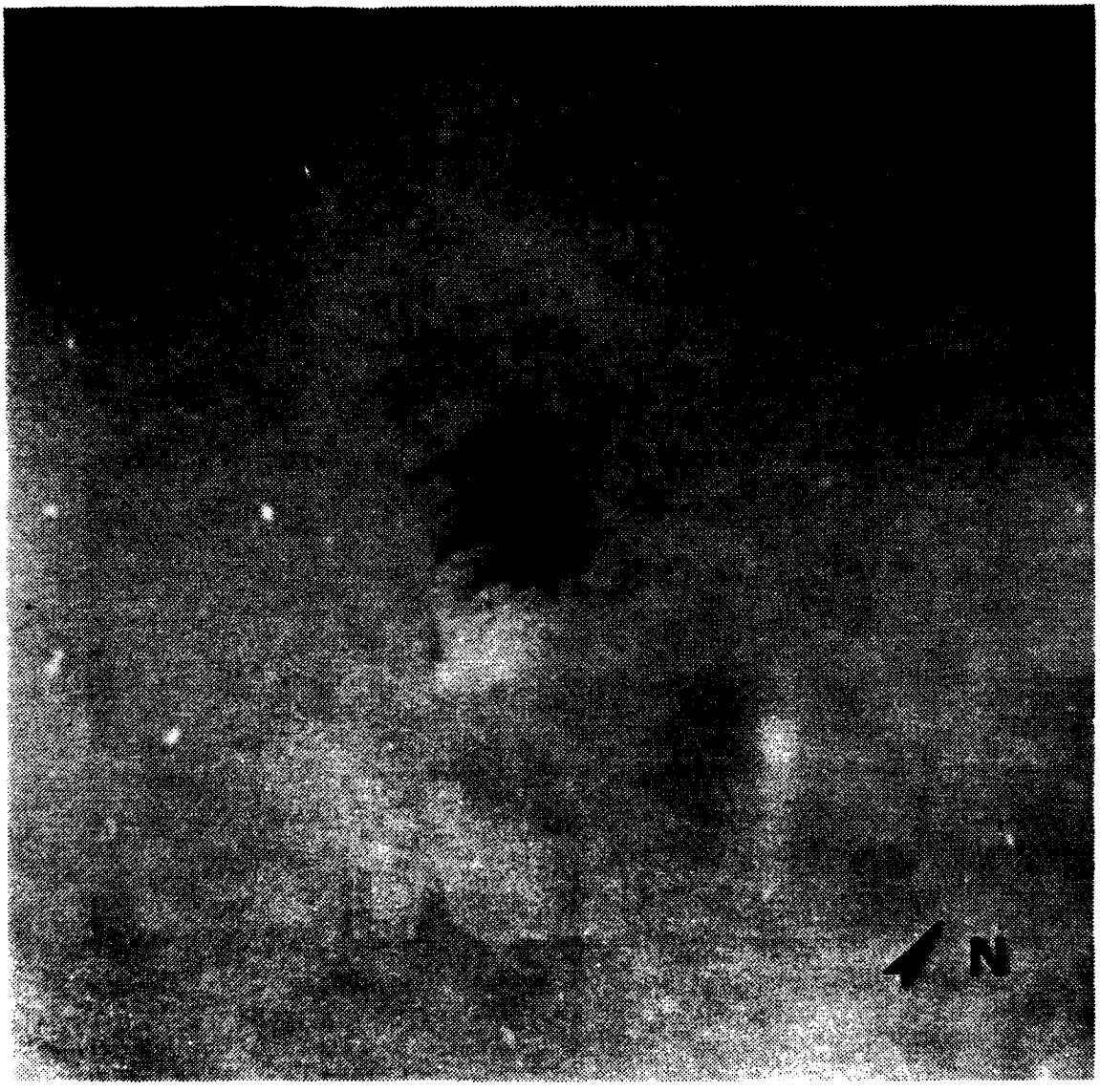

Fig. 33 Frame 1367: Hurricane Kamisy, Orbit 30 1128 GMT, 8 April 1984 (250-mm lens).

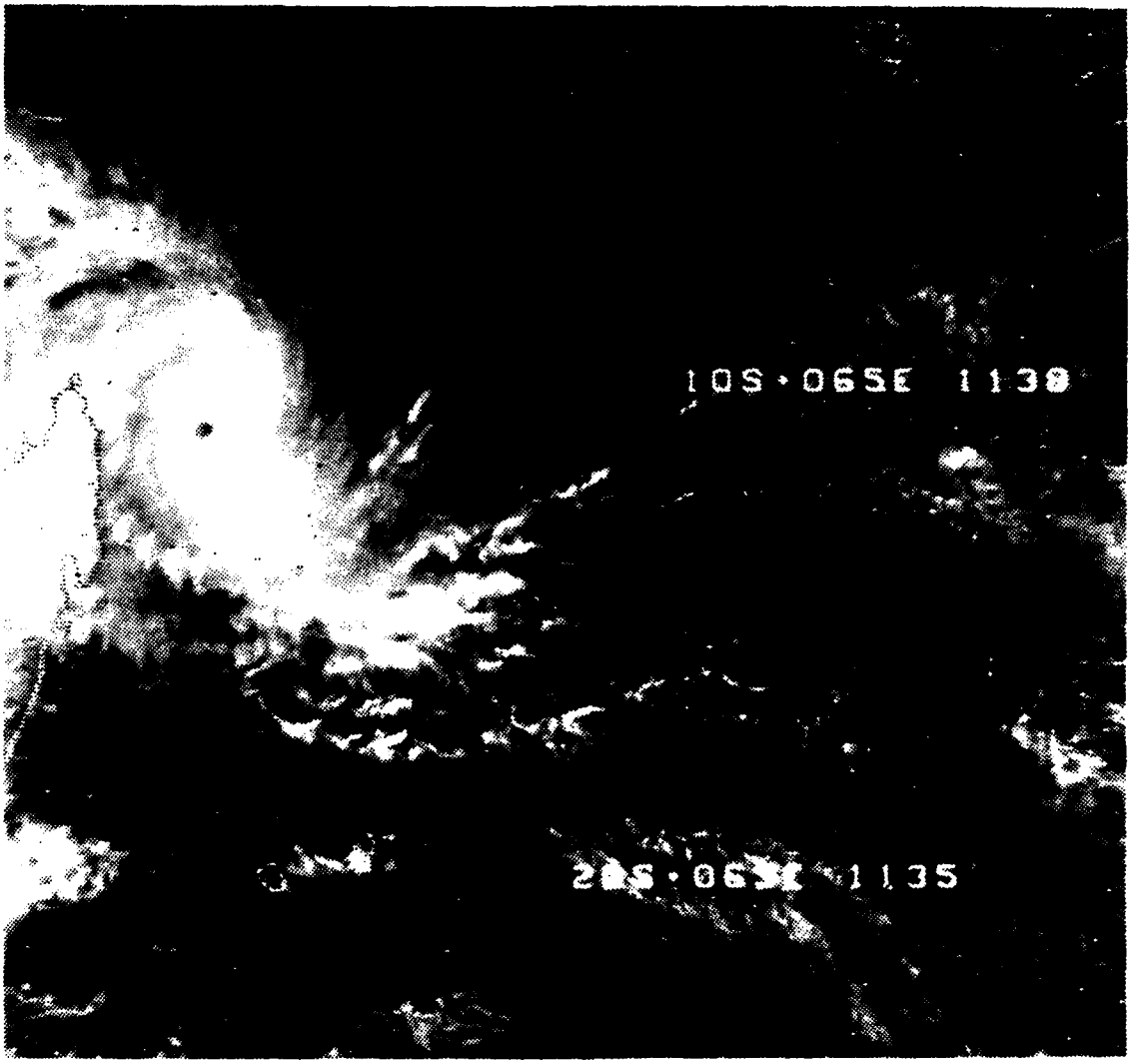

Fig. 34 AVHRR VISIBLE: Hurricane Kamisy
1153 GMT, 8 April 1984.

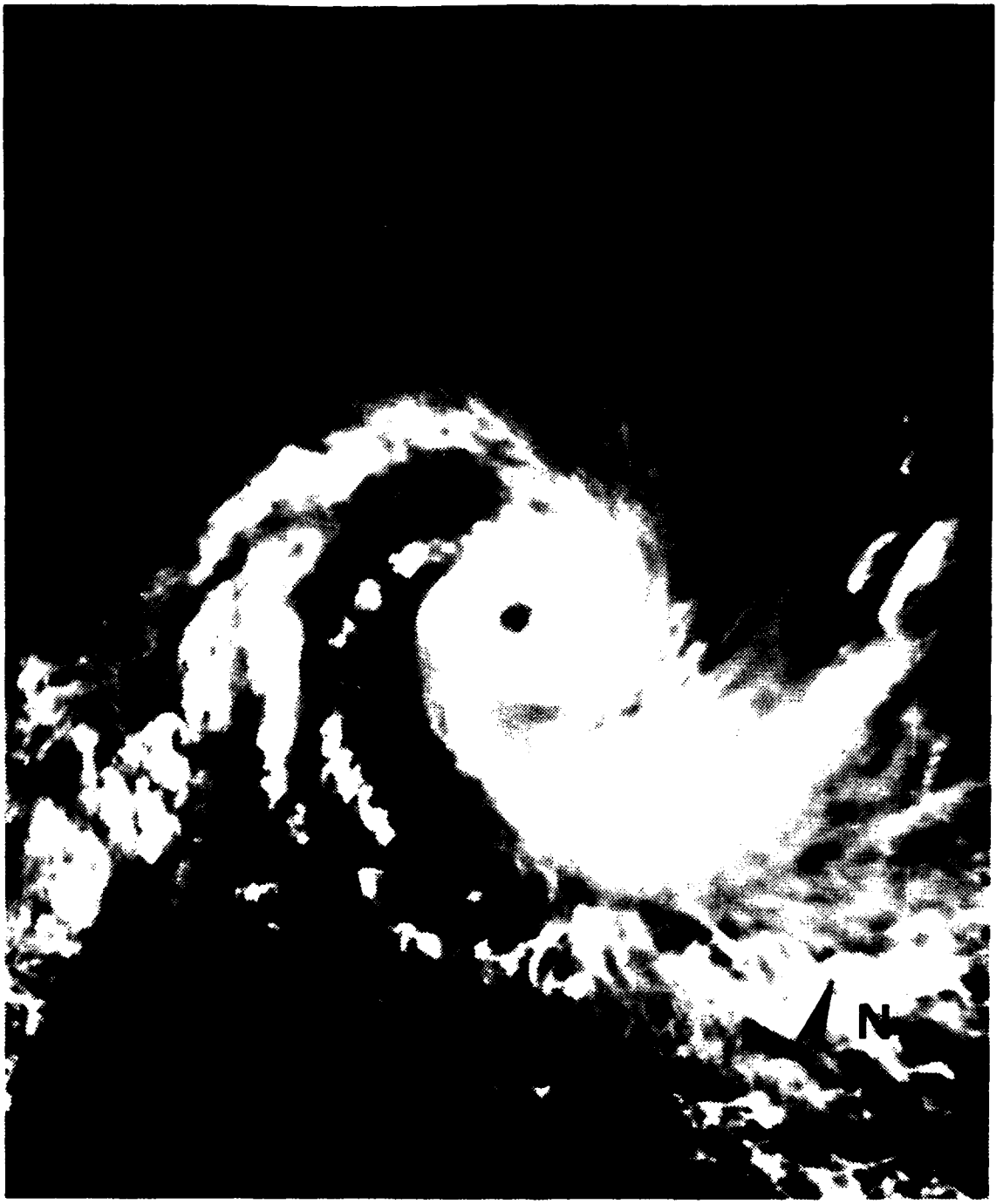

Fig. 35 DMSP IR: Hurricane Kamisy
0714 GMT, 8 April 1984.

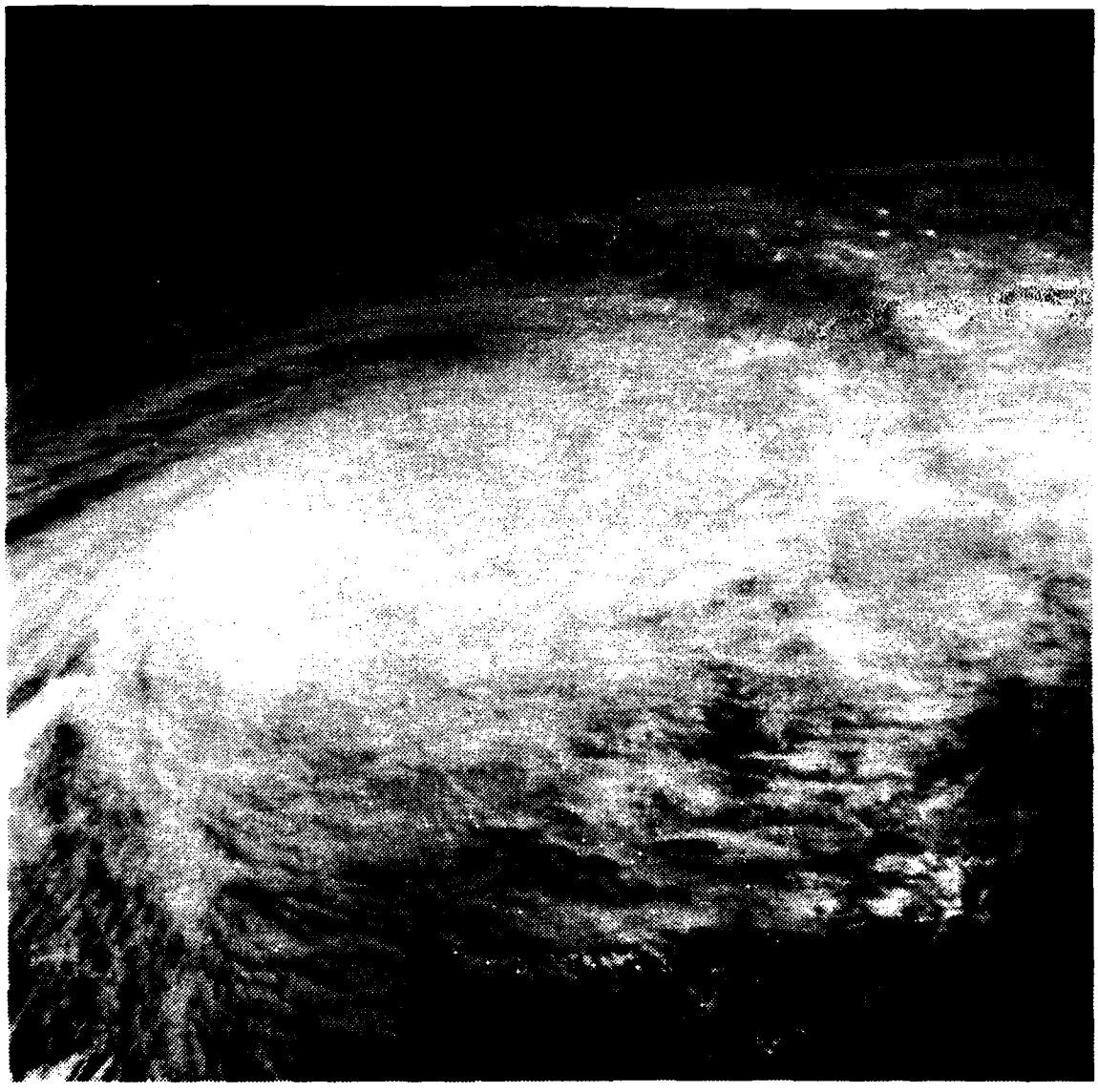

Fig. 36 Frame 2126; Hurricane Kamisy, Orbit 46 1239 GMT, 9 April 1984 (100-mm lens).

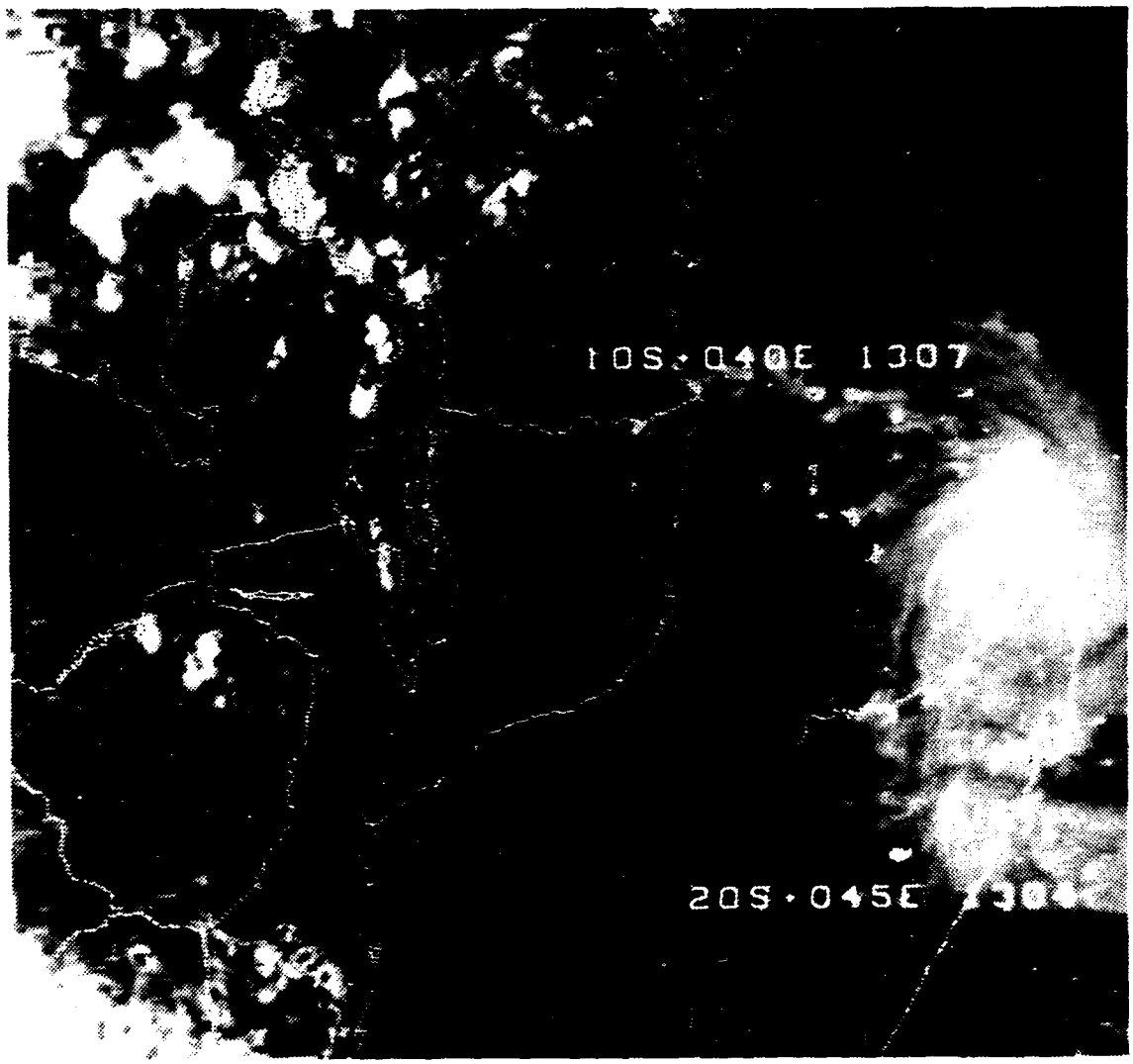

Fig. 37 AVHRR VISIBLE: Hurricane Kamisy
1322 GMT, 9 April 1984.

Fig. 38 DMSP IR: Hurricane Kamisy
1322 GMT, 9 April 1984.

AD-A159 415 USE OF SPACE SHUTTLE PHOTOGRAPHY IN THE STUDY OF METEOROLOGICAL PHENOMENA(U) NAVAL POSTGRADUATE SCHOOL MONTEREY CA F J SVETZ JUN 85 2/2

UNCLASSIFIED F/G 4/2 NL

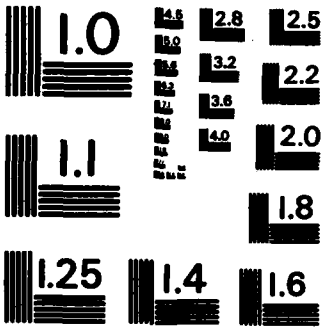

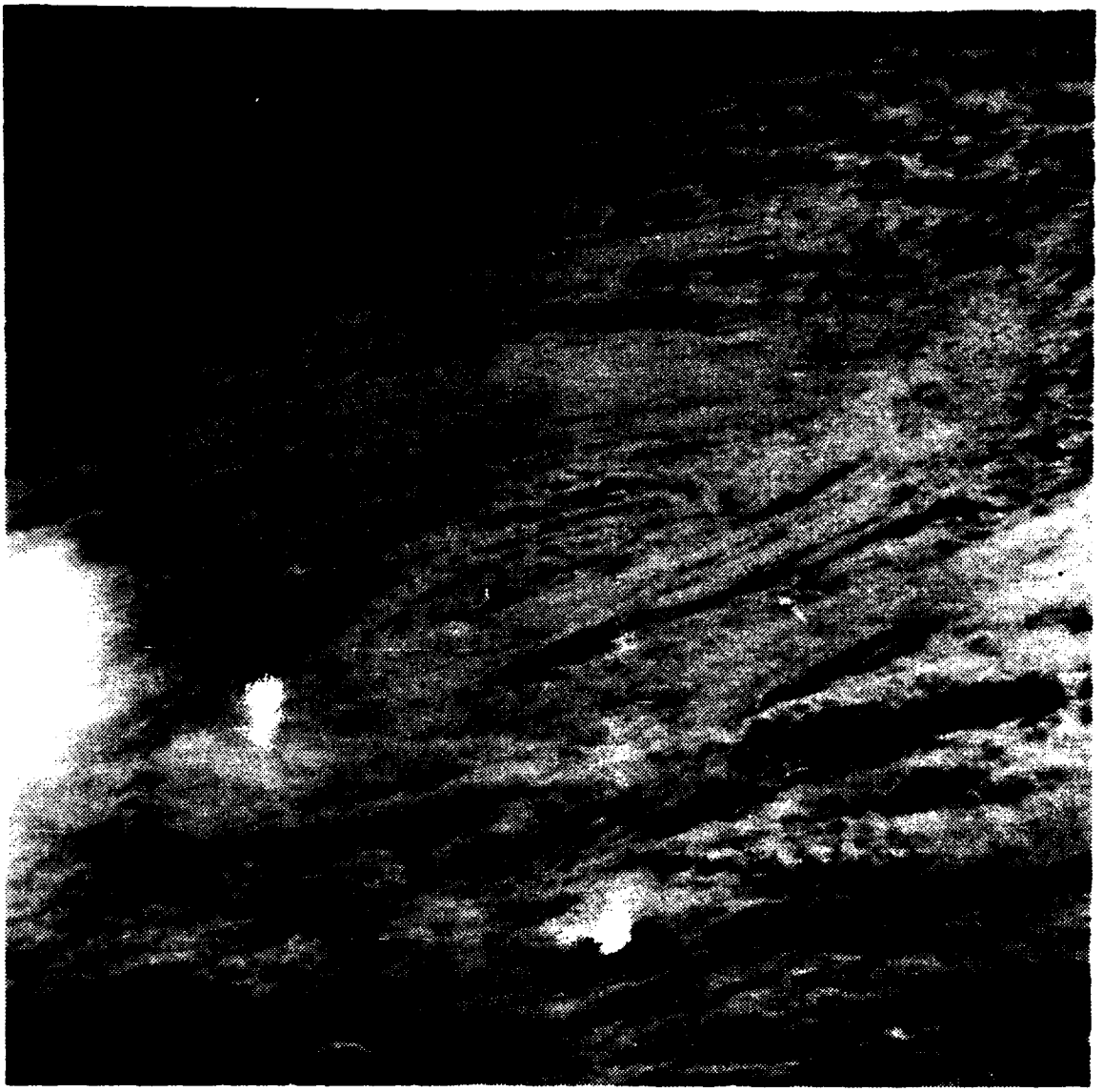

Fig. 39 Frame 1756: Unnamed Tropical Cyclone, Orbit 92
1330 GMT, 12 April 1964 (250-mm lens).

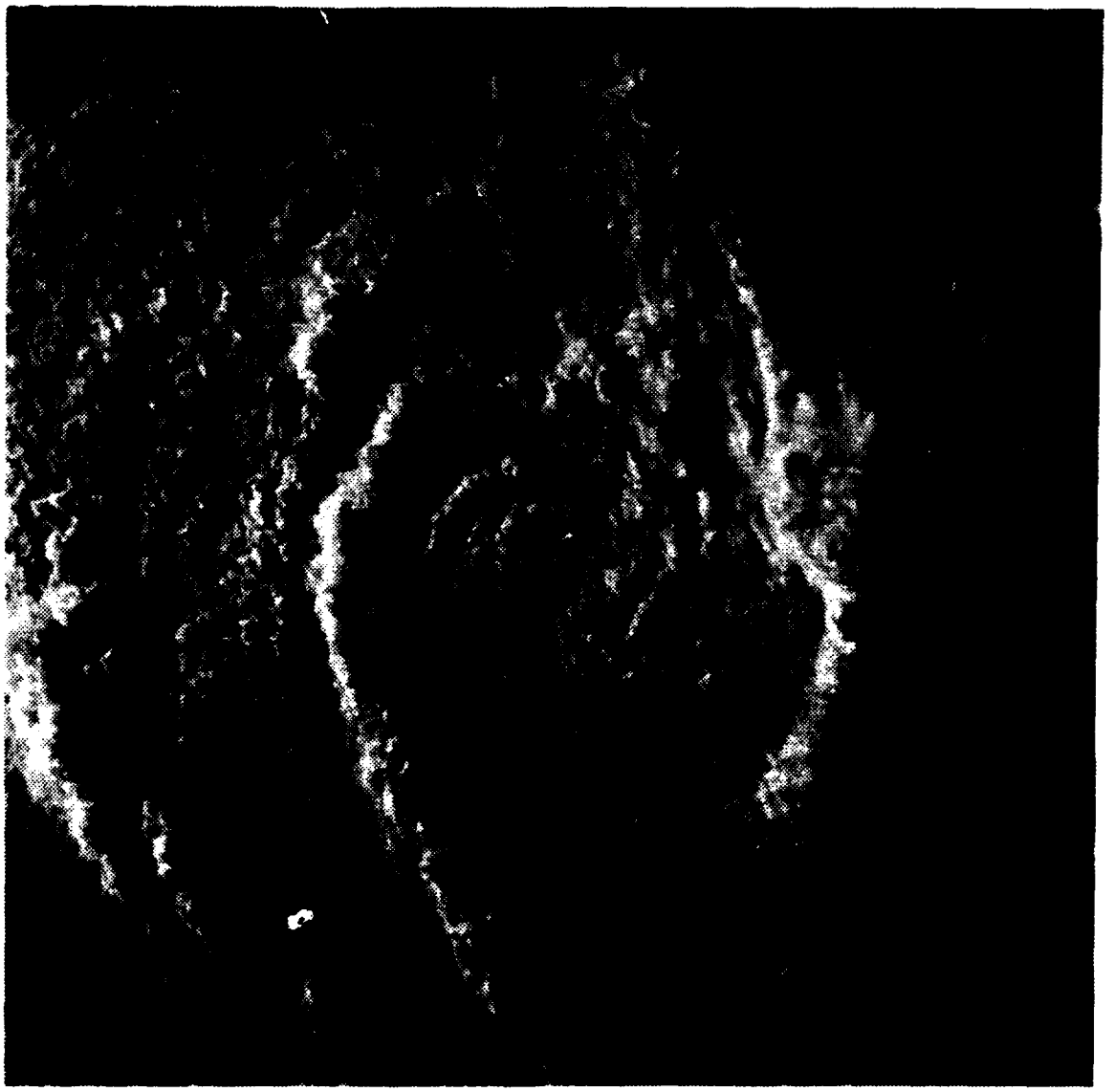

Fig. 40 Frame 1780: Unnamed Tropical Cyclone, Orbit 93
1510 GMT, 12 April 1984 (250-mm lens).

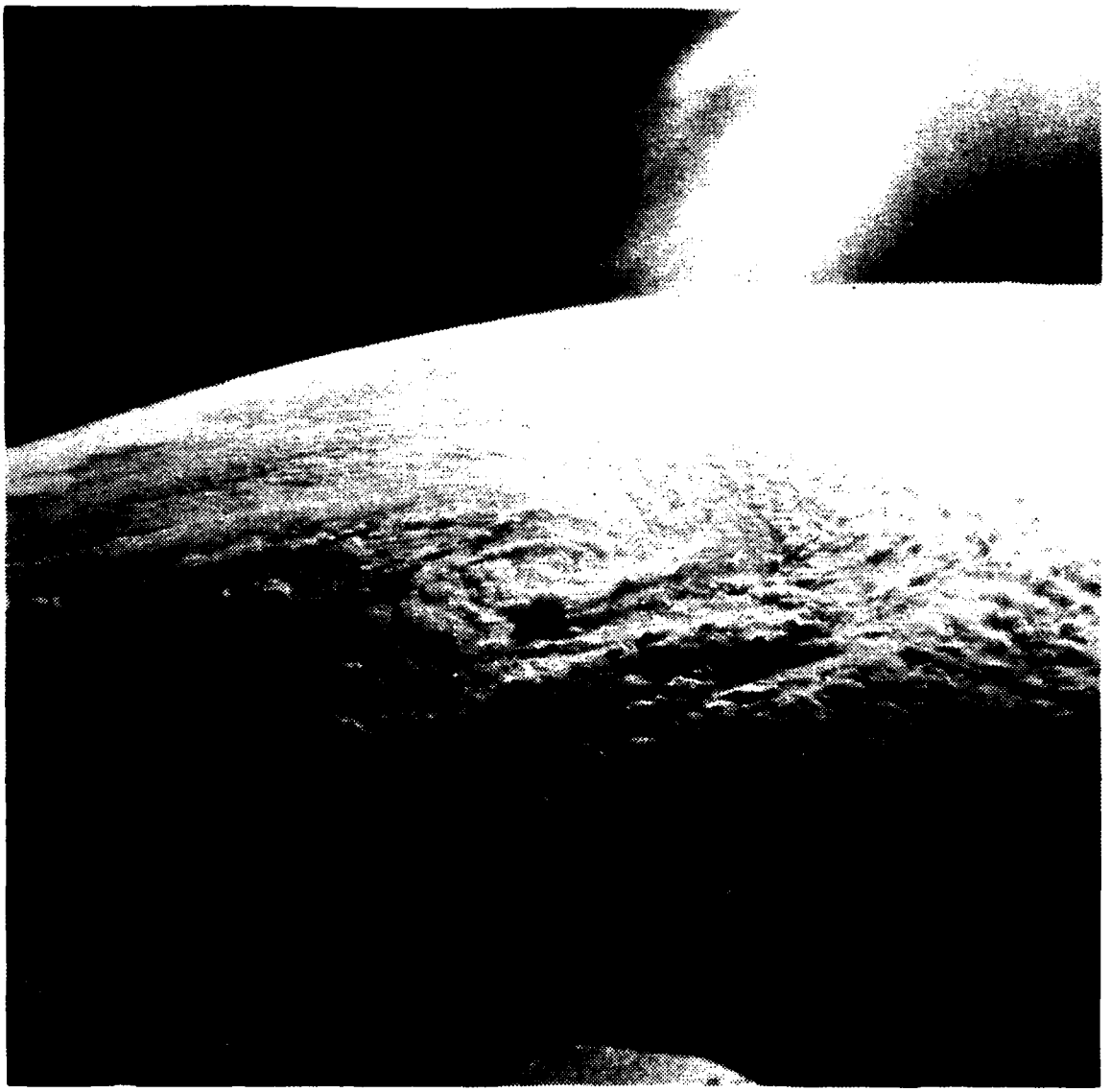

Fig. 41 Frame 1935: Unnamed Tropical Cyclone, Orbit 93 1510 GMT, 12 April 1984 (50-mm lens).

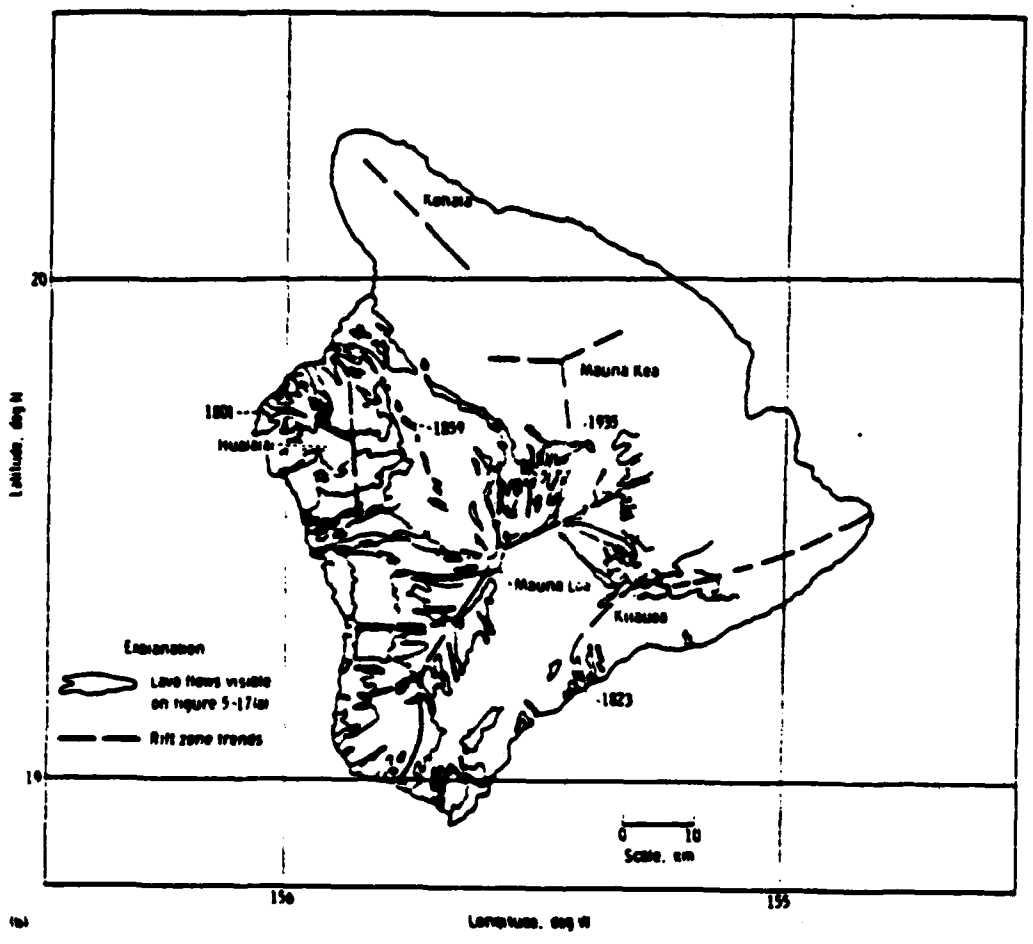

Fig. 42 The island of Hawaii, and location of its major volcanoes.

Fig. 43 Frame 1538: Island of Hawaii, Orbit 21 2051 GMT, 7 April 1984 (250-mm lens).

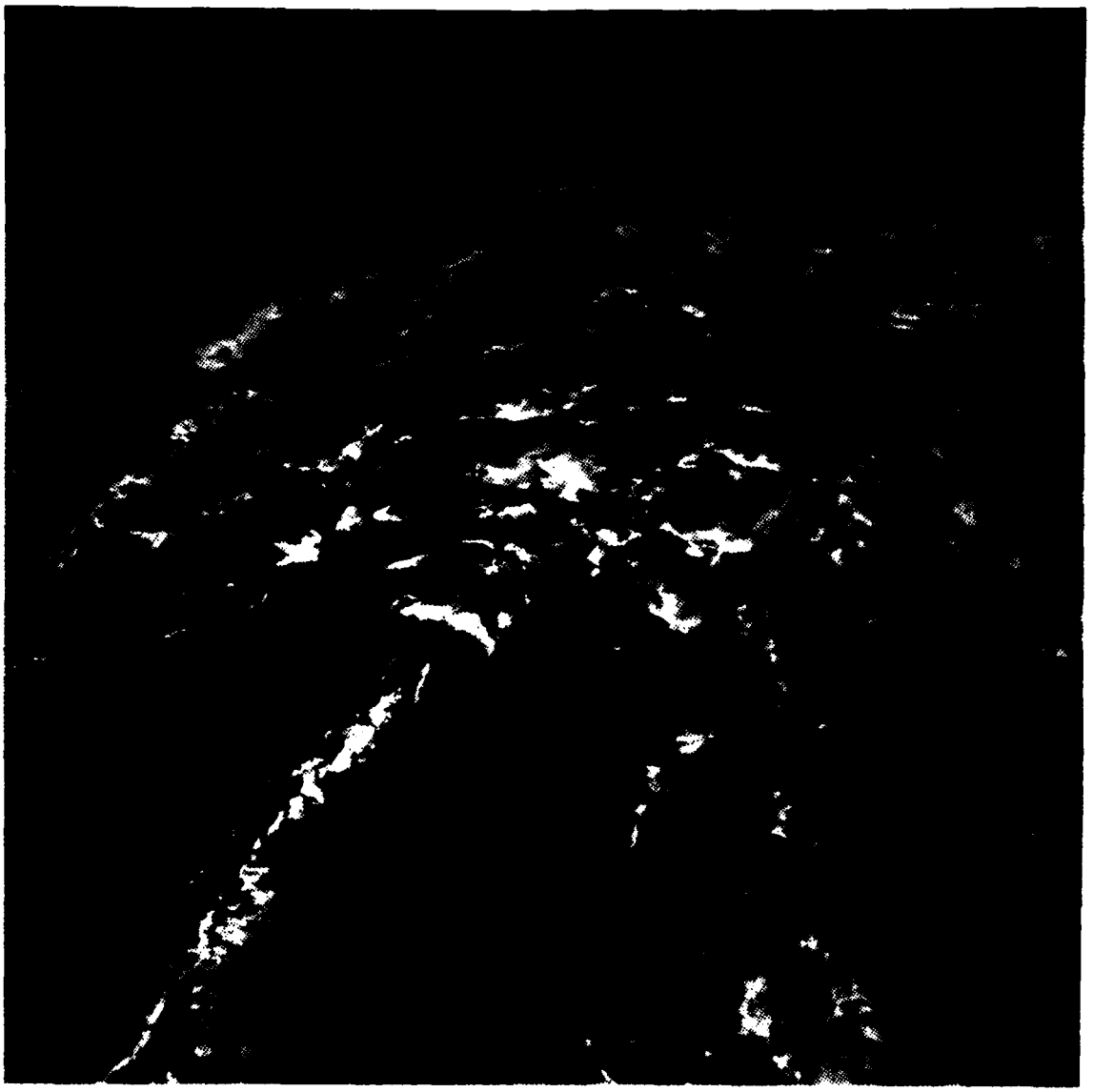

Fig. 48 Frame 1688; Island of Hawaii, Orbit 37 2205 GMT, 8 April 1984 (50-mm lens).

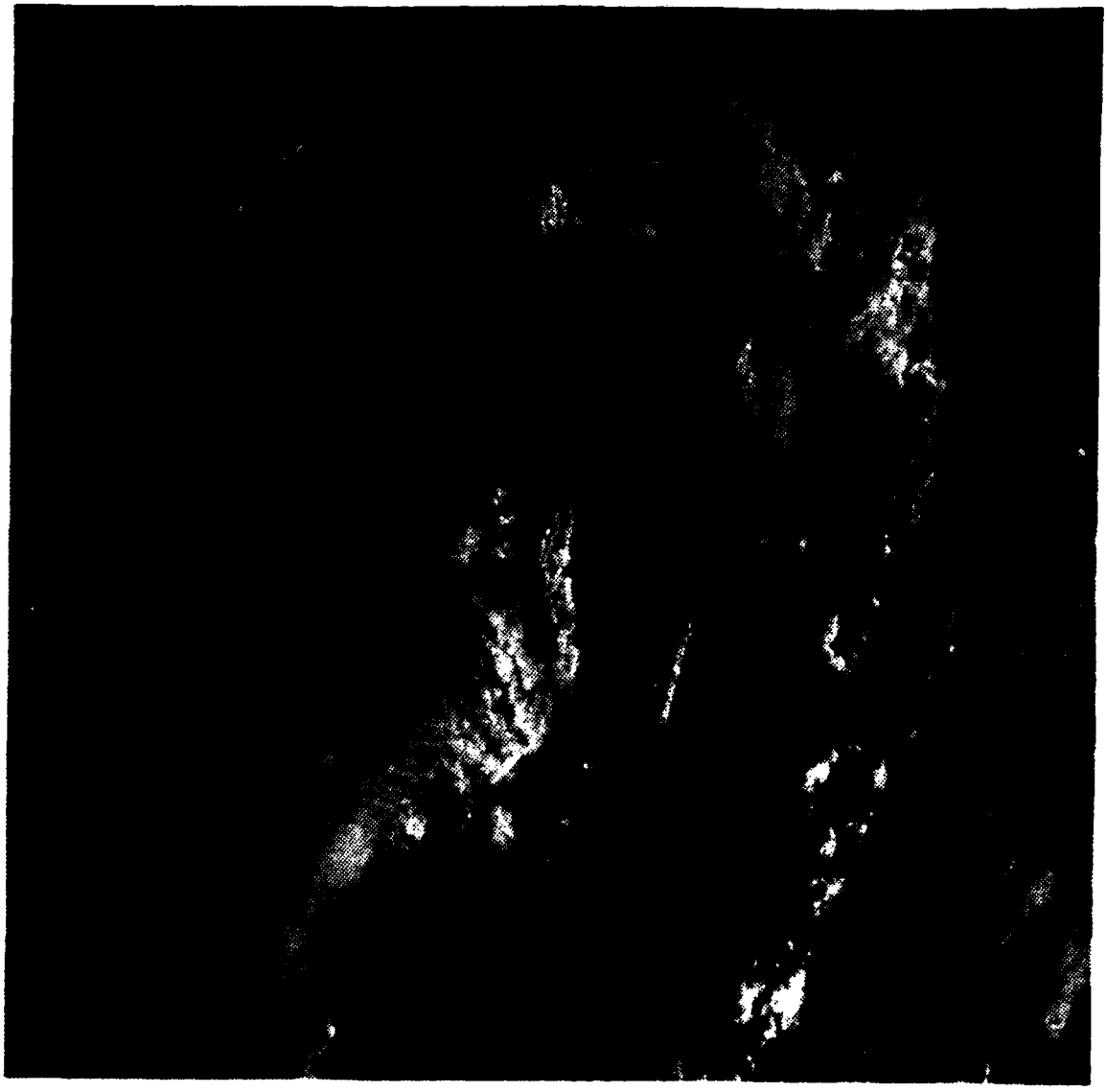

Fig. 45 Frame 1807; Island of Hawaii, Orbit 96
1951 GMT, 12 April 1984 (250-mm lens).

LIST OF REFERENCES

Anthes, R.A., 1982: Tropical Cyclones--Their Evolution, Structure and Effects. American Meteorological Society, Boston, MS, 206 pp.

Black, P.G., 1977: "Some Aspects of Tropical Storm Structure Revealed by Handheld-Camera Photographs From Space", in Skylab Explores The Earth, NASA SP-380, eds. V.R. Wilmarth, J.L. Kaltenbach, and W.B. Lenoir, NASA Lyndon B. Johnson Space Center, Houston, TX, 517 pp.

----------, 1979: Mesoscale cloud Patterns Revealed by ASTP Photographs, in Apollo-Soyuz Test Project, Summary Science Report, Volume II, NASA SP-412, eds. F. El-Baz and D.M. Warner, NASA Lyndon B. Johnson Space Center, Houston, TX, 692 pp.

Carr, G.P., 1977: Preface, in Skylab Explores The Earth, NASA SP-330, eds. V.R. Wilmarth, J.R. Kaltenbach, and W.B. Lenoir, NASA Lyndon B. Johnson Space Center, Houston, TX, 517 pp.

Chopra, K.P. and L.F. Hubert, 1965: Karman vortex streets in wakes of islands. J. American Inst. Aeronaut. & Astronaut., Vol.3, 10, 1941-1943.

El-Baz, F., D.M. Warner and R.T. Guili, 1979: Summary of Significant Results, in Apollo-Soyuz Test Project, Summary Science Report, Volume II, NASA SP-412, eds. F. El-Baz and D.M. Warner, NASA Lyndon B. Johnson Space Center, Houston, TX, 692 pp.

Fujita, T.T. and J.J. Tecson, 1977: "Mesoscale Wake Clouds in Skylab Photographs", in Skylab Explores The Earth, NASA SP-330, eds. V.R. Wilmarth, J.L. Kaltenbach, and W.B. Lenoir, NASA Lyndon B. Johnson Space Center, Houston, TX, 517 pp.

Hering, W.S., 1981: An Operational Technique for Estimating Visible Spectrum Contrast Transmittance. AFGL-TR-81-0193, Visibility Laboratory, University of San Diego, La Jolla, CA, 39 pp.

Kaufman, Y.J., 1979: Effect of the Earth's atmosphere on contrast for zenith observation. J. Geophys. Res., 84, 3165-3172

Koepke, P. and H. Quenzel, 1979: Turbidity of the atmosphere determined from satellite: calculation of optimum viewing geometry. J. Geophys. Res., 84, 7847-7856.

Kropfli, P.A. and L.J. Miller, 1975: Thunderstorm flow patterns in three dimensions. Mon. Wea. Rev., 103, 70-71.

Maul, G.A. and M. McCaslin, 1977: "An Assessment of the Potential Contributions to Oceanography From Skylab Visual Observations and Handheld-Camera Photographs", in Skylab Explores The Earth, NASA SP-380, eds. V.R. Wilmarth, J.L. Kaltenbach, and W.B. Lenoir, NASA Lyndon B. Johnson Space Center, Houston, TX, 517 pp.

Nowakowski, B.S. and W.F. Palmer, 1984: Catalog of Space Shuttle Earth Observations Hand-Held Photography: Space Transportation System (STS 41-C) Mission. JSC-20056, NASA Lyndon B. Johnson Space Center, Houston, TX, 46 pp.

National Oceanic and Atmospheric Administration, 1984: Environmental Satellite Imagery, April 1984. Key to Meteorological Records Documentation (KMRD) No. 5.4, U.S. Dept. of Commerce, Washington, D.C., 93 pp.

Norton, C.C., F.R. Mosher, B. Hinton, D.W. Martin, D. Santek and W. Kuhlow, 1982: A Model for Calculating Atmospheric Turbidity Over the Oceans From Geostationary Satellite Data, in Atmospheric Aerosols: Their Formation, Optical Properties, and Effects, ed. A. Deepak, Spectrum Press, Hampton, VA, 305-315.

Pitts, D.E., J.T. Lee, J. Fein, Y. Sasaki, K. Wagner and R. Johnson, 1977: "Mesoscale Cloud Features Observed From Skylab", in Skylab Explores The Earth, SP-380, eds. V.R. Wilmarth, J.L. Kaltenbach, and W.B. Lenoir, NASA Lyndon B. Johnson Space Center, Houston, TX, 517 pp.

Sanderson, D., 1977: "Quantitative Analysis of Atmospheric Pollution Phenomena", in Skylab Explores The Earth, NASA SP-380, eds. V.R. Wilmarth, J.L. Kaltenbach, and W.B. Lenoir, NASA Lyndon B. Johnson Space Center, Houston, TX, 517 pp.

Shapiro, M., 1983: Mesoscale Weather in the United States--Review of Regional Phenomena, in The National STORM Program, ed. R.A. Anthes, University Corporation for Atmospheric Research, Boulder, CO, 477 pp.

Skillman, W.C. and W.E. Shenk, 1977: "Meteorological Applications of Skylab Handheld-Camera Photographs", in Skylab Explores The Earth, SP-380, eds. V.R. Wilmarth, J.L. Kaltenbach, and W.B. Lenoir, NASA Lyndon B. Johnson Space Center, Houston, TX, 517 pp.

Terry, R.D., 1979: Visual Observations Over Oceans, in Apollo-Soyuz Test Project, Summary Science Report, Volume II, NASA SP-412, NASA Lyndon B. Johnson Space Center, Houston, TX, 692 pp.

Zipser, E.J., 1977: Mesoscale and convective downdrafts as distinct components of squall-line structure. Mon. Wea. Rev., 105, 1568-1589.

INITIAL DISTRIBUTION LIST

		No. Copies
1.	Defense Technical Information Center Cameron Station Alexandria, Virginia 22304-6145	2
2.	Library, Code 0142 Naval Postgraduate School Monterey, Califcrnia 93943-5100	2
3.	Air Weather Service Technical Library Scott AFB, IL 62225-5000	1
4.	Professor Robert J. Renard, Code 63 Rd Chairman, Department of Meteorology Naval Postgraduate School Monterey, CA 93943	1
5.	Professor Carlyle H. Wash, Code 63 Wx Department of Meteorology Naval Postgraduate School Monterey, CA 93943	15
6.	Chief of Satellite Operations Det 1, 1WW (MAC) Box 20 FPO San Francisco, CA 96630	10

END

FILMED

10-85

DTIC